COMMERCIAL APPLICATION OF ALUMINUM HONEYCOMB AND FOAM IN LOAD BEARING TUBULAR STRUCTURES

by

Stefano Bartolucci

B.S. in Mechanical Engineering (*cum laude*), 2002

Universita' degli Studi di Modena, Modena, Italy

Submitted to the Department of Materials Science and Engineering

in partial fulfillment of the requirements for the degree of

Master of Engineering in Materials Science and Engineering

at the

Massachusetts Institute of Technology

September 2004

Signature of Author.....
Department of Materials Science and Engineering
August 11, 2004

Certified by.....
Lorna J.Gibson
Matoula S. Salapatas Professor of Materials Science and Engineering
Thesis Supervisor

Certified by.....
Thomas W. Eagar
Thomas Lord Professor of Materials Science and Engineering
Thesis Coadvisor

Accepted by.....
Carl. V. Thomson
Stavros Salapatas Professor of Materials Science and Engineering
Chairman, Departmental Committee on Graduate Students

COMMERCIAL APPLICATION OF ALUMINUM HONEYCOMB AND FOAM IN LOAD BEARING TUBULAR STRUCTURES

by

Stefano Bartolucci

Submitted to the Department of Materials Science and Engineering

on August 11, 2004 in partial fulfillment of the requirements

for the degree of Master of Engineering in Materials Science and Engineering

Abstract

Small dimension engineering tubular structures subjected to a complex load system are designed like hollow circular shells. For minimum weight design, the ratio between the shell radius and the thickness has to be as large as possible, but its maximum value is limited by the onset of local buckling. Tubular natural structures subjected to a complex load system have often an outer shell of solid material supported by a low density, compliant core, which makes them more resistant to local buckling. Biomimicking of natural constructions offer the potential to improve the design of small diameter tubular engineering structures.

Here, the fabrication technology of biomimicked engineering tubular structures integrating aluminum foam or honeycomb as core material is discussed. A viability analysis is presented including technical performance, cost, utility, and risk assessments. Aluminum compliant core shells have potential for substituting CFRP and aluminum tubular structures in aerospace and high-level sport applications. The case of sailboat masts was considered in detail. Results of our analysis proved that use of honeycomb as core material can lead to a significant reduction of the mast weight. Business opportunities based on this application are discussed.

Thesis Advisor: Lorna J. Gibson

Title: Matoula S. Salapatas Professor of Materials Science and Engineering

To my father

Acknowledgements

Life at M.I.T. has been a great personal and intellectual adventure, and my pleasure has mainly been due to the extraordinary people around me and their professional qualities.

Principal among these, I would like to thank my advisor, Prof. Lorna Gibson, for her guidance, patience and encouragement during the course of this thesis, especially when things did not turn out well. She has taught me much about perseverance and organization in my work.

I also would like to thank Prof. Thomas Eagar for his brilliant inputs regarding my thesis: every single talk we had was a unique and valuable experience for me.

It was a pleasure to interact with the M.I.T Welding Lab group. I wish to thank in particular Joel William for a wonderful lab experience and Kris Musso for his important advice.

I would like to thank those who have been instrumental in enabling me to endure the difficult times, as well as to enjoy the glad times, in particular Diego, Alfredo, Markus, Padraig, and Paolo.

Lucy, I wish to express my deepest gratitude for the constant support, understanding, and love that I received from you through all this period.

Finally, but most important, I wish to thank my family, whose moral and financial support enabled me to study here in M.I.T. Without you, this could have not been possible.

Table of Contents

	page
Title page	*1*
Abstract	*2*
Dedication	*3*
Acknowledgements	*4*
Table of Contents	*5*
List of Tables	*9*
List of Figures	*10*
List of Notations and Symbols	*15*
Chapter 1: Introduction and Current Technology	**20**
1.1 Background and Significance	20
1.1.1 Engineering Tubular Structures	*20*
1.1.2 Natural Tubular Structures	*21*
1.1.3 Biomimicking of Natural Cylindrical Tubes	*26*
1.2 Current Technology: Aluminum Foam Manufacturing Methods	27
1.2.1 Production Methods Overview	*27*
1.2.2 CYMAT	*28*
1.2.3 ALPORAS	*29*
1.2.4 ALULIGHT/FOAMINAL	*31*
1.2.5 DUOCEL	*32*
1.3 Current Technology: Aluminum Honeycomb Manufacturing	34
1.3.1 Generality	*34*
1.3.2 Expansion Process	*34*
1.3.3 Corrugation Process	*35*
1.4 Current Technology: Bond Technologies for Aluminum Foam Sandwich Structures	37
1.4.1 Introduction to Aluminum Foam Sandwich Structures	*37*
1.4.2 Feasible Al-Foam Al-Sheet Joining Technologies	*38*

page

1.4.2.1 Mechanical Fastening Elements 38

1.4.2.2 Gluing 38

1.4.2.3 Welding 39

1.4.2.4 Soldering and Brazing 40

1.4.2.5 Transient Liquid Phase Bonding 41

1.4.2.6 Nickel Plating and Brazing 42

1.4.3 Shear Testing on Foam-Sheet Joints 43

1.4.4 Summary 45

1.5 Current Technology: Bond Technology for Aluminum Honeycomb Sandwich Structures 46

1.5.1 Adhesive Bonding 46

1.5.2 Brazing 48

1.6 Fabrication of Tubular Structures with Compliant Core 49

1.7 References of Chapter 1 51

Chapter 2: Viability Assessment **54**

2.1 Introduction 54

2.2 Technical Performance Assessment 57

2.2.1 Hollow Circular Shells 58

2.2.2 Stringers-Stiffed Isotropic Shells 61

2.2.3 Hollow Sandwich-Wall Circular Cylinder 66

2.2.4 Shells with Compliant Core 70

2.2.5 Comparison of Different Form of Constructions 74

2.2.6 Effect of Materials 76

2.3 Cost Estimation 80

2.4 Value in the Market 84

2.5 References of Chapter 2 90

Chapter 3: Sailboat Masts with Cellular Metal Core **92**

3.1 Introduction 92

page

3.2 Mast Load System 92

3.3 Mast Design: Functional Requirements 97

3.3.1 Stiffness *97*

3.3.1.1 Global Buckling *97*

3.3.1.2 Transverse Mast Stiffness $E \cdot I_{yy}$ *100*

3.3.1.3 Longitudinal Mast Stiffness $E \cdot I_{xx}$ *101*

3.3.2 Minimum Weight *102*

3.3.3 Maximum Aerodynamics Efficiency *103*

3.4 Mast Design: Materials Selection 106

3.4.1 Figures of Merit *106*

3.4.2 Wood *107*

3.4.3 Aluminum *107*

3.4.4 Steel and GRP *107*

3.4.5 CFRP *108*

3.5 Application of Cellular Metals in Sail Masts: Circular Sections 109

3.5.1 Circular Cylindrical Aluminum Extruded Tube *111*

3.5.2 Aluminum Circular Cylindrical Sandwich with Foam Core *113*

3.5.3 Aluminum Circular Cylindrical Sandwich with Honeycomb Core *116*

3.5.4 Aluminum Circular Cylindrical Shell with Foam Core *118*

3.5.5 Aluminum Circular Cylindrical Shell with Honeycomb Core *120*

3.6 Application of Cellular Metals in Sail Masts: Elliptical Sections 122

3.6.1 Estimation of the Local Buckling Stress *122*

3.6.2 Aluminum Elliptical Cylindrical Extruded Tube *124*

3.6.3 Aluminum Elliptical Cylindrical Sandwich with Foam Core *126*

3.6.4 Aluminum Elliptical Cylindrical Sandwich with Honeycomb Core *128*

3.6.5 Aluminum Elliptical Cylindrical Shell with Foam Core *129*

3.6.6 Aluminum Elliptical Cylindrical Shell with Honeycomb Core *131*

3.7 Application of Cellular Metals in Sail Masts: Discussion 133

page

3.8 References of Chapter 3 137

Chapter 4: Investment Assessment for Sailboat Masts with Cellular Core **138**

4.1 Introduction 138

4.2 Market Assessment 140

4.2.1 Generality *140*

4.2.2 Mast Market *141*

4.2.3 Sailboat Market Projections *142*

4.2.4 End Users *144*

4.2.5 Overall Marketing Strategy *144*

4.2.6 Competition *145*

4.2.7 Potential Revenue Flows *147*

4.3 Value Capture 148

4.3.1 Generality *148*

4.3.2 IP Asset and Defense *149*

4.3.3 Industry Structure *149*

4.3.4 Organizational Structure *150*

4.3.5 Probability of Value Capture Summary *151*

4.4 Investment Decision 151

4.5 References of Chapter 4 153

Chapter 5: Conclusions **154**

List of Tables

	page
Table 1.1: Applied sheet and foam materials.	43
Table 1.2: Investigated joining technologies.	43
Table 1.3: Influence of the joining technology on the theoretical maximum tensile shear stress in quasi-static loading.	44
Table 1.4: Evaluation of the investigated joining technologies.	45
Table 2.1: Experimental values of the panel efficiency coefficient.	65
Table 2.2: Materials for lightweight compression commercial hollow tubes.	76
Table 2.3: Different constructions for lightweight compression structures.	79
Table 2.4: Sandwich structures under investigation.	80
Table 2.5: Cost of materials.	81
Table 2.6: Resources consumed in making composite honeycomb/foam core shell.	82
Table 2.7: Utility of weight saving in transport systems.	85
Table 3.1: Calculation of the staying factor.	101
Table 3.2: Resistance to environmental conditions for materials employed in masts.	106
Table 4.1: Mast markets (2000).	141
Table 4.2: Sailboat retail value in the United States (2000).	143
Table 4.3: U.S. sailboat masts producers.	146
Table 4.4: Management efficiency.	150
Table 4.5: Attractiveness of different investment strategies.	152

List of Figures

page

Figure 1.1: North American porcupine quill cross section. 22

Figure 1.2: North American porcupine quill cross section: detail. 22

Figure 1.3: Old World porcupine quill cross section: detail. 23

Figure 1.4: Grass stem cross section. 23

Figure 1.5: Grass stem cross section: detail. 24

Figure 1.6: Hedgehog spine longitudinal section. 24

Figure 1.7: Hedgehog spine longitudinal section: detail. 25

Figure 1.8: Biomimicking natural tubular structure. 26

Figure 1.9: A taxonomy of metal foam manufacturing process 27

Figure 1.10: Schematic illustration of the CYMAT process. 28

Figure 1.11: Foam produced by the CYMAT process. 29

Figure 1.12: Schematic illustration of the ALPORAS process. 30

Figure 1.13: Foam produced by the ALPORAS process. 30

Figure 1.14: Schematic illustration of the powder compact process. 31

Figure 1.15: Foam produced by the powder compact process. 32

Figure 1.16: Duocell™ foam produced by investment casting. 33

Figure 1.17: Expansion manufacturing process. 34

Figure 1.18: Corrugation manufacturing process. 35

Figure 1.19: Principal honeycomb cell configurations. 36

Figure 1.20: Geometry of the samples for the shear test. 44

Figure 1.21: Flat sandwich panel produced by heated press. 46

Figure 1.22: Curve sandwich panel produced by vacuum bagging or autoclave. 47

Figure 1.23: Vacuum bag system: a flexible bag is sealed over the sandwich and the vacuum is created. 47

Figure 1.24: Schematic of the autoclave. 48

Figure 1.25: Methods for filling tubes with foam. 49

page

Figure 1.26: Comparison between foam-filled shell produced by the (a) Fraunhofer process and (b) the co-forming process. 50

Figure 1.27: Insert for honeycomb core shell. 50

Figure 2.1: The investment methodology for materials (IMM). 55

Figure 2.2: Market size and value capture as measures of attractiveness of a material innovation. 56

Figure 2.3: Schematics of cross-sections of cylindrical tubes. (a) Empty shell (b) longitudinal hat-stiffed shell (c) sandwich wall shell (d) shell with a complaint honeycomb or foam core. 57

Figure 2.4: Maximum stress for given structural index. 60

Figure 2.5: Stiffeners considered in this study. 62

Figure 2.6: Thin walled cylindrical shell with a compliant elastic core. 70

Figure 2.7: Normalized weight index plotted against normalized load index, showing curves for empty shell; longitudinal Y-stiffened shell; foam sandwich shell; honeycomb sandwich shell; shell with foam core; shell with honeycomb core; $\gamma \approx 0.5, \varepsilon_y = 0.007, \nu = 1/3; (R/t < 50.)$ 74

Figure 2.8: Normalized weight index plotted vs. load index $\gamma \approx 0.3$, $(50 < R/t < 200)$ 75

Figure 2.9: Normalized weight index plotted vs. load index $\gamma \approx 0.2$, $(R/t > 200)$ 75

Figure 2.10: Material selection chart for commercial hollow tubes, plotted on the density-modulus chart. 77

Figure 2.11: Shape factors for hollow, honeycomb- and foam-core shells. 78

Figure 2.12: Unit cost plotted against production volume for honeycomb sandwich shell. 83

Figure 2.13: Unit cost plotted against production volume for foam sandwich shell. 83

Figure 2.14: Performance-cost tradeoff for structural compression lightweight tubes. 85

page

Figure 2.15: Types of Performance/Cost Substitution for cellular metal shells. 86

Figure 2.16: Value chain in material innovation. 87

Figure 2.17: Market applications for maturity of application and system complexity. 88

Figure 3.1: Forces on a sailing yacht. 93

Figure 3.2: Sail loads on rigging. 94

Figure 3.3: Mast load system. 95

Figure 3.4: Mast compressive load calculation. 96

Figure 3.5: Types of rig considered in the study. 98

Figure 3.6: Types of staying. 99

Figure 3.7: Reference system. 99

Figure 3.8: Panel notation for the different types of rigs. 100

Figure 3.9: Pressure distribution along a sail. 103

Figure 3.10: Flow around a mast/sail combination. 104

Figure 3.11: Wing-mast concept; creating a mast from an existing airfoil. 104

Figure 3.12: Profiles of masts of different dimension (measured in % of the total chord). 105

Figure 3.13: YD-40 rig. 110

Figure 3.14: Circular cylindrical hollow section. 111

Figure 3.15: Weight per unit length plotted against the radius for hollow circular shell. 113

Figure 3.16: Circular sandwich shell section with foam core. 113

Figure 3.17: Weight per unit length plotted against the radius for foam core sandwich shells with different relative densities. 115

Figure 3.18: Circular sandwich shell section with honeycomb core. 116

Figure 3.19: Weight per unit length plotted against the radius for honeycomb-core sandwich shells with different relative densities. 117

Figure 3.20: Circular cylindrical hollow section with foam core. 118

page

Figure 3.21: Weight per unit length plotted against the radius for foam core shells with different relative densities. 119

Figure 3.22: Circular cylindrical hollow section with honeycomb core. 120

Figure 3.23: Weight per unit length plotted against the radius for honeycomb core shells with different relative densities. 121

Figure 3.24: Geometry of elliptical cylindrical shell. 122

Figure 3.25: Elliptical cylindrical hollow section. 124

Figure 3.26: Weight per unit length plotted against the equivalent radius for elliptical cylindrical hollow shell. 125

Figure 3.27: Elliptical sandwich shell section with honeycomb core. 126

Figure 3.28: Weight per unit length plotted against the radius for elliptical foam- core sandwich shells with different relative densities. 127

Figure 3.29: Elliptical sandwich shell section with honeycomb core. 128

Figure 3.30: Weight per unit length plotted against the radius for elliptical honeycomb-core sandwich shells with different relative densities. 129

Figure 3.31: Elliptical cylindrical hollow section with foam core. 129

Figure 3.32: Weight per unit length plotted against the radius for elliptical foam-core shells with different relative densities. 130

Figure 3.33: Elliptical cylindrical hollow section with honeycomb core. 131

Figure 3.34: Weight per unit length plotted against the radius for elliptical honeycomb-core shells with different relative densities. 132

Figure 3.35: Weight per unit length plotted against the radius for hollow circular shell, foam-core sandwich shell, foam reinforced hollow shell, honeycomb-core sandwich shell, honeycomb reinforced hollow shell. 134

Figure 3.36: Weight per unit length plotted against the radius for hollow elliptical shell, foam-core sandwich shell, foam reinforced hollow shell, honeycomb-core sandwich shell, honeycomb reinforced hollow shell. 135

Figure 4.1: Investment assessment. 138

page

Figure 4.2: Market assessment. 140

Figure 4.3: Sailboat sells in the United States by category. 142

Figure 4.4: Market penetration of CFRP in boats' hulls. 147

Figure 4.5: Value capture assessment. 148

Figure 4.6: Value created by the technology under investigation. 151

Figure 5.1: The carbon fiber mast of the trimaran Sergio Tacchini, produced by Espace Composite (Lunel, France). 155

List of Notations and Symbols

A = area of the cross section;

A_{st} = stiffener area;

$B \approx 0.58$ = Allen coefficient;

$C_{m,i}$ = cost of the material i;

C_t = cost of tooling;

$\dot{C}_L$ = overhead rate;

C_e = cost of energy;

$\dot{C}_S$ = cost of space;

$\dot{C}_{ip}$ = royalty payments, cost of intellectual properties;

$\dot{C}_{LO}$ = basic overhead rate;

C_C = cost of capital;

b = radius of bore hole;

c = cell size;

d = core thickness;

E_c = Young's modulus of core;

E_f = Young's modulus of shell;

F = compressive force acting on the mast;

F_{crit} = maximum compressive force acting on the mast;

f = total material utilization fraction;

h = height above the deck to the highest sail carrying forestay;

I = moment of inertia of the cross section;

i = stiffeners interspacing;

K = buckling coefficient;

$$k_1 = \frac{\left(1 - \frac{1}{2}\frac{\rho_c}{\rho_f}\right)\sqrt{1-\nu^2}}{\gamma};$$

$$k_2 = \frac{4\rho_c}{\pi\rho_f}\frac{\gamma}{\sqrt{1-\nu^2}};$$

J = torsional moment of inertia;

l = length of column;

l_{eq} = equivalent length of column;

L = length of shell;

L_f = load factor;

$\mathrm{N} = P/(2\pi R)$;

N = ellipse major semiaxis;

$\dot{n}$ = production rate;

n = production volume;

$n_{xx} = n_{yy}(p)$ = half-wavelength in buckled shape;

$$\mathrm{M} = B\left(\frac{E_c}{E_f}\right)^{\frac{2}{3}};$$

M = ellipse major semiaxis;

$$M_1 = \frac{\left(E\phi_B^e\right)^{1/2}}{\rho} = \text{performance index};$$

m_i = mass of the material i;

P = axial compressive load;

p = panel number;

R = radius to mid-plane of thickness;

$R_s = \frac{M}{N^2}\left\{1+\left[\left(\frac{N}{M}\right)^2 - 1\right]\cdot\left(\frac{y}{M}\right)^2\right\}^{3/2}$ = radius of curvature of surface;

$R_N = \frac{M^2}{N}$;

$R_0 = (N \cdot M)^{\frac{1}{2}}$ = equivalent radius;

s = circumferential coordinate;

sf = traverse stability factor;

T = transverse force applied in the masthead;

t = thickness of shell;

$\bar{t} = (A_{st}/i) + t$ = effective face thickness;

t_t = tooling life (units);

t_c = capital write-off time;

U = utility coefficient;

W = shell weight;

$\alpha = (\pi^2 K)^{\frac{1}{4}}\left(\frac{\varsigma_f \cdot t}{i \cdot \bar{t}}\right)^{\frac{1}{2}}$;

β = shroud angle;

ζ = safety factor;

$$\chi = \left(\pi^2 K\right)^{\frac{1}{4}} \left(\frac{\varsigma \cdot t}{i \cdot \bar{t}}\right)^{\frac{1}{2}};$$

δ = half beam;

$$\varepsilon_y = \frac{\sigma_y}{E_f};$$

$$\eta = \frac{\rho_c}{\rho_s} = \text{ relative density;}$$

κ = knockdown factor shell parameter;

$$\phi_B^e = \frac{4\pi I}{A^2} = \text{flexural shape factor;}$$

$$\phi_T^e = \frac{4\pi K}{A^2} = \text{torsional shape factor;}$$

γ = knockdown factor;

$$\Lambda = \frac{1}{\varepsilon_y}\left[1 + 5 \cdot \frac{\rho_c}{\rho_f} \cdot \left(\frac{\lambda_{cr}}{t}\right)\right];$$

λ_{cr} = critical buckling wavelength parameter;

ς = section radius of gyration;

$\varsigma_f \approx \bar{t}/\left(2\sqrt{3}\right)$ = radius of gyration of an unstiffened panel of thickness $\bar{t}$;

ν_c = Poisson's ratio of core;

$\nu = \nu_f$ = Poisson's ratio of shell;

ρ_c = density of core;

ρ_s = density of parent material;

$\rho = \rho_f$ = density of shell;

$$\Psi = \left(\frac{\sqrt[4]{6}}{\sqrt{2\pi}} \right)^{-\frac{2}{3}} \cdot \alpha^{-\frac{4}{3}};$$

ψ = righting moment lever arm;

$$\Sigma = \frac{1}{M}\left[1 + 5 \cdot \frac{\rho_c}{\rho_f} \cdot \left(\frac{\lambda_{cr}}{t} \right) \right];$$

$\sigma_a = N/t$;

σ_1 = global buckling axial stress;

σ_2 = local buckling axial stress;

σ_y = yielding axial stress;

σ_{wr} = wrinkling stress;

σ_{dm} = face dimpling stress;

$$\tau = \left(\frac{\pi}{4} \right)^{\frac{1}{3}} \cdot \gamma^{\frac{1}{3}} \cdot \frac{1}{\left[3 \cdot (1 - \nu^2) \right]^{\frac{1}{6}}};$$

$\xi = M/N$ = ellipticity;

Chapter 1

Introduction and Current Technology

"When Nature builds large load-bearing structures,
She generally uses cellular materials: wood, bone, coral.
There must be good reasons for it"

M. F. Ashby

1.1 Background and Significance

1.1.1 Engineering Tubular Structures

Cylindrical shells are used in a variety of applications [1]: examples include tubular trusses, silos, tanks, submarines, aircraft fuselages, rockets, and legs of offshore platforms [1]. These components are generally subjected to a complex system of loads: compression, torsion, and bending. For a given material, the resistance to a particular mode of load depends on the shape of the component. To consider this, Ashby [2] has introduced a cross-sectional shape factor for each mode of loading. Defining I as the second moment of inertia and A is the cross area of the section, for axial compression and bending, the shape factor is [2]:

$$\phi_B^e = \frac{4\pi I}{A^2}; \qquad (1.1)$$

In the same way, for torsion, defining J the torsional moment of inertia:

$$\phi_T^e = \frac{4\pi J}{A^2}; \qquad (1.2)$$

The shape factor measures the efficiency of a cross-sectional shape to resist buckling, bending, and torsion. For a hollow circular shell, the shape factor is simply given by the ratio between the shell radius, R, and the wall thickness, t. Therefore, tubular sections become more efficient as the ratio between the shell radius and wall thickness increases. The shape factor can be augmented, enhancing the efficiency of tubular sections, up to a limit determined by the onset of local buckling or by manufacturing constraints.

Maximum shape factors for commercial aluminum and steel circular hollow tubes, which are designed against local buckling, are respectively 25 and 30 [2]. On the other side, wood hollow tubes, due to the anisotropy of the material and machining difficulties, have a maximum shape factor of four [2]. When local buckling is the limiting factor, bracing can suppress it. Shells stiffened by longitudinal stringers and stabilized at intervals by lateral stiffeners, such as ribs or formers, are common in engineering applications, such as aircraft fuselages or legs of offshore structures. For these structures, values of the shape factor of the order of 10^2 or 10^3 are common [1]. However, if the diameter of the shell decreases, the stiffeners have to become thinner and deeper [1]: this sets a lower limit to the radius of stiffened shells, which cannot be less than one meter.

1.1.2 Natural Tubular Structures

Solid sections and hollow tubes of the types used in engineering applications are widespread in nature, for example in tree trunks. Karam in his Ph.D. dissertation described different types of tubular structures, which can be found in nature [1]: he showed that animal quills, plant stems, and spines present a dense outer shell with a more compliant cellular core. He distinguished four different microstructures. The first structure, which can be found for instance in the North American porcupine quills, is a shell completely filled with foam-like material (see Figure 1.1). Figure 1.2 shows the cellular structure more in detail. The second type of structure, which can be observed for instance in the Old World porcupine, is a shell filled with foam but with an additional thin, longitudinal stiffener running radially from the outer shell of the quill toward the center (see Figure 1.3). Another variant of the first type is a shell filled with foam but with a central hole; this microstructure can be found in most plant stems (see Figure 1.4). Figure 1.5 shows the microstructure of the core in detail. The fourth microstructure, which can be observed in the spines of the hedgehog (Figure 1.6), presents closely spaced longitudinal and radial stiffeners and resemble a square-cell honeycomb (Figure 1.7). Gibson [3] observed that sandwich structures with a foam or honeycomb core are also diffuse in Nature, as in the human skull or in the tall leaves of the marshy plants such as cattails and iris.

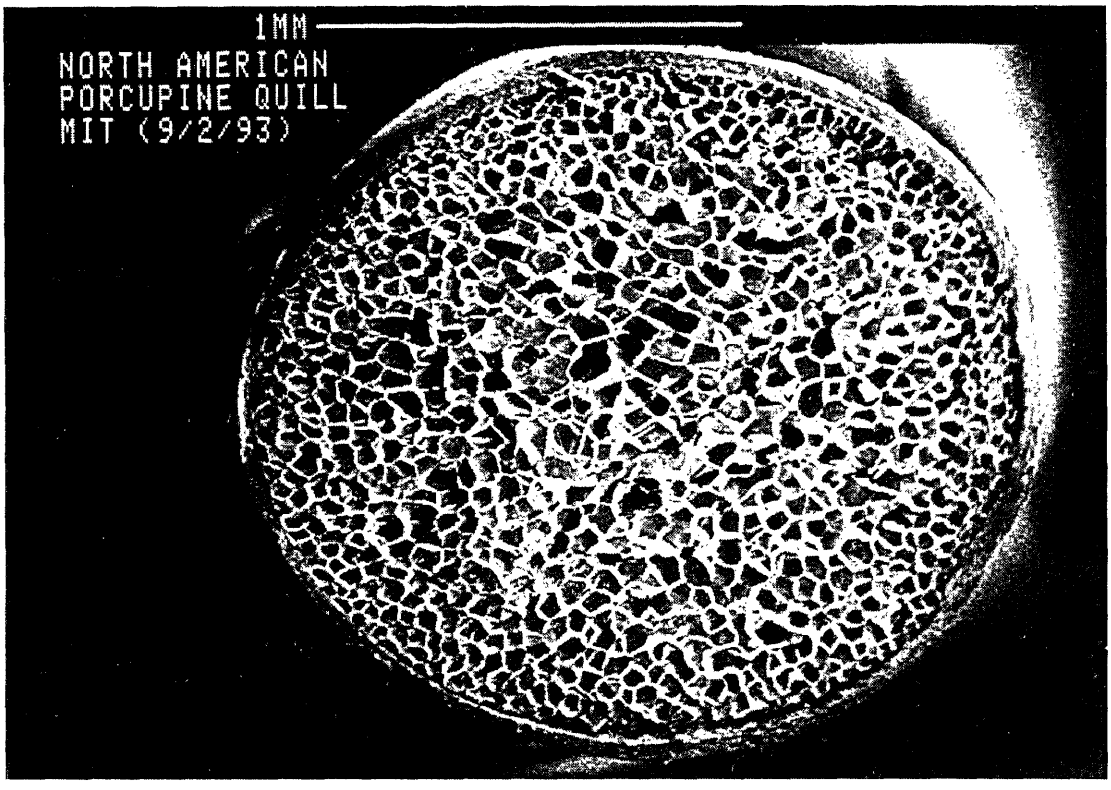

Figure 1.1: North American porcupine quill cross section [4]

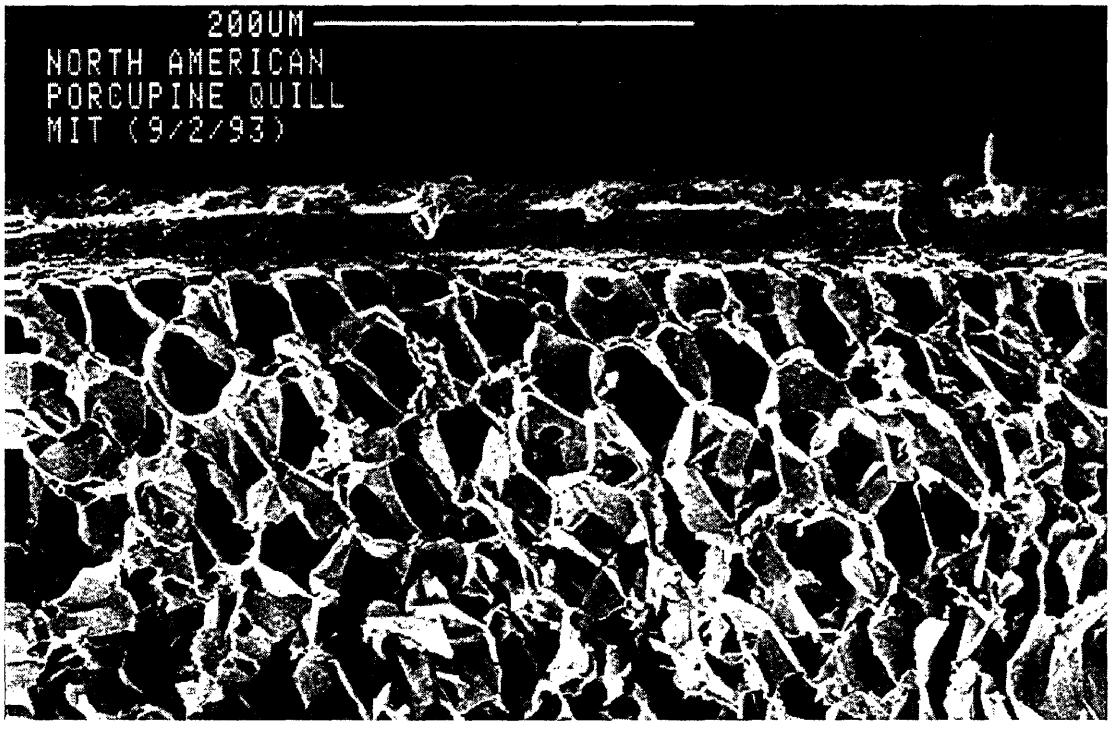

Figure 1.2: North American porcupine quill cross section: detail [4]

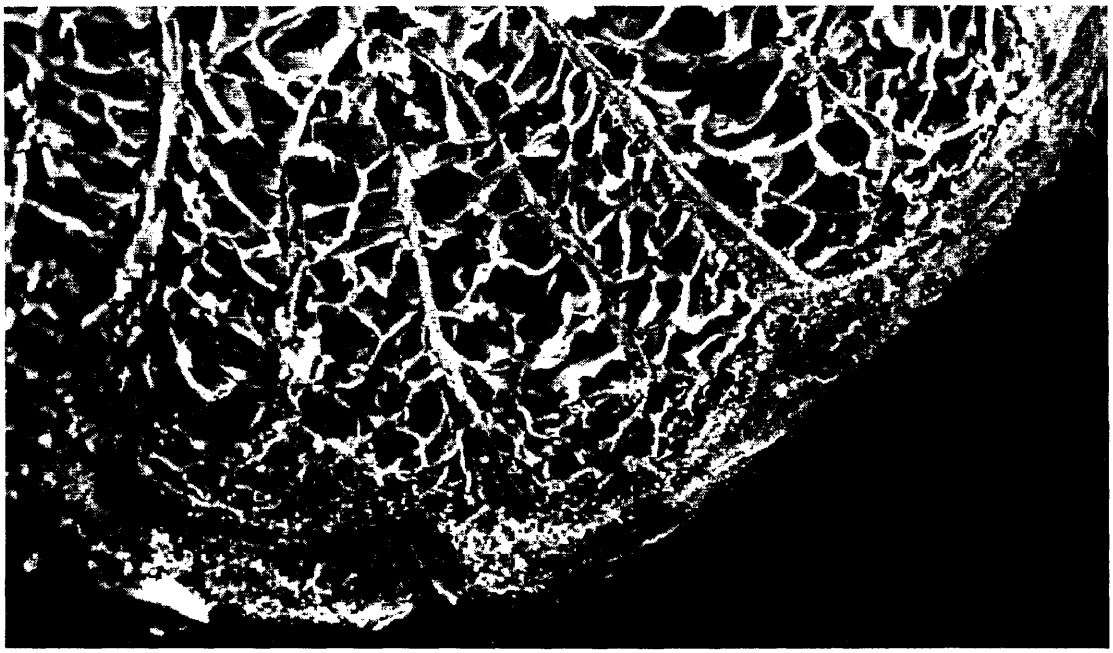

Figure 1.3: Old World porcupine quill cross section: detail [1]

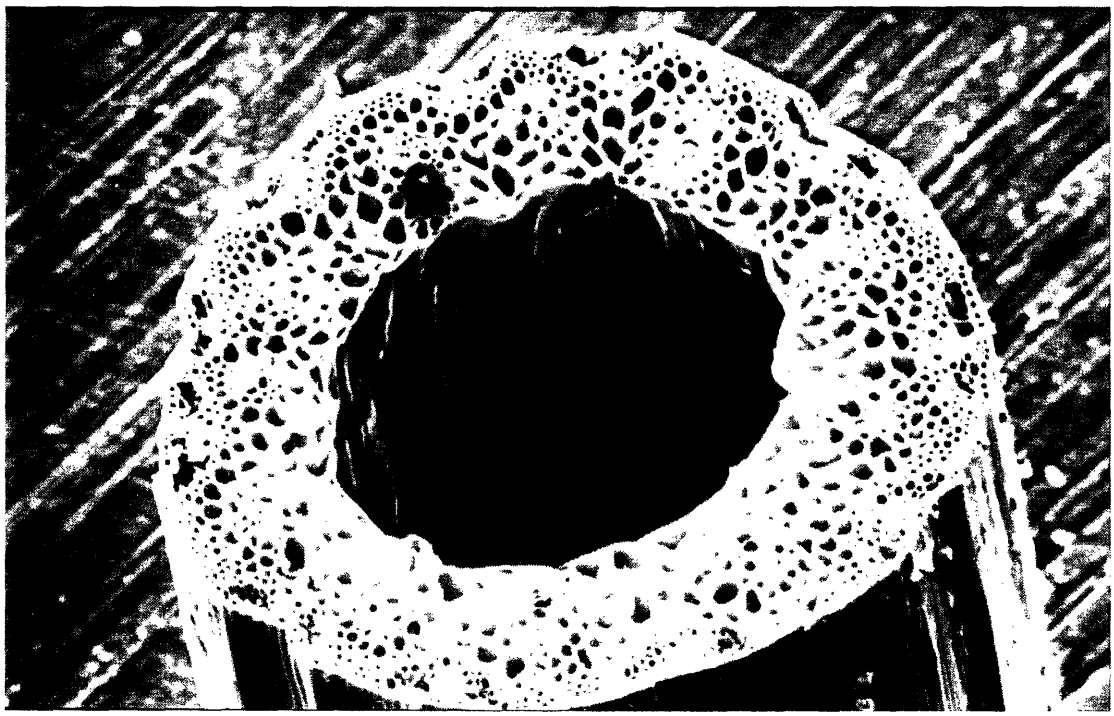

Figure 1.4: Grass stem cross section [4].

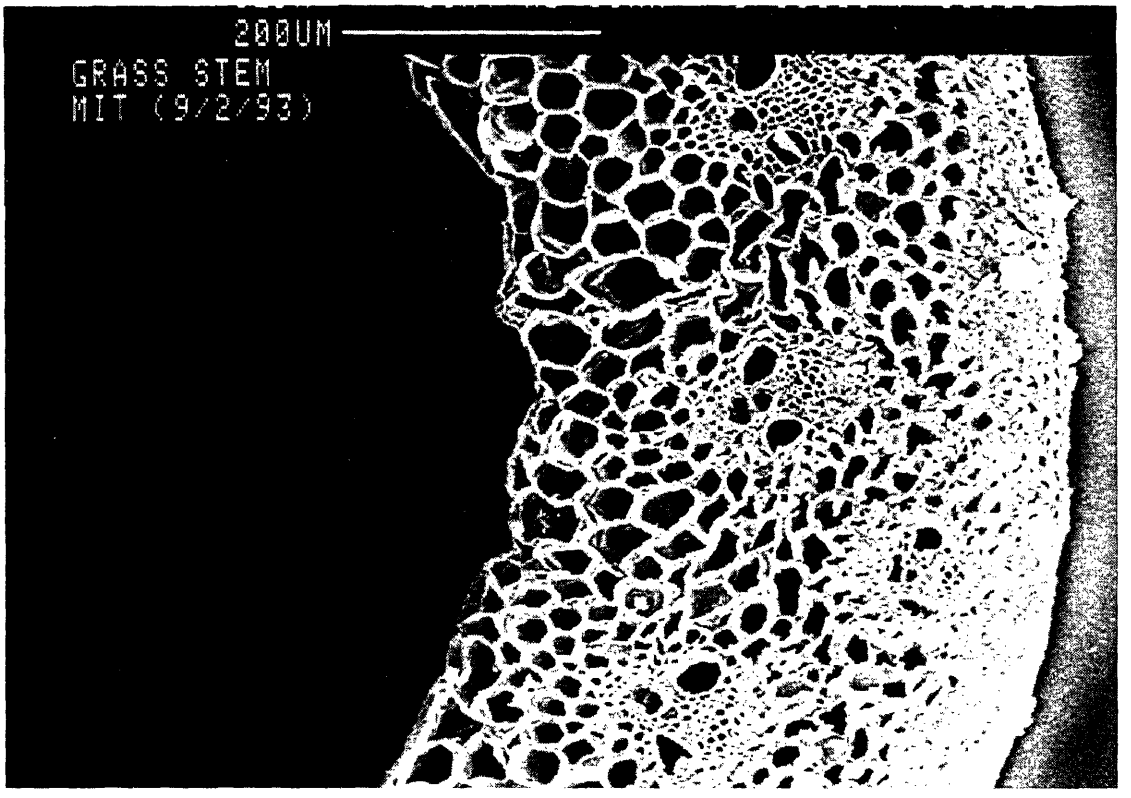

Figure 1.5: Grass stem cross section: detail [4].

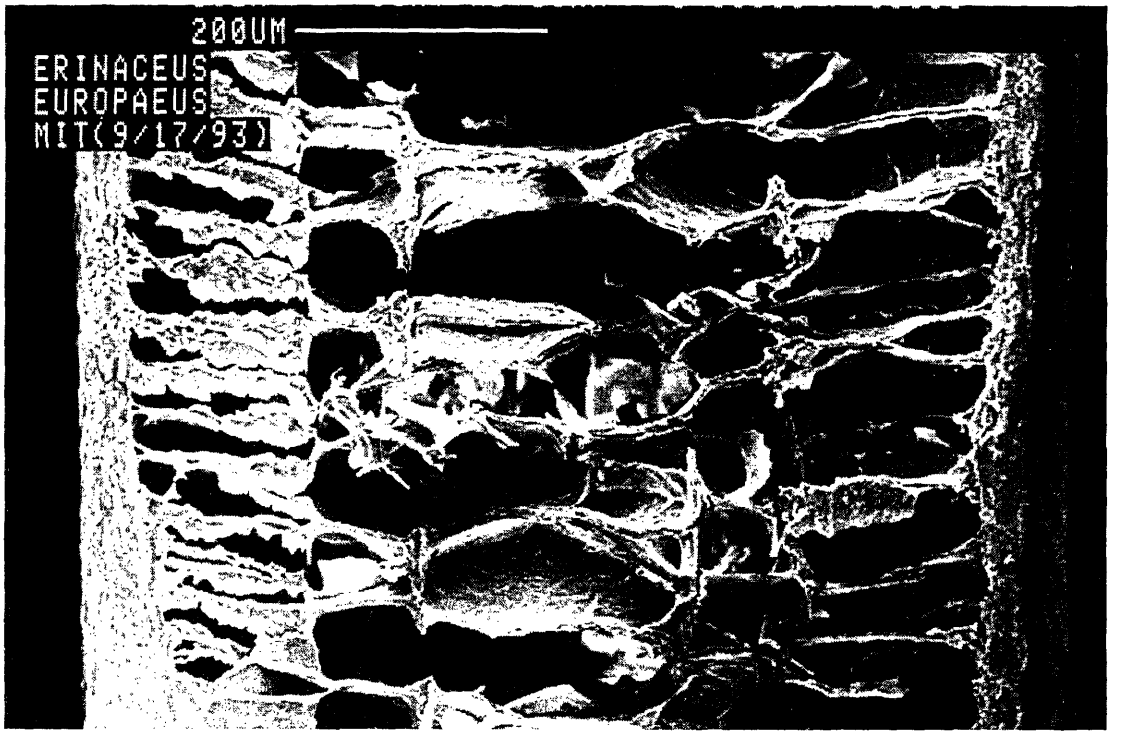

Figure 1.6: Hedgehog spine longitudinal section [4].

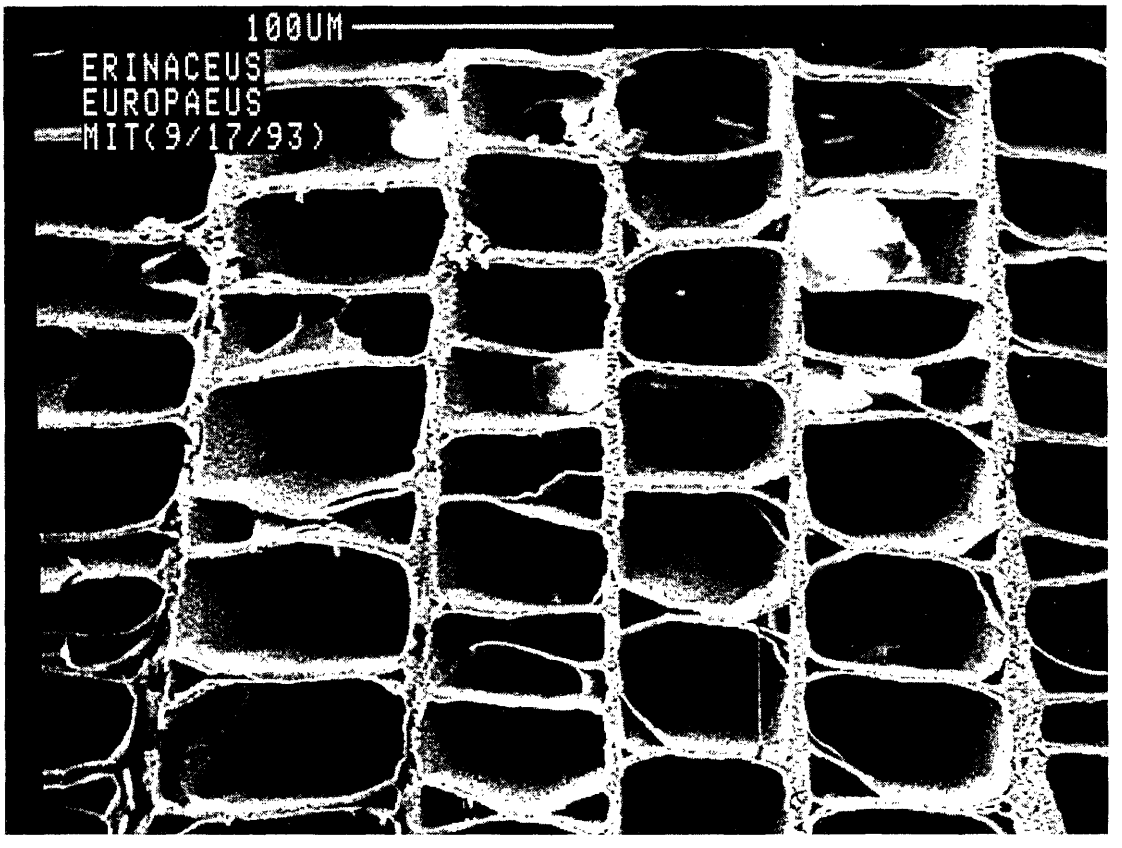

Figure 1.7: Hedgehog spine longitudinal section: detail [4].

In the early 16th century, Leonardo da Vinci was writing: "*Observe the Nature and learn from Her.. No action of the Nature can be made in a more efficient way with the same resources*. (Code Arundel)". Natural structures are the result of years of evolution and, consequently, are often optimized. Analyses of the mechanical behavior of the compliant core natural shells ([1]- [5]) showed that in all cases, the structures are loaded by some combination of bending and axial load and that the compliant core, acting as an elastic foundation, increases the resistance to local buckling. As result, for a given buckling resistance, the weight of the structure, and therefore the total biomass, is reduced respect to a hollow shell [1]. It is remarkable that the shells represented in Figures 1.1-1.7 have an outer radius, R, $0.5 \leq R \leq 1$ mm, and wall thickness, t, $t \approx 40\,\mu m \Rightarrow 15 \leq R/t \leq 25$ [1]. These natural cylindrical shells are therefore small on the absolute scale, but characterized by relatively large values of R/t.

1.1.3 Biomimicking of Natural Cylindrical Tubes

In the previous section, we have seen that some natural cylindrical tubular structures, subjected to combined axial and bending load, present a light, compliant core with a microstructure that resembles that of honeycomb or foam. We have also seen that these natural shells are small in dimension but characterized by relatively large values of the shape factor. Conversely, engineering tubular structures with large shape factors using stringers and ribs are characterized by large diameters. Biomimicking of natural constructions can therefore offer the possibility for the design of small diameter tubular engineering structures that are more efficient and lighter than ones existing today [4]. Natural constructions can be replicated using a foam or honeycomb core joined to a solid outer layer (see Figure 1.8).

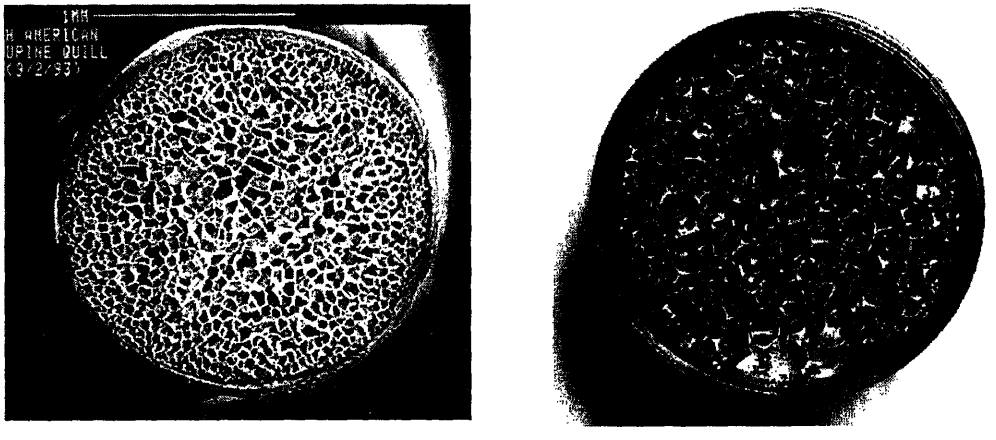

Figure 1.8: Biomimicking natural tubular structure [4]-[6].

The objective of this thesis is to analyze the performance, the manufacturability, and viability of load-bearing tubular structures employing cellular metals, in view of their commercialization. Chapter 1 reviews the current methods to manufacture cellular metals and conventional joining techniques, which are feasible for compound structures integrating aluminum foam and honeycomb. Chapter 2 examines the viability of metal compliant core shells in terms of their technical attributes, cost, and risk of investment. In Chapter 3, we compare the design of a sailboat mast incorporating cellular metals to current mast designs. Chapter 4 describes the business plan of a company producing cellular metal sailboat masts. In Chapter 5, the conclusions of this work are summarized.

1.2 Current Technology: Aluminum Foam Manufacturing Methods

1.2.1 Production Methods Overview

In this section, we describe the manufacturing methods to produce cellular aluminum foams. Metal foams were for the first time obtained by B. Sosnik in 1948 [7]: the method he used was based on adding a volatile phase, e.g. mercury, to the metal to be foamed, e.g. aluminum, inside a pressure vessel, melting the metal and suddenly reducing the pressure to allow foaming [7]. Metal foams produced in this way were expensive, irregular and, more important, contained traces of toxic metals. After then, many advances have been made and today several techniques are known for producing metal foam [8] (see Figure 1.9). Although the foaming always takes place in the liquid phase, Ashby *et al.* distinguished four major manufacturing routes, each corresponding to different initial states of the metal to be foamed: liquid metal, powder metal, metal vapor and metal ion solution [9]; of these, only the first two find commercial application and are represented in Figure 1.9.

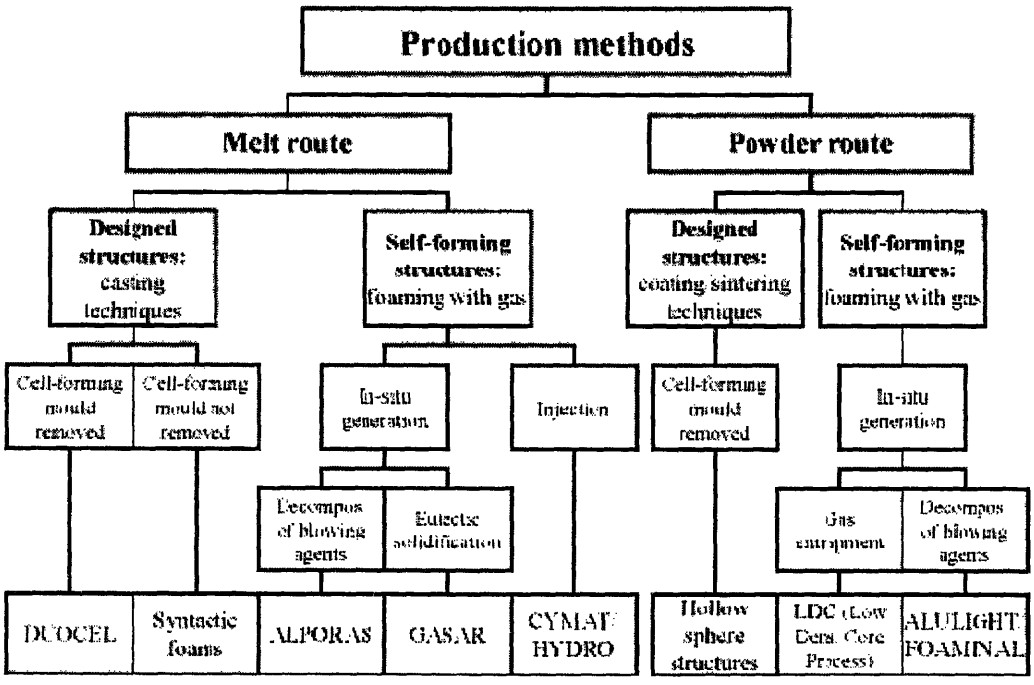

Figure 1.9: A taxonomy of metal foam manufacturing processes [10].

A second level of classification is the strategy to generate porosity (see Figure 1.9): self-formation or pre-design [10]. The former includes all the methods in which the porosity is obtained through the nucleation and subsequent growth of gas bubbles; foams produced in this way have a stochastic structure [11]. In the latter, the resulting structure is determined by a cell-forming mold [10]. The third level of classification is the gas source used to create porosity: foaming can be obtained injecting a gas or by the decomposition of gas releasing particles [12]. All the techniques represented in Figure 1.9 are suitable for aluminum, but only four have reached the commercial state. They have taken a commercial name, given by the manufacturer, i.e. CYMAT, ALPORAS, DUOCEL, and ALULIGHT/FOAMINAL. In the following, these production methods are discussed in more detail.

1.2.2 CYMAT

In the CYMAT process, aluminum foam is produced injecting gas in the melt metal [13] (see Figure 1.10). One of the problems of this approach is that normally the gas bubbles injected in the melt would tend naturally to rise to the surface and to escape [14]. The gaseous bubbles can be retained increasing the viscosity of the metal. In the CYMAT approach [13], a dispersion of finely grinded particles of a refractory, generally silicon carbide is added to the melt. Good viscosities are obtained adding 5-15% by volume fraction of SiC particles smaller than 20 μm [13]. Gas is then added to the melt using a rotating impeller (see Figure 1.10) and a liquid foam forms at the surface.

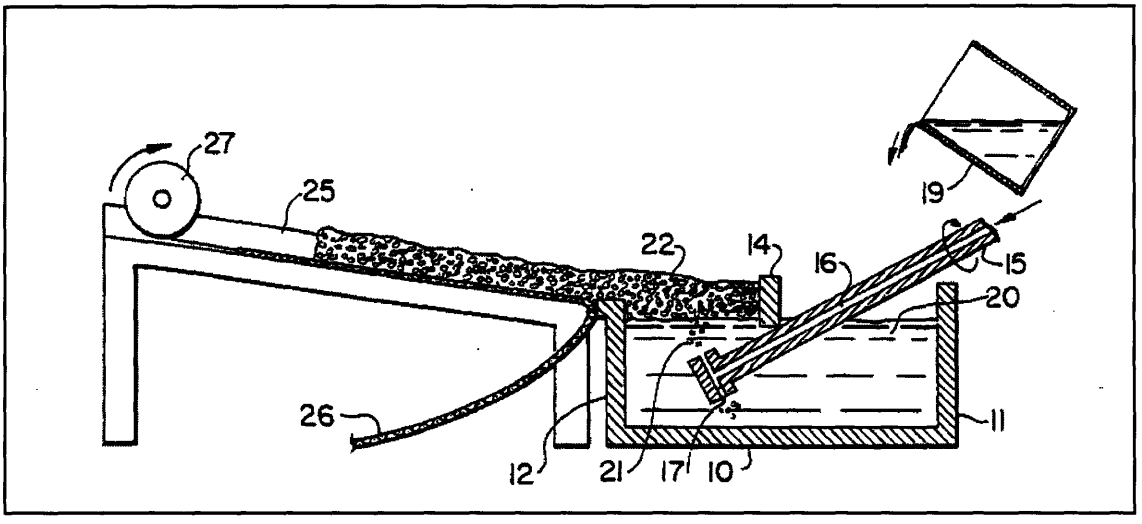

Figure 1.10: Schematic illustration of the CYMAT process [13]

The foam liquid is then cooled below the liquidus temperature of the melt and solidified. There are several options for this step. In the method represented in Figure 1.10, the foam is drawn off the liquid surface with a conveyor belt. The most successful variant consists of pulling off the foam from the surface of the molten metal vertically using a pair of moving belts [15]: this has the advantage to reduce the effect of the gravity during the drainage of the foam [14]. Other methods can be found in literature [16-18]. Advantages of the CYMAT process are represented by the low cost and simplicity of production, low cost starting material (recycled MMC scrap), economy of scale and good density control [8]. The main disadvantage of this method is that only a relatively small number of large bubbles is generated, which leads to rather coarse and irregular shaped pore distribution [10] (see Figure 1.11). In the next section, we describe a technique in which a large number of gaseous bubbles are created by the thermal decomposition of solid ingredient.

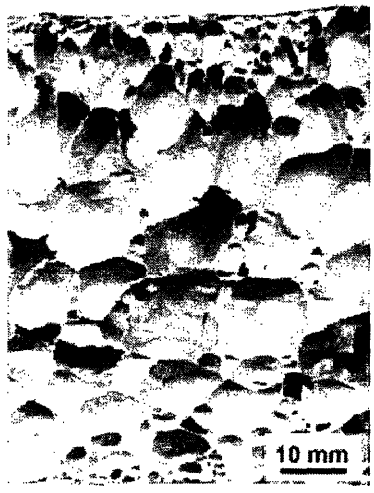

Figure 1.11: Foam produced by the CYMAT process [19]

1.2.3 ALPORAS

Shinko Wire Company, Ltd. Japan attempted another approach to foam metal melts [20]. Rather than inject gas into the molten metal, a blowing agent is added, typically titanium hydride (TiH_2) [20]. The blowing agent is stable at room temperature, but when heated up, it decomposes, releasing gas which propels the foaming process (see Figure 1.12) [21].

The advantage of using a solid foaming agent is that it is possible to disperse the gas more uniformly throughout the melt [22]. The result is that the microstructure of this foam, which is commercialized with the trade name of ALPORAS, is very homogeneous (see Figure 1.13). One disadvantage of the technique is that the viscosity of the melt still needs to be adjusted and this is usually done by adding 1.5% by volume of Calcium [22], which is toxic. Another limit comes from the absence of economies of scale, which is inherent in the batch nature of the process. For this reason, ALPORAS foams are among the most expensive in the marketplace.

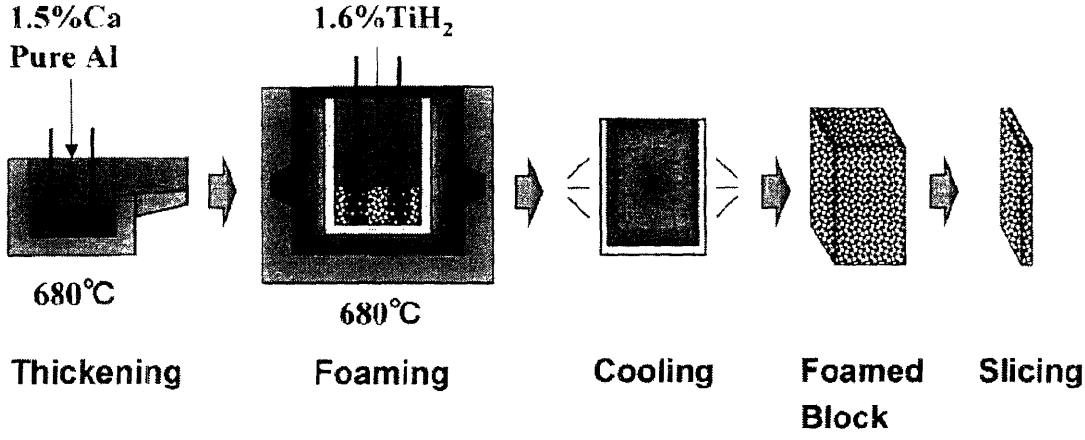

Figure 1.12: Schematic illustration of the ALPORAS process [22].

Figure 1.13: Foam produced by the ALPORAS process [14]

1.2.4 ALULIGHT/FOAMINAL

In this section, we discuss the powder-metallurgical route to produce metal foams following the process invented and patented at the Fraunhofer-Institute, Germany by Baumeister [23-24]. A schematic diagram of the process is shown in Figure 1.14.

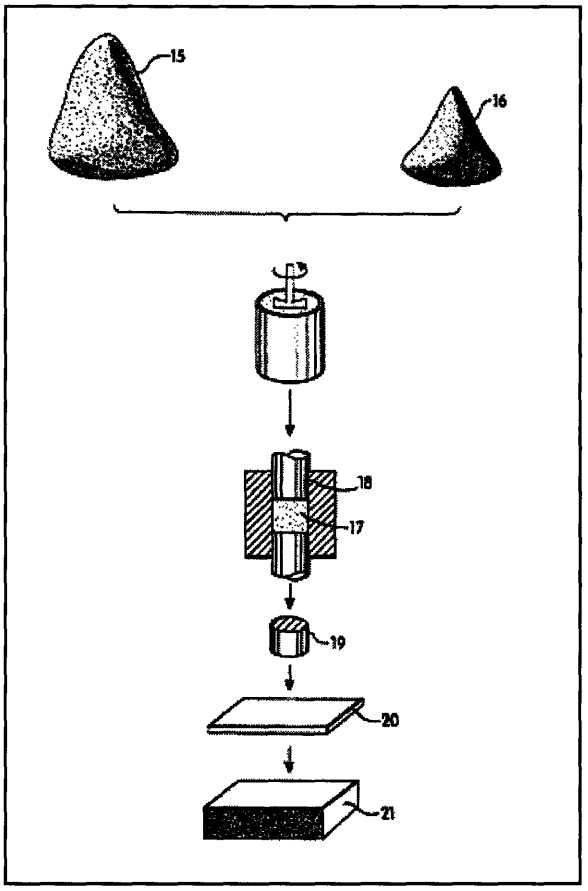

Figure 1.14: Schematic illustration of the powder compact process [24].

The most important feature of this method is that both the metal to be foamed and the foaming agent, typically titanium hydride, are introduced in the solid state as powders. The production process begins mixing the two types of powders [25]. This mix is then compacted to yield a dense semi-finished product called "foamable precursor material" [26]. In Figure 1.14, the compaction of the powder is done by axial compression, but also other methods as extrusion or powder rolling can be used [25]. At this point, the precursor can be formed or machined in the desired size and shape (number 20 in Figure 1.14) [8]. In the last step, the precursor is heated up. At 465 °C, the TiH_2 melts and the

released gas forces the material to expand creating the foam [25]. Figure 1.15 shows a typical cross section of foam obtained through the Fraunhofer process. Advantages of this technique are represented by the simplicity of the process, the extensive range of shapes and densities, which can be obtained, and the possibility to create aluminum sandwich structures (AFS) in one-step process. Disadvantages incluse the cost of the powders, size limitations, difficulties in controlling the pore size and the mechanical properties of the final component. The most commercialized foam produced with the Fraunhofer process is produced by ALULIGHT International GmbH with the trade name ALULIGHT.

Figure 1.15: Foam produced by the powder compact process [8].

1.2.5 DUOCEL

DUOCEL, produced by ERG Materials and Aerospace, Oakland, California, is the only pre-designed foam with commercial applications. Although the manufacturing method of this foam is a trade secret and no patent has ever been filed, it is generally believed [14] that DUOCEL is obtained by investment casting from a "dummy" polymer foam. A schematic description of the process is given by Ashby [9] and Banhart [9]. In first place, a polymer foam mould is selected and filled with a slurry of heat resistant material [9], e.g. plaster [8]. After curing the polymer foam is then removed and a melt metal is cast into the cavity which replicate the original polymer foam structure [8]. After solidification the mould material is removed by pressurized water and metallic open-cell foam, replicating the original polymer foam, remains [8]. Advantages of this method are

given by the high grade of regularity and reliability of the foam (see Figure 1.16), the possibility to obtain porosities as high as 98% and complex shapes. Main disadvantages are represented by the complexity of the process, the cost of the foam and obvious difficulties to scale up the process.

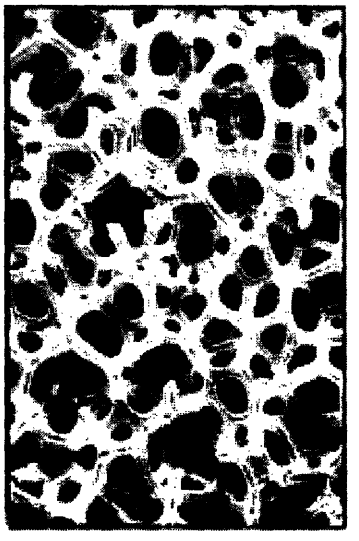

Figure 1.16: Duocell^{TM} foam produced by investment casting [8].

1.3 Current Technology: Aluminum Honeycomb Manufacturing

1.3.1 Generality

There are five methods to manufacture metal honeycomb, based on the way in which the nodes are attached [27]. These methods are resistance adhesive bonding, welding, brazing, diffusion bonding, and thermal diffusion [27]. Probably more than 95% of honeycombs are produced through adhesive bonding [27]. The limitation of adhesive bonded honeycomb is represented by the maximum temperature that it can withstand, usually 399 °C with polyimide or 204 °C with nylon epoxy and nitrile phenolic adhesives [27]. When higher operational temperatures or severe environmental conditions are required, cores can be manufactured using resistance welding, brazing, or diffusion bonding, even though these processes are more expensive than adhesive bonding [27].

There are two basic techniques to convert a sheet of metal into honeycomb: the expansion process and the corrugation process.

1.3.2 Expansion process

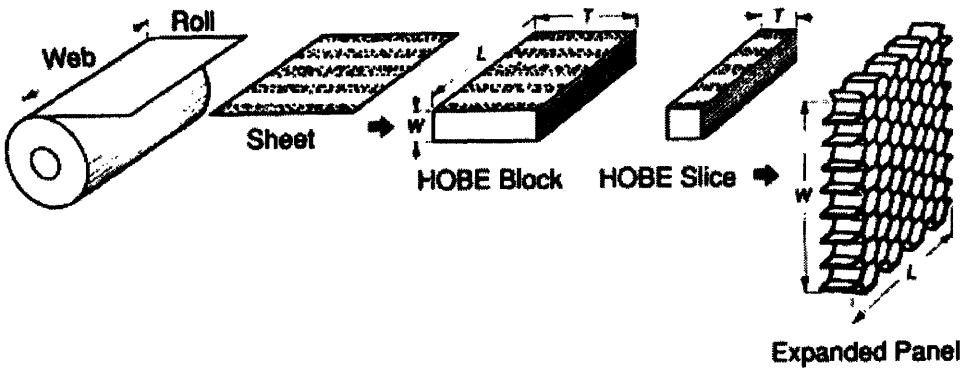

Figure 1.17: Expansion manufacturing process [27]

The majority of the adhesive bonded cores are made by the expansion process shown in Figure 1.17. At first, a corrosion resistant coating is applied to the foil sheets and

adhesive lines are printed. After the sheets are cut and stacked one upon the other. The HOBE is brought to the autoclave, where the adhesive is cured under high temperature and pressure. Then the HOBE is cut into slices of the required thickness and expanded: when the metallic cores are expanded, the sheets yield plastically at the node-free wall joints and thereby retain their expanded geometric shape [27].

The method described is working for metallic honeycomb; for non-metallic honeycomb, like the Nomex^{TM}, the process is a little different. Here is enough to say that the honeycomb after the expansion has to be held in a rack. Then the honeycomb block is dipped in liquid resin and oven cured [27].

1.3.3 Corrugation process

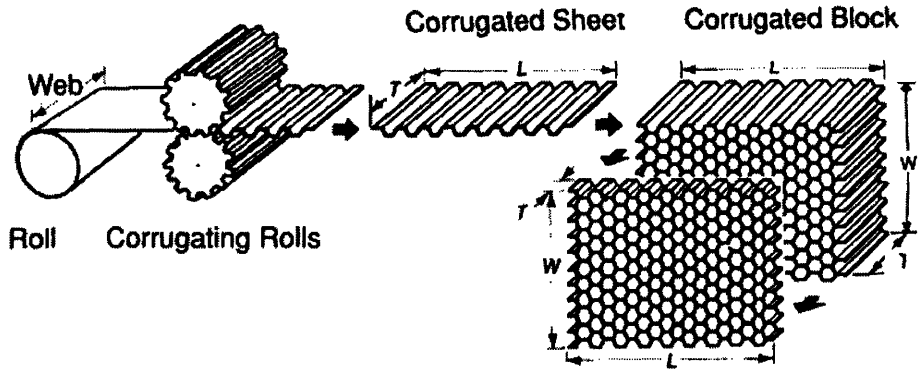

Figure 1.18: Corrugation manufacturing process [27].

The corrugation method, invented by Hexcel, was the first used to produce aluminum honeycomb. This system is still used today to produce high-density metallic cores, even though is expensive [27].

The method is shown in Figure 1.18. In the process, the sheets are first corrugated and adhesive is placed at the nodes (now this is done automatically). Then the sheet are piled up and cured in the oven. As the sheets cannot be compressed much during the curing, a thick layer of adhesive is required. Generally the quantity of adhesive needed in the corrugation process can be ten times that needed in the expansion manufacturing process.

Brazing, diffusion bonding or spot-welding are just different variants of the corrugation process, in which the nodes are welded instead to being adhesively bonded. Corrugated aluminum honeycomb is made because above 12 pcf it becomes impossible to expand the HOBE. In Figure 1.19 are represented the most common cell configurations manufactured [27].

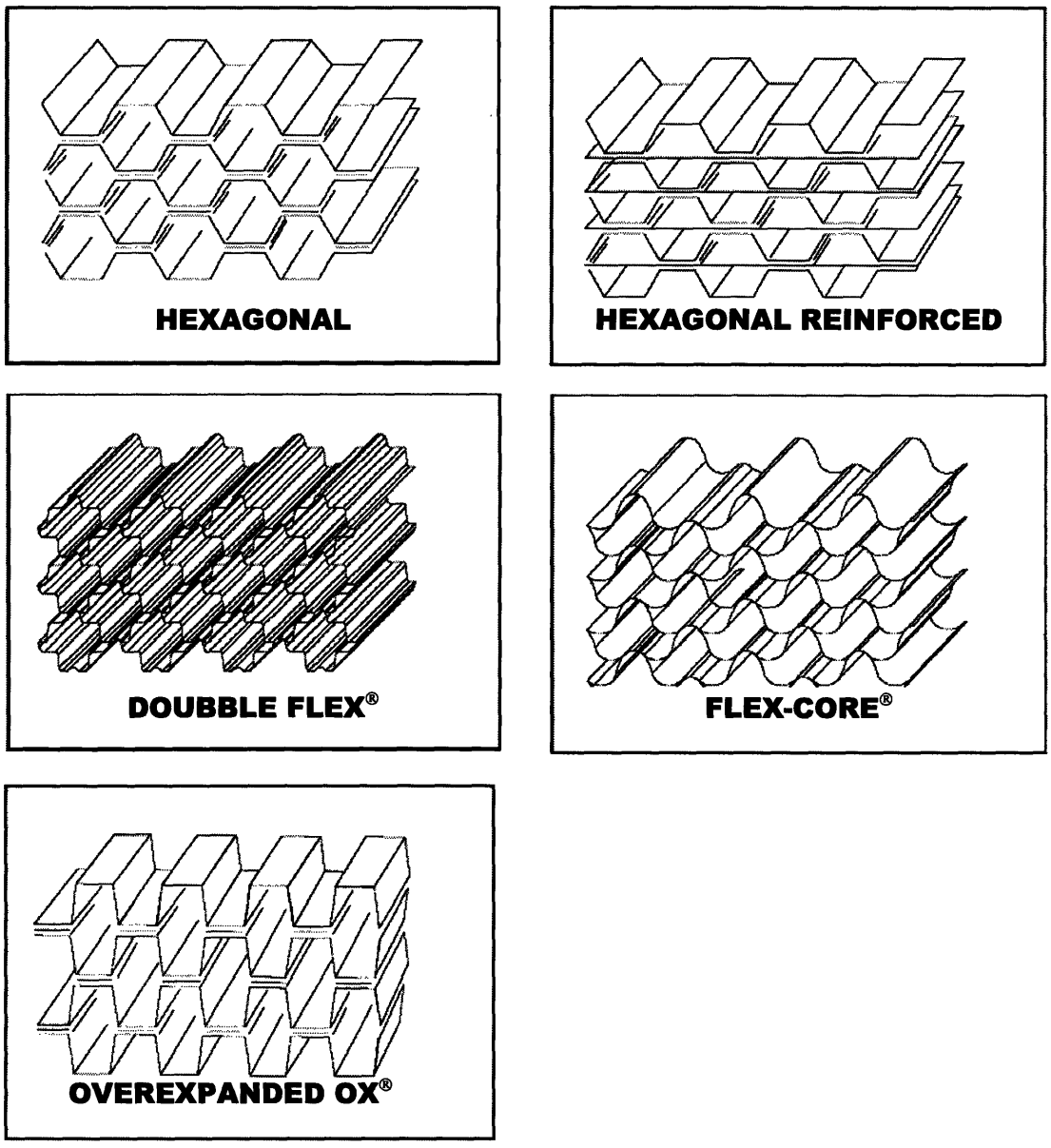

Figure 1.19: Principal honeycomb cell configurations (elaborated from [28])

1.4 Current Technology: Bond Technologies for Aluminum Foam Sandwich Structures

1.4.1 Introduction to Aluminum foam sandwich structures

For structural applications metal foam has to be used in combination with conventional dense metal structures, such as sheets, tubes or more complex-shaped hollow structures: this allows for optimized mechanical properties in a given situation.

Aluminum foam sandwich (AFS) panels can be produced very elegantly by roll-cladding face sheets to a sheet of foamable precursor material, then creating the desiderated shape in an optional working step, and finally foaming the entire composite [29] (Fraunhofer process). Foaming will create a highly porous core structure without melting the face sheets if the melting points of the foam and the face sheets are different and the process parameters are chosen appropriately.

One consequence of the production process for aluminum foam sandwich panels (AFS) as described is that the performance of the sandwich is not as good as its components will allow [30]. For the precursor to foam, the sandwich panel must be heated close to the melting point of the precursor alloy. To keep the facings intact, the melting point of the foam alloy must be kept low. This is generally achieved by using an alloy with high (7 - 12%) Si content. These alloys have mechanical properties that are considerably less than typical aluminum alloys. In addition, the alloy used for the facings cannot be dependent on heat treatment for its properties, due to the high foaming temperature. Another limitation is represented by substantial cost of the powders. As a result, aluminum foam sandwich panels produced through the Fraunhofer process present modest mechanical properties and utility compared to the panels produced by joining facings and core after foaming. In this report an overview of feasible conventional joining technologies between metal foams and sheets is presented.

1.4.2 Feasible Al-foam Al-sheet Joining Technologies

1.4.2.1. Mechanical fastening elements

Foams have a cellular structure resembling, in some ways, that of wood. Because of this, foam sandwich panels can be developed in ways similar to wood sandwich panels: in particular using mechanical fastening elements [9]. There are many mechanical fastening elements available, ranging from hollow spheres- to metal-plugs, as well as nails, screws and rivets, even though experiments show that there are only a few suitable technologies in which the strength of the joint is approximately the strength of the applied cellular material [31]. In general, fasteners using not only a frictional-, but a form-fitting mechanism as well are preferred: for this reason screws and blind rivets are preferred to nails [31]. Other solutions, like the integration of screw sockets into the foam structure have proved to be not viable, especially in light of cost considerations [32]. Mechanical fastening elements although cost attractive, are strongly limited by the non-uniform distribution of the stress inside the structure and the additional space required [32].

1.4.2.2 Gluing

Adhesive bonding is the most obvious and straightforward technology that can be used to produce AFS structures [33]. Epoxy-based systems curing at 180 °C for 30 minutes are available as conventional glues or as expanding glues, which are very convenient for bridging high tolerances and for integrating foam bodies into hollow extruded profiles [31]. The joining is caused by adhesive forces between the surface of the substrate and the glue: consequently, well-glued sample should not fail at the interface, as the adhesive forces caused by ionic bonding or polar interactions should be higher than the cohesive forces in the glue or the substrate [33]. When the foam does not present casting skin, joining is still possible, even though a greater consumption of adhesive is to be expected (weight increase, cost) because of the significantly enlarged surface area [31]. Other drawbacks of the technique are low thermal stability, mismatch of expansion coefficient and the possible creation of thermal and electrical isolation barrier [9].

1.4.2.3 Welding

Welding processes that have been shown suitable for joining aluminum foams are laser-beam welding [34] and ultrasonic welding [35].

In *laser-beam welding* the sheet material and the underlying foam structure are melted by the heat input of the laser and the metallic connection is created when the material re-solidifies [34]. Advantages of this technique are represented by the high welding speed, the keyhole effect and the locally limited energy input [36]. This feature in particular makes laser welding particularly attractive to join cellular metal, because unlike other systems, e.g. TIG, large collapse of the cellular structure is avoided. However early experiments at the Laser Zentrum in Hannover [37] showed that in applying laser welding to cellular metals special care is needed: in fact, the molten material can flow into the foam cells, filling them partially and a seam groove can form. Solutions to this problem using different types of filler materials and modifying the process parameters are know [34], but control of the technique is still complex [31].

In the *ultrasonic welding* system an ultrasonic generator, a converter and a booster convert the main voltage into high frequency mechanical oscillation [35]. The actual bonding of the joining partners takes place through the transfer of this high frequency shear oscillation via the connecting surface of the welding tool into the sheet material [35]. At the same time a static pressure, perpendicular to the oscillation direction, is brought up [35]. A characteristic of the ultrasonic welding process is that it is a joining process in the solid state based on friction and consequently not a real welding process, where both joining partners are transferred into the liquid state for joining [31]. In comparison to other joining techniques, ultrasonic spot welding is characterized by low energy input, short welding times, < 3 s, as well as relatively low welding temperatures, $<$ 300 °C and by allowing the joining without causing significant damage or deformation in the joining partners [38]. To realize ultrasonic roll seam welding of sheet material with Al-Foams it is necessary to insert more energy in the bonding zone [38]. As a consequence higher temperatures, up to 650 °C, melting of the aluminum joining partners and local deformations occur in the bonding zone [38]. Thus to realize roll seam welding appears to be more difficult than spot welding [38].

1.4.2.4 Soldering and Brazing

Soldering and brazing of aluminum foams is impeded by their oxide layer, which has to be removed before and during the soldering process [31]. The oxide layer can be removed in two ways: one is mechanical destruction by scratching, brushing, or ultrasonic vibration; the other is the application of a flux [31]. The latter causes serious corrosion problems if it is not removed properly [31]. In consequence, the joint requires good accessibility so that the flux can be washed out after the soldering process. This makes soldering with flux unsuitable for sheet-foam composites [31], where a connection along the whole surface is desired. When removing the oxide layer mechanically, the use of foam with a casting skin is advantageous, as the oxide layer is easier to remove [31].

Soldering

The S-bond ™ is special alloy, developed by Euromat, to solder light alloys, that can be implemented in air, without fluxing agents and at relative low temperatures (far from the melting point of the joining partners) [39]. The S-bond ™ alloy can be divided in two categories: the Sn-based solders with a melting point from 208 to 238 °C and the Zn-based solders with a melting point from 380-426 °C. Other alloy components are Titanium, in which finely distributed inter-metallic phases lead to a strength increase; Silver and/or Copper, which are present to reduce the surface tension of the liquid solder; Gallium, which enhances the wetting of the metallic base solder. The S-bond process consists of different phases. In the first step, the solder alloy is deposited on the bonding surfaces of both the partners and the temperature is raised to the soldering point. Secondly, the two soldering surfaces are brought together and through relative movement of the two parts, the oxide film present between the melt solder and the metal is broken. The oxides on the substrate material are also partially broken during the process, so that a metallurgical interaction can take place. As relative movement between parts is necessary during soldering with a flux-free soldering, both surfaces have to be as plane as possible, so that the wetting of the substrate can take place everywhere. Alternatively, the oxide film could be broken with ultrasonic waves with a frequency of 60 kHz and amplitude of 2μm. The latter system could be particularly effective in a fully automatic production line. If there is not a casting skin, the solder flows into the pores, but in contrast to glued

samples does not form a material-fitting joint with cell walls, as the oxide layer of the molten solder in the pores can not be torn properly during the relative movement of the parts. Consequently, the remaining joining area would be limited to the number of the present cell edges, which would result in a reduced strength of the structure. The technique is already well established for graphite-foam Al-sheet joining. Although flux-free soldering technology can be transferred to aluminum foams, corrosion preventing measures have to be taken as the Sn- and Zn-based alloys can cause corrosion problems in combination with aluminum.

Brazing

Brazing (T>450°C) is a feasible joining process for aluminum foams [40]. Although non-corrosive fluxes are available for brazing, it advisable to coat the structure to protect it from humidity. The brazes are preferably Al-based and the furnace atmosphere should be inert. An alternative is the use of a porous filler material, which expands during the brazing process. This prevents a sudden change in porosity from foam to bulk. The working temperature of the filler material has to be low enough that the porous base material does not deform during the expansion of the filler material. Although this process has not been treated deeply in the literature, it is known that aerospace companies have incorporated aluminum foam into sandwich panels by using it. A current project at the University of Erlagen, is investigating the fundamentals of brazing techniques, first for flat and later for formed compounds with emphasis to the selection of suitable brazing materials and joining partners under consideration of different process parameters as, for example, temperature, hold time and surface preparation.

1.4.2.5 Transient Liquid Phase (TLP) bonding

In the transient liquid bonding (TLP) the Al-foam and the Al-sheet are joined together by sandwiching a thin layer of melting point depressant between them (in general a Cu-based alloy) and heating [41]. If the right interlayer material and conditions are chosen, we can heat the assembly to a temperature at which the bulk remains solid and where a region exists near the interface which is initially liquid but subsequently undergoes isothermal solidification. TLP bonding has a number of advantages over other joining

processes, combining positive aspects of both liquid and solid state techniques. For example, the presence of a liquid phase (in which solute can diffuse much more quickly than in solid material) means that joints can be produced without the imposition of any external pressure, as capillary forces will naturally cause the liquid to flow and eliminate interfacial porosity. On the other hand, it shares with solid-state techniques the advantages afforded by low processing temperatures and homogenous compositions near the joint. These factors mean that properties such as strength and re-melting temperature can approach those of the parent material.

Despite these advantages, the time required to join Al-foam and Al-sheet using this technique is considerable. As a consequence, TLP is not a valid alternative for large production of AFS panels.

1.4.2.6 Nickel Plating and Brazing

Soldering and brazing of aluminum foam is a feasible process, but at the current stage of the technology not commercially attractive because of their limitations and high costs.

An alternative approach for brazing aluminum solid metal with foam is to first nickel-plate the foam and then braze it with the foil using conventional fluxes, which solidify to produce a phase between the two brazing mates that is stronger than the foam itself. Such approaches are commercially available. The aluminum oxide film is removed prior to plating by a special pre-plating procedure called zincating. The nickel deposit acts as an impermeable layer, protecting the foam from erosion and has a positive effect in the brazing process, because of its excellent wetting properties, in particular short wetting time, good capillarity penetration, and "spreadability". Using this method, aluminum foams and solid metals can be brazed quickly, reliably and at low costs. The quality of the joints produced using this technique is currently under investigation by the present author.

1.4.3. Shear Testing on Foam-Sheet Joints

The quality of a joint is characterized mainly by its load-carrying capability. For this reason some of the joining technologies discussed above have been tried in quasi-static shear tests ([31-32] and [42]). Table 1.1 lists the materials used in the tests. Table 1.2 lists the investigated technologies.

Sheet Materials	**Core**
Al-alloy	*Al-foam*
AA6182 – t=1.3 mm	Powder metallurgically produced Alloy: AA6016 – Density = 0.3 g/cm^3

Table 1.1: Applied sheet and foam materials [31].

Type of the joint	**Mechanical**	**Metallurgical**	**Adhesive**
Joining Technology	Riveting/ Screwing	Laser beam welding/ Flux-free soldering	1C-Glue Expanding Glue
Formation of the Joint	Point contact	Line/Area contact	Area contact
Process conditions	All blind rivets: Ø = 6.4 mm Self tapping screw: M6;	Welding: 2.5 m/min; 2.5kW Soldering: 250°C- 15 min	Curing: 180 °C 30 min
Joining class	Mechanical	Thermal	Adhesive

Table 1.2: Investigated joining technologies[32].

Figure 1.20 shows a sketch of the test. The test consists in finding the load-deformation behavior of the specimen up to failure of the joint. The maximum theoretical shear stress is then defined by

$$\tau_{th,\max} = \frac{F_{\max}}{A_{th}}; \quad (1.3)$$

where $F_{\max}$ is the maximum applied load and $A_{th} = m \times n$ is the theoretical contact area (see Figure 1.20), which is the same in all cases considered.

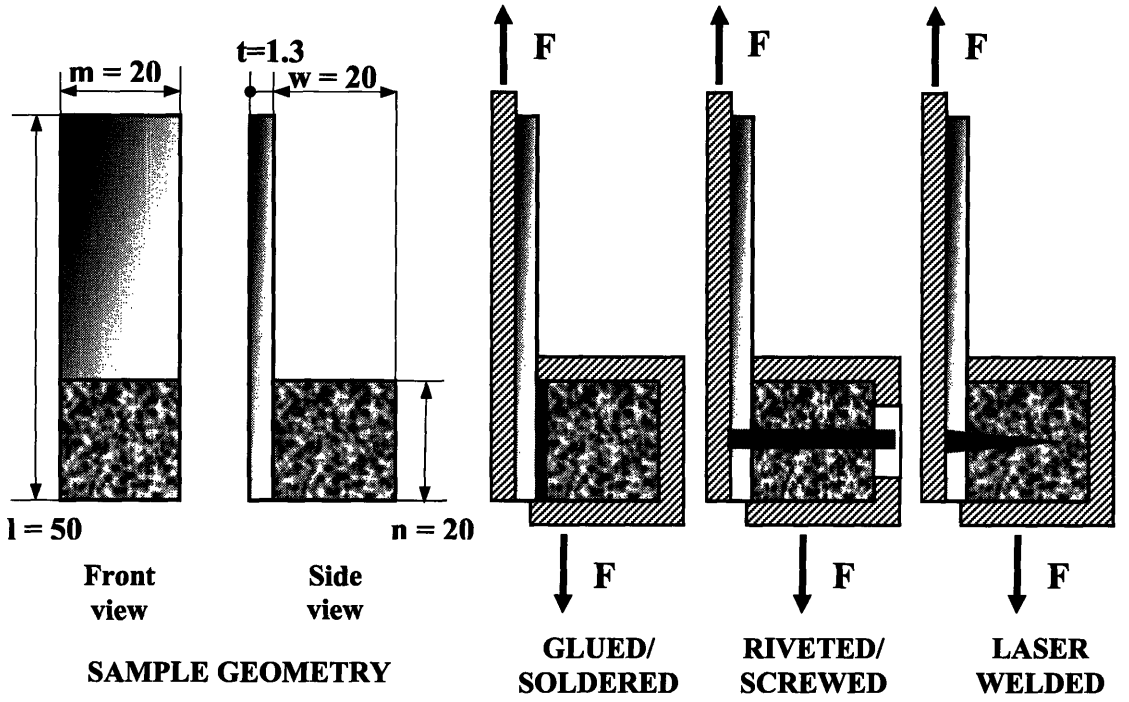

Figure 1.20: Geometry of the samples for the shear test. All the dimensions are in millimeters. The testing speed was 5mm/min. The Al facing is bonded to a sheet plate. The foam block is encapsulated in a steel box (elaborated from [31]).

The maximum shear stress allowed by the sandwich structure as a function of the joining technology, is summarized in Table 1.3.

Joining method	F_{max} (N)	$\tau_{th,max}$ (MPa)
Riveting	997 ± 91	2.5 ± 0.2
Screwing	1282 ± 130	3.2 ± 0.3
Laser-beam welding (1 seam weld)	580 ± 116	1.3 ± 0.3
Gluing	2043 ± 220	5.1 ± 0.6
Flux-Free Soldering	2112 ± 596	5.3 ± 1.5

Table 1.3: Influence of the joining technology on the theoretical maximum tensile shear stress in quasi-static loading [31].

The real contact area between the foam and the sheet, A, in point- and line-contact joining technologies (see Table 1.2) is much less than the one in area-contact welding.

Assessment of the actual contact area A for laser-beam welded samples [33] (defined as the width of the welding seam at the lower side of the sheet multiplied by the length of the seam) showed that the actual maximum shear stress is about $\tau_{act,\max} = F_{\max}/A = 4.3$ MPa. Similar assessments for riveted and screwed sample are difficult: the problem lies in the different mechanism of failure [31]. Area- and line-contact joints fail in the foam close to the joining zone [31]. Rivets and screws fail by foam break in the core [31].
The porosity of the foam influences significantly the behavior under shear loading. Based on regression of experimental data, Bernard [33] showed that the maximum shear strength of a laser-welded joint is related to the foam density by the approximate relation:

$$\tau_{act,\max} = C \cdot \rho_c^2; \qquad (1.4)$$

where ρ_c is the foam density and $C = 28.8 \cdot MPa \cdot cm^6 / g^2$; for $\rho_c = 2.7\, g/cm^3$ we find $\tau_{act,\max} = 210$ MPa, which is the strength of a sheet-sheet joint. Note that if $\rho_c = 0.6\, g/cm^3 \Rightarrow \tau_{act,\max} = 10.5$ MPa, but if $\rho_c = 0.15\, g/cm^3$ gives $\tau_{act,\max} = 0.6$ MPa!

1.4.4. Summary

Table 1.4 [31] gives a final overview of the mechanical properties including a technological assessment of the investigated joining technologies.

Technique	Mechanical performance	Accessibility	Costs	Recycling	Cycle time	Transferability on structural components
Mechanical Fastening	–	++	++	++	O	+
Gluing	+	O	O	O	-	++
Welding	O/+	–	–	++	++	++
Soldering	O	O	–	+	O	+
TLP	{++}	O	—	++	--	+
Ni plating + Brazing	{+}	{O}	{+}	{+}	{O}	{+}

Table 1.4: Evaluation of the investigated joining technologies [31] (++ very good, + good, O overage, - bad). Values in {} are estimated.

1.5 Current Technology: Bond Technologies for Aluminum Honeycomb Sandwich Structures

All the methods described in the last sections to join aluminum foam with aluminum sheets are feasible also to manufacture aluminum honeycomb sandwich structures. However, two techniques dominate in aluminum honeycomb fabrication: adhesive bonding and brazing. In this section, these two manufacturing systems are described.

1.5.1 Adhesive Bonding

Adhesive bonding of aluminum honeycomb and aluminum faces is straightforward: it is enough to interleave the adhesive layers between the face and the core, apply the temperature and the pressure required by the adhesive resin to cure and cool down the sandwich [43]. There are three variant of this process [44]:

1. *heated press*, used exclusively for the production of flat board or simple preformed panels (see Figure 1.21);

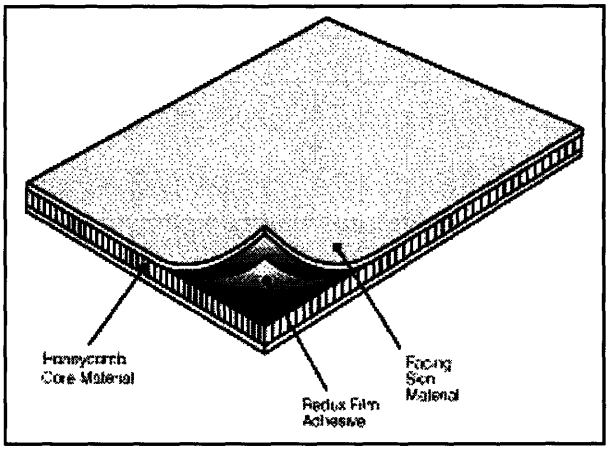

Figure 1.21: Flat sandwich panel produced by heated press [44].

2. *vacuum bag processing*, used for the manufacture of curved and complex form panel (see Figure 1.22); this technique involves the placing and sealing of a flexible bag over a composite lay-up and the subsequent evacuation of all the air from under the bag (see Figure 1.23). The curing of the panel is done in an oven

while holding it in the vacuum [27]. The pressure during the curing procedure is 0.10 MPa [27].

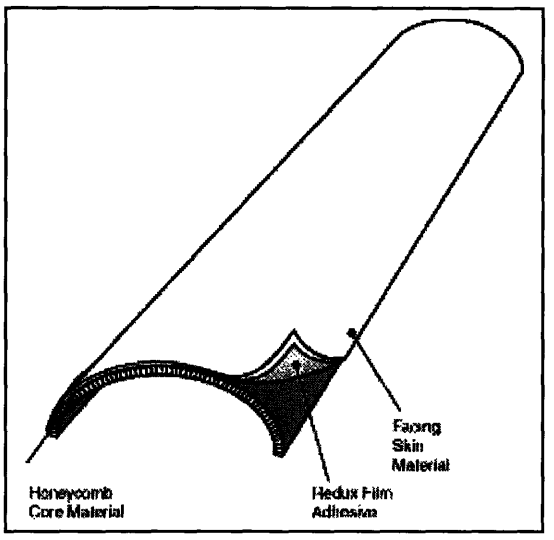

Figure 1.22: Curve sandwich panel produced by vacuum bagging or autoclave[44].

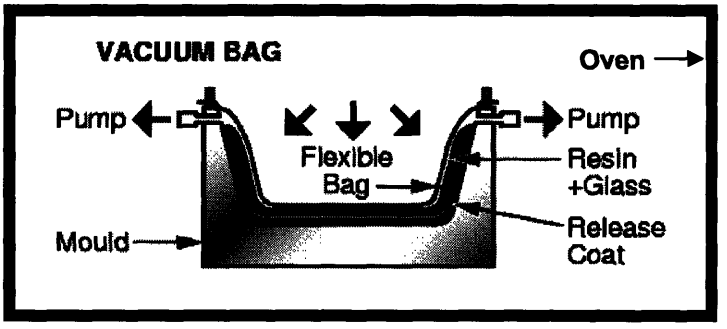

Figure 1.23: Vacuum bag system: a flexible bag is sealed over the sandwich and the vacuum is created [45].

3. *autoclaves* are also used for curved shapes and complex shapes. Figure 1.24 shows a schematic of the apparatus: in the autoclave the vacuum bag is still present, but the oven is replaced by a pressure vessel. This method allows higher cure pressures, which has a positive effect to minimize the creation of voids in the resin and generally the quality of the panels. However, long cure cycles are required because the large autoclave mass takes a long time to heat up and cool down: typical cure cycles are either 121 °C or 177 °C for about 1 hour after an heat rate of 1-2 °C/min with a pressure of 0.48 MPa [27].

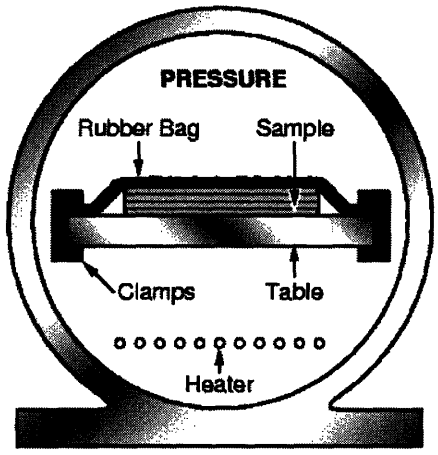

Figure 1.24: Schematic of the autoclave [45].

1.5.2 Brazing

Brazing of structural elements of metallic sandwich structure may be carried out following different approaches [46-52]. One technique comprises coating the cell walls with a brazing powder suspended in a binder [47-48]. Other methods include placing thin sheets of brazing materials between the core and the faces [46]; plating the core material and/or the facings with a suitable braze alloy [49-50] and placing the braze alloy in the core by means of braze foil segments, which are spot welded between the core nodes [51]. Regardless of the method chosen to place the brazing alloy, the structure is placed under a heating press. Selecting adequate pressures and temperatures, the braze material melts and is drawn by capillary attractions to the cell nodes and edges adjacent to the end panels [46-52]. When the sandwich structure is cooled down, an integral sandwich structure is formed. Although brazing of aluminum honeycomb/sheet metal has proved to be a suitable joining technique, with good transferability to structural parts and reliability, costs associated are high and justified only when adhesive bonding is not applicable [27].

1.6 Fabrication of Tubular Structures with Compliant Core

In Section 1.1 of this Chapter, we discuss the opportunity to mimic the design of natural shells with a compliant core. This Section describes techniques to manufacture sandwich or reinforced hollow shells for load-bearing components, integrating cellular metals.

Methods are known to create solid-shell component with an inner foam-core in one-step [25], based on the "powder-metallurgic" route. The basic concept of these methods is that the precursor material (see Figure 1.14 number 19) can be extruded in different shapes and when placed in furnace it will start to expand inside the shell (see Figure 1.25).

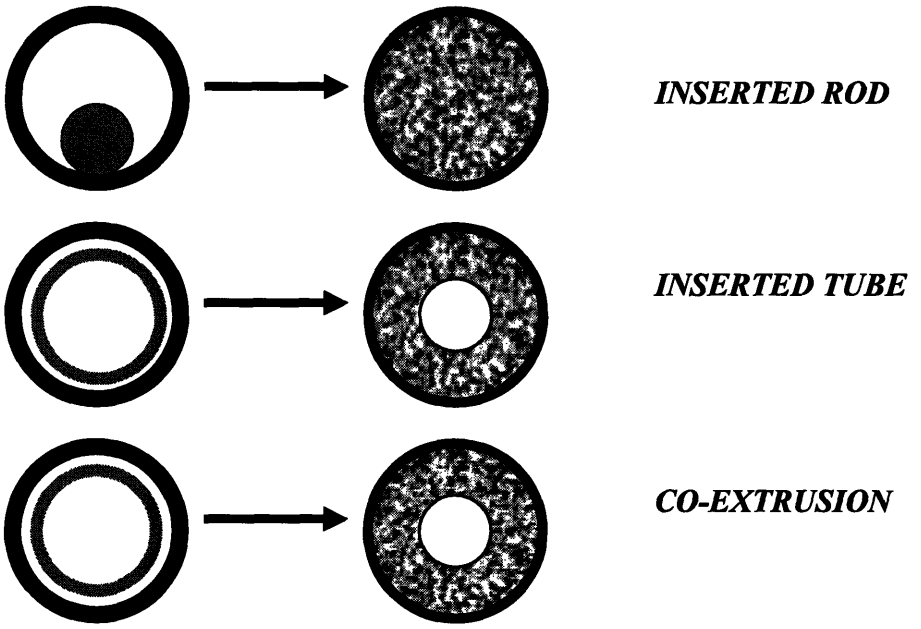

Figure 1.25: Methods for filling tubes with foam [25].

Problems affecting these types of constructions were already highlighted in Section 1.4.1. The main limit is represented by the shrinkage of the foam, whereas little or no shrinkage occurs in the tube, thereby creating a gap between the metal foam and the tube [6]. Methods have been proposed to solve this problem [6] based on the co-forming of a powdered metal tube with a polymeric foam coated with metal powder: when the component is heated-up the polymeric foam volatizes, while the powder solidifies leaving the final structure [6]. Figure 1.8 (right) shows a picture of the shell with compliant core produced according to this method. An advantage of this method is that it eliminates any

gaps associated with the shrinkage of the foam by allowing the powdered metal component to shrink with the foam, but information on the quality of the joint is still missing [6]. Figure 1.26 compares a conventional shell manufactured through the Fraunhofer process to one fabricated according to this system.

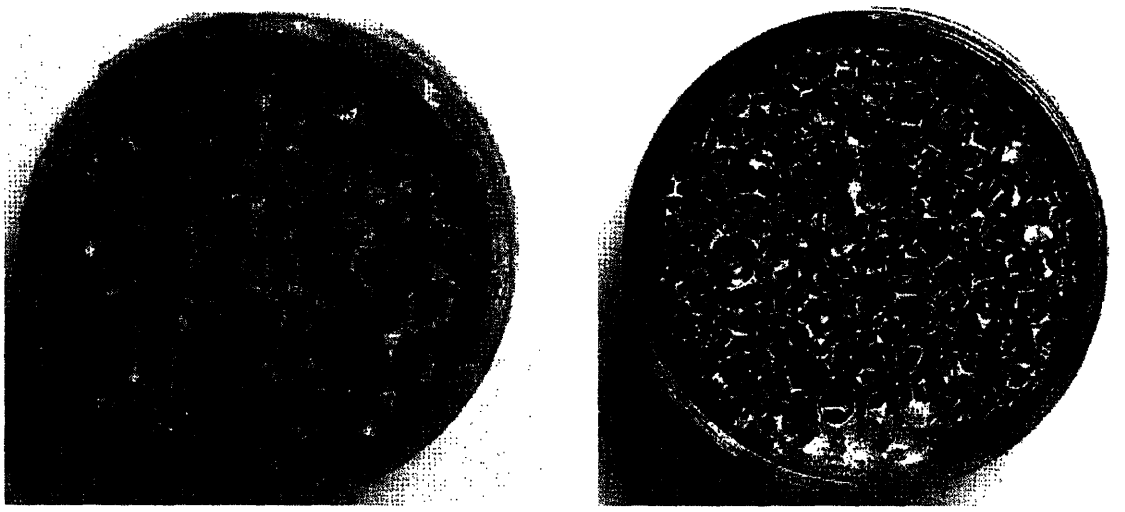

Figure 1.26: Comparison between foam-filled shell produced by the Fraunhofer process (left) and the co-forming process (right). In the left picture it is visible a large gap between the outer shell and the foam core [6].

A feasible way to produce foam-filled shells with known reliability is to bond the face sheet to the foam: in this case the initial foam has to be shaped as a hollow tube. Note that autoclave and vacuum-bag cannot be used here, due to the rigidity of the foam: if adhesive bonded is desired, special solutions have to be found, i.e. those described in Reference [53]. In this case, soldering and brazing seems more appropriate.

Different is the case of honeycomb sandwich shells, which can be fabricated in an autoclave [54]. Special care has to be taken for the free ends: in order to compensate the expansion of the panel, an insert of the type represented in Figure 1.27 can be used [54].

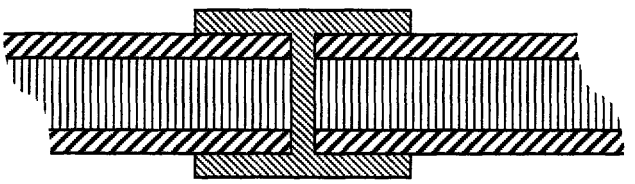

Figure 1.27: Insert for honeycomb core shell.

1.7 References

[1] G.N. Karam, "Elastic Stability of Cylindrical Shells with Soft Elastic Core: Biomimicking Natural Tubular Structures", *Ph.D. Dissertation,* Massachusetts Institute of Technology, **1994.**

[2] M.F. Ashby, *Materials Selection in Mechanical Design*, Butterworth-Heinemann. Oxford **1992**

[3] L.J. Gibson and M.F. Ashby, *Cellular Solids: Structure and Properties*, 2nd ed., Cambridge University Press, Cambridge **1997.**

[4] G.N. Karam and L.J. Gibson, "Elastic buckling of cylindrical shells with elastic cores – I. Analysis" in *Int. J. Solids Structures*, **1995**, *32*, p. 1259-1283.

[5] K. J. Nicklas, *Plant Biomechanics: An Engineering Approach to Plant Form and Function*, University of Chicago Press, **1992.**

[6] D.P. Haack *et al.*, U.S. Patent 6 706 239, **2004.**

[7] B. Sosnick, U.S. Patent 2 434 775, **1948.**

[8] J. Banhart, "Manufacture, characterization and application of cellular metal and metal foam", *Progress in Materials Science,* **2001,** *46*, p. 559-632.

[9] M.F. Ashby, A. G. Evans, N.A. Fleck, L.J. Gibson, J.W. Hutchinson, H.N.G. Wadley, *Metal Foams: a Design Guide*, Butterworth-Heinemann, Oxford **2000**.

[10] C. Körner, R. Singer, "Processing of Metal Foams – Challenges and Opportunities", *Advanced Engineering Materials*, **2000**, *4*, p. 159-165.

[11] F. Simancik, "The Strange World of Cellular Metals", *Handbook of Cellular Metals,* Wiley, **2002,** p. 1-4.

[12] H.N.G. Wadley, "Cellular Metals Manufacturing", *Advanced Engineering Materials*, **2002**, 10, p. 726 -733.

[13] Jin *et al.*, U.S. Patent 4 973 358, **1990.**

[14] J. Banhart, "Manufacturing Routes for Metallic Foams", *The Minerals, Metals and Materials Society,* **2000**, *52*, p. 22-27

[15] Sang, U.S. Patent 5 334 236, **1994.**

[16] Thomas *et al.*, U.S. Patent 5 622 542, **1997.**

[17] Kenny *et al.*, U.S. Patent 5 281 251, **1994.**

[18] Gesing *et al.*, U.S. Patent 5 409 580, **1995.**

[19] D. Curan, *Metal Foams*, http://www.msm.cam.ac.uk/mmc/people/dave/dave.html, **2001.**

[20] Akiyama *et al.*, U.S. Patent 4 713 277, **1987.**

[21] N. Babcsan, J. Banhart, D. Leitlmeier, "Metal Foam – Manufacture and Physics of Foaming", *International Conference "Advance Metallic Materials"*, Smolenice, Slovakia, **2003.**

[22] T. Miyoshi, "ALPORAS Aluminum Foam: Production Process, Properties and Applications", *Advanced Engineering Materials*, **2000**, *4*, p. 179-183.

[23] J. Baumeister, German Patent, DE 40 18 360, **1990.**

[24] J. Baumeister, U.S. Patent 5 151 246, **1988.**

[25] J. Baumeister, J. Bahnart, "Production Methods for Metallic Foams", *Mat. Res. Soc. Symp. Proc*, **1998**, *521*, p. 121-130.

[26] J. Banhart, F. Baumgärtner, I. Duarte, "Industrialization of Powder-Compact Toaming Process", *Adv. Eng. Mater.* **2000**, *2*, (No.4) p. 168-174.

[27] T. Bitzer, *Honeycomb Technology*, Chapman & Hall, London, **1998.**

[28] Hexcel Composite, *Hexweb™ Honeycomb Selector Guide*, **2004.**

[29] W. Seelinger, "Manufacture of Aluminum Foam Sandwich (AFS)" in *Advanced Engineering Materials*, **2002**, *10*, p. 753.

[30] P. Van Nieuwkoop, http://www.sml.lr.tudelft.nl/research/r_pr_foam.html, **2004.**

[31] H.-P. Degischer, B. Kriszt, *Handbook of Cellular Metals: Production, Processing, Applications,* Wiley-VCH Verlach, Weinheim, **2002.**

[32] T. Bernard, C. Haberling, H.W. Bergmann, H.-G.Haldenwanger, „Joining Technologies for Al-foam/Al-sheet Compound Structures", *Adv. Engineering Materials,* **2002**, *10,* p. 798-802

[33] T. Bernard, J.Burzer, H.W. Bergmann, *Porous and Cellular Materials for Structural Applications,* D.S. Schwartz, D.S. Smith, A.G. Evans, H.N.G. Wadley (eds), MRS Symp. Proc. Vol.521, MRS, Warrendale, PA **1998**, p.159.

[34] H. Haferkamp, J. Bunte, D. Herzog and A. Osterdorf, „Laser Based Welding of Cellular Aluminum", *Science and Technology of Welding and Joining,* **2004**, *9*, p. 65-71.

[35] C. Born *et al.*, "Ultraschallsweißen Metallischer Schäume mit Blechen", *Mat.-wiss. U. Werkstofftech*, **2000**, *31*, p. 547-549

[36] W.W. Duley, *Laser Welding*, Hoboken, GA, Wiley, **1998.**

[37] T. Böllinghaus *et al.*, "Laserstrahlschweißen von schäumbaren Aluminiumhalbzeug", *UTF Science,* **2000,** *11*, p. 23-26.

[38] DFG, „Ultrasonic Welding of Metalfoams to Sheet Metals", http://www.spp-metallschaeume.uni-erlangen.de/Projects/Project_CF6/project_cf6.html, **2004.**

[39] D. Pickart-Castillo, F. Hillen, I. Rass, *Materwiss. Werkstofftechn.* **2000**, *31*, 553.

[40] K.-J. Matthes, H. Lang, *Materwiss. Werkstofftechn.* **2000**, *31*, 558.

[41] H.K.D.H. Bhadeshia, "Joining of Commercial Aluminum Alloys" in *Proceeding in International Conference of Aluminum,* Aluminum Association of India, Bangalore, **2003**

[42] T. Bernard, H.W. Bergmann, *Materwiss. Werkstoffetechn.* **2000**, *31*, p. 436

[43] K.F. Karlsson and T. Åström, "Manufacturing and Application of Structural Sandwich Components", *Composites Part A*, **1997**,*28A*, p. 97-111.

[44] Hexcel Composite, *HexWeb™ Honeycomb Sandwich Design Technology Manufacture,* www.hexcelcomposite.com, **2004.**

[45] CES, *The Cambridge Engineering Material Selector*, Granta Design Ltd, **1999.**

[46] C. Wirsing, U.S. Patent 3 030 703, **1962.**

[47] O.W. Langhans, U.S. Patent 3 057 057, **1962.**

[48] R.J. Lindstrom, U.S. Patent 3 068 565, **1962.**

[49] T.A. Herbert, U.S. Patent 3 106 015, **1963.**

[50] Blair *et al.,* U.S. Patent 3 656 224, **1972.**

[51] Ittner *et al.,* U.S. Patent 4 333 598, **1982.**

[52] C.L. Holland and L. Jennings, U.S. Patent 4 477 012, **1984.**

[53] Seelinger *et al.*, U.S. Patent, 6 090 232, **2000.**

[54] D. Zenker, *The Handbook of Sandwich Construction,* EMAS, London, **2000.**

Chapter 2

Viability Assessment

"A beautiful idea has a much greater chance to be a correct idea than an ugly one."

Roger Penrose, The emperor's new mind

2.1 Introduction

In the first chapter, the possibility of mimicking load-bearing tubular natural structures with an inner elastic core was considered. Shells incorporating foam or honeycomb are already manufactured using different techniques and find applications in weight-sensitive components like energy absorbers, silencers, vibration dumpers, and heat exchangers [1]. The use of these structures in load-bearing components is characterized by different requirements in terms of price, quality of the joints, characteristics of the core material, resistance to failure, etc. For this reason, tailored manufacturing techniques have to be developed for this specific application: these developments can involve, for instance, the adaptation of existing methods for joining the cellular core with the solid metal or employment of new cellular metals. The process of developing new structural materials and manufacturing products from it may be very expensive, and take 10 to 20 years [2]. This time is excessively long for most potential users, who require a payback in 5 years, and an initial sales volume from $5 to $50 million per year to justify investment [3].

The high risk and the long gestation time associated with the development and commercialization of a new structural material can be reduced through a though technology assessment and an aimed investment policy [3]. E. Maine and M. Ashby have developed a special tool for this purpose called investment methodology for material (IMM) [4]. The IMM is characterized by three different assessments [4]: *viability analysis*, *market assessment,* and *value capture assessment* (see Figure 2.1).

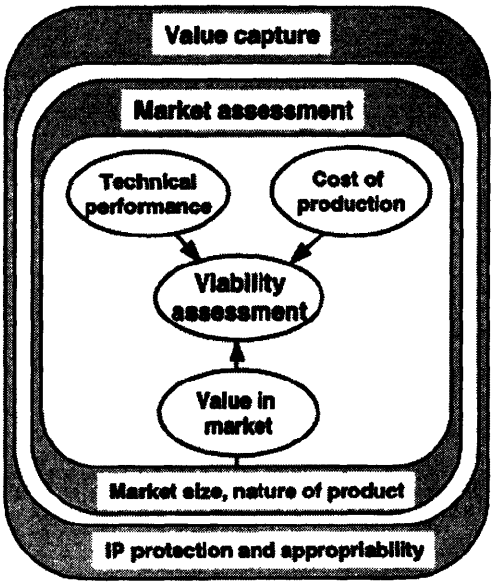

Figure 2.1: The investment methodology for materials (IMM) [4].

The viability of the new material is assessed by analyzing its technical performance, the projected manufacturing cost, and customer utility. In the technological assessment, performance metrics for the materials or structures are established and compared with those of other materials or structures. This stage acts as a preliminary barrier in the development phase, because investment in new materials can be justified often only when these show superior technical performances [2]. In the cost section, the projected manufacturing costs of the new material are calculated through a cost model. Modeling costs for materials at the laboratory stage and the sensitivity of the cost to the production volume can be hard, because often manufacturing processes are not completely developed and/or information for a cost model may be missing. In this case, an estimation of the costs can still be a guide to spot the limiting manufacturing barriers. The value assessment examines the impact of the new material in the marketplace, trying to establish its degree of acceptance [2]. This is traditionally done comparing the cost and the performance metric of the new and existing competitive materials and establishing trade-off surfaces through an utility analysis [5]. K. Musso [6] in his Ph.D. dissertation criticized the usefulness of the utility analysis in value assessment of the IMM. He believes that the intuitive premise of assessing the value of a new material on the cost and performance metric is oversimplifying and that other factors affecting the use of

advanced materials have to be considered such as barriers to entry and switching costs [6]. In the *market assessment*, results from the viability assessment are used to evaluate potential market sectors, where better or cheaper products could be created from the new material and to forecast future production volumes [4]. It should be observed that the IMM market assessment is based on the assumption of replacing materials into existing products through substitution [4]; the case of more innovative applications, where the materials are used to design completely new products is not taken into consideration. Tools used in the market assessment are marketing, supply chain, market size analyses, and historical observation of the adoption and penetration rates of new material in the same market niche [4]. The *probability of value capture* is assessed analyzing the intellectual properties, the industry, and organization structure [4]. In the IMM, this is done using traditional business tools like the Porter's Five Forces analysis and the model of appropriability of Teece.

Through these three assessments, it is possible to characterize the material using the two metrics of size of markets and value capture (see Figure 2.2). In Figure 2.2 are indicated some remarkable examples. The position of the new material in the Figure 2.2 is information that can be used to establish the attractiveness of investment, as well as the strategy of investment [4].

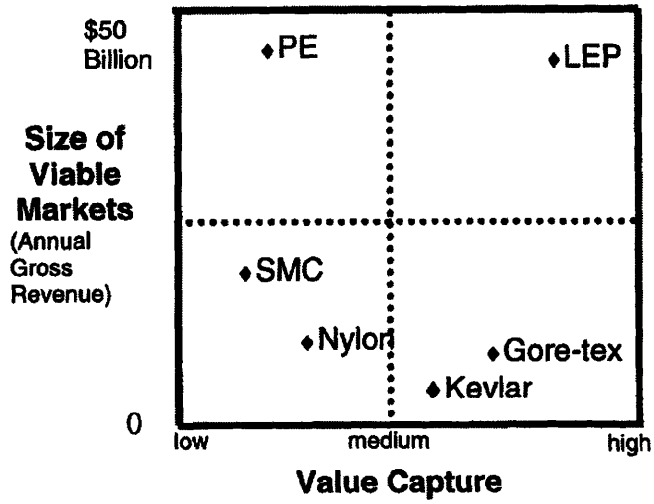

Figure 2.2: Market size and value capture as measures of attractiveness of a material innovation. [2] In Figure LEP means light-emitting polymers; PE is polyethylene; SMC is sheet molding compound.

Shells with foam or honeycomb cores can be treated as composite materials. In this chapter, the viability of these structures is assessed using the IMM and focusing on their application as structural materials. Technical performance is discussed in the next section. In the third section, an estimation of the manufacturing costs is presented. This information is used in the fourth section for the market value assessment: different markets are addressed and a tentative breakthrough application is selected on the base of minimal entry barriers. The market and value capture assessments will be considered in the chapter 4, together with the investment analysis.

2.2 Technical Performance Assessment

There are four principal configurations for cylindrical tubes/shells (Figure 2.3):

1. Empty;
2. With longitudinal stiffeners;
3. With honeycomb or foam sandwich wall;
4. With honeycomb or foam core.

In this paragraph, we will compare the efficiency of these different forms of construction loaded in axial compression on the base of the minimum weight criterion.

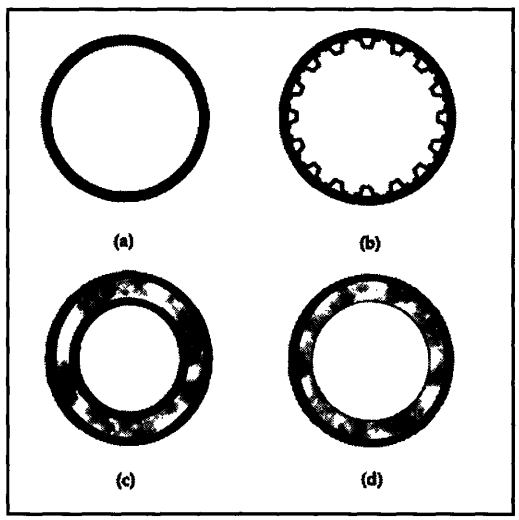

Figure 2.3: Schematics of cross-sections of cylindrical tubes. (a) Empty shell (b) longitudinal hat-stiffed shell (c) sandwich wall shell (d) shell with a complaint honeycomb or foam core.

2.2.1 Hollow circular shells

The minimum weight analysis of thin wall circular cylindrical shells has been treated by Gerard [7] and Budiansky [8]. The weight of a column of uniform cross section is:

$$W = \rho \cdot L \cdot A; \qquad (2.1)$$

where ρ is the material density, L is the length of the column, and A is the cross-sectional area. Substituting $A = P/\sigma$, where P is the applied load and σ is the axial stress acting on a point of the cross-section, gives:

$$\frac{W}{\rho L^3} = \frac{1}{\left(\frac{\sigma}{E}\right)} \cdot \left(\frac{P}{EL^2}\right); \qquad (2.2)$$

where E is the material Young's modulus. According to equation (2.2), the minimum weight of the column per given structural index $P/(EL^2)$ is achieved when the stress is maximum, i.e. $\sigma = \sigma_{max}$. Upper limits for the allowable stress σ are given by the Euler (global) buckling conditions, the local buckling condition and the yielding of the face. Considering pinned-pinned ends, the Euler buckling condition can be expressed as [9]:

$$\frac{\sigma}{E} \le \frac{\sigma_1}{E} = \frac{\pi^2 I}{AL^2}; \qquad (2.3)$$

where σ_1 is the Euler buckling stress and I is the cross-sectional moment of inertia. Defining t, the thickness of the shell, and R, the mean radius, if the ratio R/t>10 (thin shell assumption), we can rewrite (2.3) as:

$$\frac{\sigma}{E} \le \frac{\sigma_1}{E} = \frac{\pi^2}{2}\left(\frac{R}{L}\right)^2; \qquad (2.4) \quad \text{(Euler Buckling)}$$

From $\sigma = P/(2\pi Rt)$, we can write:

$$\frac{P}{EL^2} = 2\pi\left(\frac{R}{L}\right)^2\left(\frac{t}{R}\right)\frac{\sigma}{E}; \qquad (2.5)$$

Substituting equation (2.5) in (2.4), we can express the global buckling condition in a more convenient form:

$$\frac{\sigma}{E} \le \frac{\sqrt{\pi}}{2}\left(\frac{R}{t}\right)^{\frac{1}{2}}\left(\frac{P}{EL^2}\right)^{\frac{1}{2}}; \qquad (2.6)$$

The local buckling condition is [9]:

$$\frac{\sigma}{E} \le \frac{\sigma_2}{E} = \frac{\gamma}{\sqrt{3\cdot(1-\nu^2)}}\frac{t}{R}; \qquad (2.7) \quad \text{(Local Buckling)}$$

where γ is a knockdown factor inserted in order to correct the disparity between theory and experiment. Budiansky [8] takes γ as function of R/t according to the formula recommended by NASA [10]:

$$\gamma = 1 - 0.901\cdot\left(1 - e^{-\kappa}\right) \qquad (2.8)$$

where

$$\kappa = \frac{1}{16}\sqrt{\frac{R}{t}}; \quad \left(\frac{R}{t} < 1500\right) \qquad (2.9)$$

The yielding of the wall is given by:

$$\frac{\sigma}{E} \le \frac{\sigma_y}{E} = \varepsilon_y; \qquad (2.10) \quad \text{(Plastic Yielding)}$$

where σ_y is the yielding stress. Gerard [7] observed that in absence of plastic yielding, the minimum weight, which corresponds to the maximum allowable stress, is attained when the two buckling modes occurs simultaneously, i.e. $\sigma_{max} = \sigma_1 = \sigma_2$ (see Figure 2.4). According to this observation, equaling equations (2.4) and (2.7):

$$\left(\frac{R}{L}\right)^2 = \frac{2}{\pi^2}\cdot\frac{\gamma}{\sqrt{3\cdot(1-\nu^2)}}\left(\frac{t}{R}\right); \qquad (2.11)$$

Substituting equations (2.4) and (2.11) in (2.5) gives:

$$\left(\frac{t}{R}\right)^3 = \frac{P}{(EL^2)} \cdot \frac{3\pi\left(1-\nu^2\right)}{4\gamma^2}; \qquad (2.12)$$

and

$$\frac{\sigma_{\max}}{E} = \tau \cdot \left[\frac{P}{(EL^2)}\right]^{\frac{1}{3}}; \qquad (2.13)$$

where

$$\tau = \left(\frac{\pi}{4}\right)^{\frac{1}{3}} \cdot \gamma^{\frac{1}{3}} \cdot \frac{1}{\left[3\cdot(1-\nu^2)\right]^{\frac{1}{6}}}; \qquad (2.14)$$

For $\nu = 0.3$ and $10 < \frac{R}{t} < 100$, $0.72 < \tau < 0.66$. Substituting equation (2.2), finally:

$$\frac{W_{\min}}{\rho L^3} = \frac{1}{\tau} \cdot \left(\frac{P}{EL^2}\right)^{\frac{2}{3}}; \qquad (2.15)\ \text{(Elastic Region)}$$

Equation (2.15) is valid if $\sigma_{\max}/E \le \varepsilon_y$, or $P/(EL^2) \le \left(\varepsilon_y/\tau\right)^3$; for $P/(EL^2) \ge \left(\varepsilon_y/\tau\right)^3$:

$$\frac{W_{\min}}{\rho L^3} = \frac{P}{\varepsilon_y \cdot EL^2}; \qquad (2.16)\ \text{(Plastic Yielding)}$$

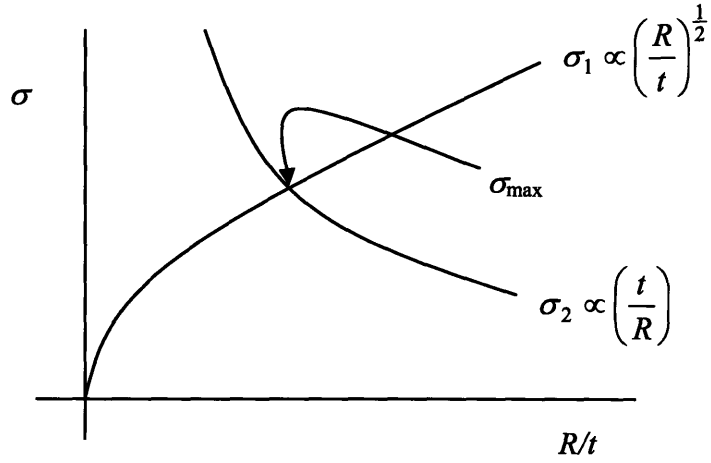

Figure 2.4: Maximum stress for given structural index $P/(EL^2)$; σ_1 = Euler buckling stress from equation (2.6) , σ_2 = local buckling stress from equation (2.7) [8].

2.2.2 Stringers-stiffed isotropic shells

The minimum weight design of hat-stringer-stiffed cylinder has been treated by Agarwal and Sobel [11]. In their work, optimum designs were obtained based on the "smeared" shell theory, which accounts for the effects of stiffener eccentricity [12], and numerical simulations [11]. In this work, a simplified analytic approach is taken and it is assumed that the shells behave like wide flat panels. This assumption neglects the increase in buckling strength of the curved skin for small values of the ratio R/t [7]. However, efficient applications of this form of construction are characterized by large values of the ratio R/t, where the assumption is valid [7]. The optimization of stringers-stiffened panels received particular attention after the WWII, both by NACA [13], which tested hundreds of panels, and other organizations like Lockheed [14], Bristol Aeroplane [15], Vickers-Armstrong [16] and has been revised recently by Budiansky [8].

According to Gerard [7], the conditions for minimum weight design of a compression structure are that the applied stress and allowable stress be equal and that the possible forms of buckling occurs simultaneously. From $\mathrm{N} = P/(2\pi R)$, the applied stress can be defined as [7]:

$$\sigma_a = \mathrm{N}/\bar{t} \qquad (2.17) \text{ (Applied stress)}$$

, where

$$\bar{t} = (A_{st}/i) + t \qquad (2.18)$$

In equation (2.18) $\bar{t}$ is the effective face thickness, t is the skin thickness, i is the stiffener interspacing and A_{st} stiffener area. The Euler buckling condition is still expressed by equation (2.3). Observing that $I = A \cdot \varsigma^2$, where ς is the section radius of gyration, we can rewrite equation (2.3) as [7]:

$$\frac{\sigma_a}{E} \le \frac{\sigma_1}{E} = \frac{\pi^2 \varsigma^2}{L^2}; \qquad (2.19) \text{ (Euler Buckling)}$$

Different types of stringers are used in practice [7]. We consider the types tested by NACA [13], i.e. riveted Z, hat and Y stringers, which are represented in Figure 2.5.

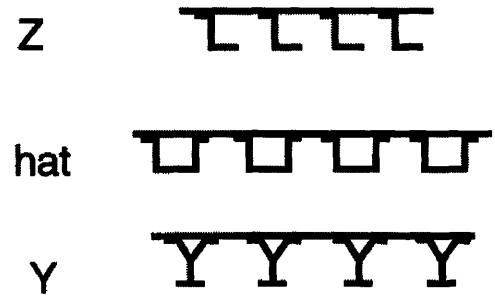

Figure 2.5: Stiffeners considered in this study [8].

The local buckling, which corresponds to the buckling of the skin between the rows of fasteners attaching the skin to the stringers, is given by [8]:

$$\frac{\sigma}{E} \leq \frac{\sigma_2}{E} = K \cdot \left(\frac{t}{i}\right)^2; \qquad (2.20) \text{ (Local Buckling)}$$

where the coefficient K depends on the particular skin-stringer combination. Other modes of failure, like stringer torsional instability or crippling, can be neglected, as they do not occur in optimal designed shells [7]. Equations (2.18), (2.19) and (2.20) can be combined in the following form:

$$\sigma_a^2 \cdot \sigma_1 \cdot \sigma_2 = \frac{E \cdot \pi^2 \varsigma^2}{L^2} \cdot \frac{E \cdot K \cdot t^2}{i^2} \cdot \frac{N^2}{\bar{t}^2}; \qquad (2.21)$$

In the minimum weight design, $\sigma_{opt} = \sigma_a = \sigma_1 = \sigma_2$. Consequently [7]

$$\frac{\sigma_{opt}}{E} = \left(\pi^2 K\right)^{\frac{1}{4}} \left(\frac{\varsigma \cdot t}{i \cdot \bar{t}}\right)^{\frac{1}{2}} \left(\frac{N}{EL}\right)^{\frac{1}{2}}; \qquad (2.22)$$

Equation (2.22) shows that the optimum stress is maximum when the ratio $t/\bar{t}$ gets close to one (relatively thick skins), the stringer spacing i becomes smaller, while the buckling coefficient K and the radius of gyration ς are as large as possible [7].

However, it should be noticed that in optimum design, these parameters are not independent and are linked by the condition $\sigma_{opt} = \sigma_a = \sigma_1 = \sigma_2$, i.e.,

$$N/\bar{t} = \frac{\pi^2 \varsigma^2}{L^2};$$

$$\frac{\pi^2 \varsigma^2}{L^2} = K \cdot \left(\frac{t}{i}\right)^2;$$

$$K \cdot \left(\frac{t}{i}\right)^2 = N/\bar{t};$$

Equation (2.22) can be rewritten, according to Zahorski [14]:

$$\frac{\sigma_{opt}}{E} = \chi \left(\frac{N}{EL}\right)^{\frac{1}{2}}; \qquad (2.23)$$

where

$$\chi = \left(\pi^2 K\right)^{\frac{1}{4}} \left(\frac{\varsigma \cdot t}{i \cdot \bar{t}}\right)^{\frac{1}{2}}; \qquad (2.24)$$

is a coefficient, that can be taken as a measure of the structural efficiency of the shell. At this point, defined ς_f as the radius of gyration of a stringer panel of effective thickness $\bar{t}$, it is convenient to introduce the panel efficiency coefficient α [14]:

$$\alpha = \left(\pi^2 K\right)^{\frac{1}{4}} \left(\frac{\varsigma_f \cdot t}{i \cdot \bar{t}}\right)^{\frac{1}{2}}; \qquad (2.25)$$

Therefore, we can rewrite equation (2.23) as

$$\frac{\sigma_{opt}}{E} = \alpha \cdot \left(\frac{N}{EL}\right)^{\frac{1}{2}} \cdot \left(\frac{\varsigma}{\varsigma_f}\right)^{\frac{1}{2}}; \qquad (2.26)$$

For large shell radius R, the ratio ς/ς_f does not depend much on the particular shape of the stringers; it keeps into account of the increased moment of inertia of a shell respect to a flat panel. Consequently, it can be approximated with the ratio between the radii of

gyration of an unstiffened panel of thickness $\bar{t}$, i.e. $\varsigma_f \approx \bar{t}/\left(2\sqrt{3}\right)$ and radius of gyration of an unstiffened shell, i.e., $\varsigma \approx R/\sqrt{2} \Rightarrow \varsigma/\varsigma_f = \sqrt{6}\,R/\bar{t}$. With this assumption and observing that N = $P/(2\pi R)$, equation (2.26) can be expressed in the following form:

$$\frac{\sigma_{opt}}{E} = \frac{\sqrt[4]{6}}{\sqrt{2\pi}} \cdot \alpha \cdot \left(\frac{L}{\bar{t}}\right)^{\frac{1}{2}} \cdot \left(\frac{P}{EL^2}\right)^{\frac{1}{2}}; \qquad (2.27)$$

As consequence of the initial assumption that the curved stringer panel behaves in the same manner as a wide flat panel and from equations (2.17) and (2.23), the effective thickness of the shell is [7]:

$$\left(\frac{\bar{t}}{L}\right)_{opt} = \frac{\sigma_{opt}}{E} \cdot \frac{1}{\chi^2} \approx \frac{\sigma_{opt}}{E} \cdot \frac{1}{\alpha^2}; \qquad (2.28)$$

Substituting equation (2.28) in (2.27), gives:

$$\frac{\sigma_{opt}}{E} = \left(\frac{\sqrt[4]{6}}{\sqrt{2\pi}}\right)^{\frac{2}{3}} \cdot \alpha^{\frac{4}{3}} \cdot \left(\frac{P}{EL^2}\right)^{\frac{1}{3}}; \qquad (2.29)$$

As the weight is given by:

$$W = \frac{\rho PL}{\sigma}; \qquad (2.30)$$

we obtain

$$\frac{W_{\min}}{\rho L^3} = \Psi \cdot \left(\frac{P}{EL^2}\right)^{\frac{2}{3}}; \qquad (2.31)\ \text{(Elastic Region)}$$

where

$$\Psi = \left(\frac{\sqrt[4]{6}}{\sqrt{2\pi}}\right)^{-\frac{2}{3}} \cdot \alpha^{-\frac{4}{3}}; \qquad (2.32)$$

By writing the minimum weight equation in the form of equation (2.31), it is possible to confine further considerations to the effects of the geometrical configurations of the panel to the value of the panel efficiency coefficient α. Due to the analytical difficulties to

determine this coefficient [7], NACA embarked in the early 50s a series of experiments testing different stringers geometry [7]. The experimental values of the panel efficiency coefficient α, given in Table 2.1 are still considered the most reliable [8].

Stringer Type	α	ψ
Z section	1.02	1.33
Hat section	0.99	1.39
Y section	1.15	1.14

Table 2.1: Experimental Values of the Panel Efficiency Coefficient [7].

Equation (2.31) is valid if $\sigma_{\max}/E \le \varepsilon_y$, or $P/(EL^2) \le (\varepsilon_y/\Psi)^3$; for $P/(EL^2) \ge (\varepsilon_y/\Psi)^3$

$$\frac{W_{\min}}{\rho L^3} = \frac{P}{\varepsilon_y \cdot EL^2}; \qquad (2.33)\ \text{(Plastic Yielding)}$$

2.2.3 Hollow Sandwich-Wall Circular Cylinder

The optimization of sandwich-wall cylinder with honeycomb cores has been considered by Agarwal and Sobel [11], while the case of sandwich shells with metal foam cores was treated more specifically by Hutchison and He [17]. The procedure followed here elaborates on the work of Budiansky [8]. Considered a sandwich-wall hollow cylinder, with core thickness *d*, sheet thickness *t*, mean radius *R*, and length *L*, the weight is given by the relation:

$$W = \left[4\pi\rho_f \cdot R \cdot t + 2\pi\rho_c \cdot R \cdot (d-t)\right]L \qquad (2.34)$$

From $P = 4\pi\sigma \cdot R \cdot t$, defined ρ_f as the density of the face sheet, ρ_c as the density of the core, E_f as the Young's modulus of the face and E_c as the Young's modulus of the core, follows that:

$$\frac{W}{\rho L^3} = \frac{\left(1-\frac{1}{2}\frac{\rho_c}{\rho_f}\right)\frac{P}{E_f L^2}}{\sigma/E_f} + \frac{2\pi\rho_c}{\rho_f}\left(\frac{R}{L}\right)^2\frac{d}{R} \qquad (2.35)$$

In the analysis, the contribution of the core to the column buckling stiffness is neglected [8]. In addition, the contribution of the compressive stress in the core is also neglected [8], as well as the reduction of the column buckling strength due to transverse shear compliance [8]. With these assumptions for small d/R, we can approximate the buckling stress σ_1 with equation (2.4). The local buckling stress of the sandwich cylinder can be expressed as [18]:

$$\frac{\sigma}{E_f} \le \frac{\sigma_2}{E_f} = \frac{\gamma}{\sqrt{(1-\nu^2)}}\frac{d}{R}; \qquad (2.36)\ \text{(Local Buckling)}$$

where γ is the knock-down factor defined in equation (2.8). According to [10], now:

$$\kappa = \frac{1}{16\cdot(3)^{1/4}\sqrt{d/R}}; \qquad (2.37)$$

In absence of face yielding or wrinkling, the condition of minimum weight is still given by $\sigma_1 = \sigma_2 = \sigma_{max}$. Consequently, equation (2.35) can be rewritten as:

$$\frac{W}{\rho L^3} = \frac{k_1}{(d/R)}\left(\frac{P}{E_f L^2}\right) + k_2\left(\frac{d}{R}\right)^2; \qquad (2.38)$$

where:

$$k_1 = \frac{\left(1 - \frac{1}{2}\frac{\rho_c}{\rho_f}\right)\sqrt{1-\nu^2}}{\gamma}; \qquad k_2 = \frac{4\rho_c}{\pi\rho_f}\frac{\gamma}{\sqrt{1-\nu^2}}; \qquad (2.39)$$

The optimum weight is given by the condition that:

$$\left.\frac{\partial\left(\frac{W}{\rho L^3}\right)}{\partial\left(\frac{d}{R}\right)}\right|_{opt} = 0; \qquad (2.40)$$

, that is:

$$\left.\frac{d}{R}\right|_{opt} = \sqrt[3]{\frac{k_1\left(\frac{P}{E_f L^2}\right)}{2 \cdot k_2}}; \qquad (2.41)$$

, which substituting in (2.38) gives:

$$\frac{W_{min}}{\rho L^3} = \left(\sqrt[3]{2} + 1/\sqrt[3]{4}\right) \cdot \sqrt[3]{k_1^2 k_2} \cdot \left(\frac{P}{E_f L^2}\right)^{\frac{2}{3}}; \qquad (2.42)\ \text{(Elastic Range)}$$

This result applies up to the value of $P/\left(E_f L^2\right)$ relative to face yielding or face wrinkling onset. According to Hutchinson and He [17], these two modes of failure mutually exclude each other.

Face yielding occurs if the core density satisfies the condition [17]:

$$\rho_c > \rho_f \left(\frac{\varepsilon_y}{B\alpha^{2/3}} \right)^{\frac{3}{4}}; \qquad (2.43)$$

where B is a coefficient given by Allen [19] equal to 0.58 and $\alpha \approx 1$ for most commercial materials. Equation (2.43) is verified by most metallic foam. Assuming this condition, face yielding occurs when the load reaches the value $N = 2t\sigma_y$, where $N = P/(2\pi R)$ [17]: this is equivalent to say $P/(E_f L^2) \geq |P/(E_f L^2)|_y$, where $|P/(E_f L^2)|_y$ can be obtained from $P = 4\pi\sigma \cdot R \cdot t$, and equations (2.4) and (2.10):

$$\left| \frac{P}{EL^2} \right|_y = \frac{8}{\pi} \frac{t}{R} \varepsilon_y^2; \qquad (2.44)$$

where [17]

$$\frac{t}{R} = \frac{a_1}{3a_2} \cdot \left(\frac{\rho_c}{\rho_f} \right)^2; \qquad (2.45)$$

and [17]

$$a_1 = 2/\sqrt{1-\nu^2}, \quad a_2 = 8/\left[3\alpha \cdot (1-\nu^2)\right]; \qquad (2.46)$$

In minimum weight designs, face yielding and local buckling are both active [17], i.e. $\sigma_y = \sigma_2$. Consequently:

$$\left. \frac{d}{R} \right|_{opt} = \sqrt{\frac{(1-\nu^2)\varepsilon_y^2}{\gamma_y^2}}; \qquad (2.47)$$

and

$$\frac{W}{\rho L^3} = \frac{\left(1 - \frac{1}{2}\frac{\rho_c}{\rho_f}\right)\frac{P}{E_f L^2}}{\varepsilon_y} + \frac{4\rho_c}{\pi\rho_f} \frac{\varepsilon_y^2}{\gamma_y} \sqrt{1-\nu^2}; \qquad (2.48) \quad \text{(Face Yielding Active)}$$

Face wrinkling occurs if $\rho_c < \rho_f \left(\frac{\varepsilon_y}{B\alpha^{2/3}} \right)^{\frac{3}{4}}$ when the load reaches the value $N = 2tB\left(E_f E_c^2\right)^{\frac{1}{3}}$. The limiting stress at this point is:

$$\frac{\sigma}{E_f} \le \frac{\sigma_{wrink}}{E_f} = B\left(\frac{E_c}{E_f}\right)^{\frac{2}{3}}; \qquad (2.49)$$

This condition is equivalent to $P/\left(E_f L^2\right) \ge \left|P/\left(E_f L^2\right)\right|_{wrink}$, where:

$$\left|\frac{P}{EL^2}\right|_{wrink} = \frac{8B^2}{\pi}\left(\frac{E_c}{E_f}\right)^{\frac{4}{3}}\frac{t}{R}; \qquad (2.50)$$

and t/R is still given by (2.45). Both face wrinkling and local buckling are active in minimum weight designs [17], i.e. $\sigma_{wrink} = \sigma_2$ and therefore

$$\frac{d}{R} = B\left(\frac{E_c}{E_f}\right)^{\frac{2}{3}} \cdot \frac{\sqrt{1-\nu^2}}{\gamma_{wrink}}; \qquad (2.51)$$

The corresponding vale of $W_{\min}$ can still be found substituting equation (2.49) and (2.51) in (2.35):

$$\frac{W_{\min}}{\rho L^3} = \frac{\left(1 - \frac{1}{2}\frac{\rho_c}{\rho_f}\right)\frac{P}{E_f L^2}}{B\left(\frac{E_c}{E_f}\right)^{\frac{2}{3}}} + \frac{4\rho_c}{\pi\rho_f}\left(\frac{E_c}{E_f}\right)^{\frac{4}{3}}\frac{\sqrt{1-\nu^2}}{\gamma_{wrink}}B^2; \qquad (2.52)\ \text{(Face Wrinkling Active)}$$

2.2.4 Shells with compliant core

Consider a cylindrical shell with foam or honeycomb core, face thickness t, mean radius of the face R and core thickness d (Figure 2.6). In the minimum weight analysis, we neglect the contribution of the core to column bending stiffness. In addition, we assume that the compressive loads are carried by the outer shell only. Effects of the transverse shear compliance will be also neglected.

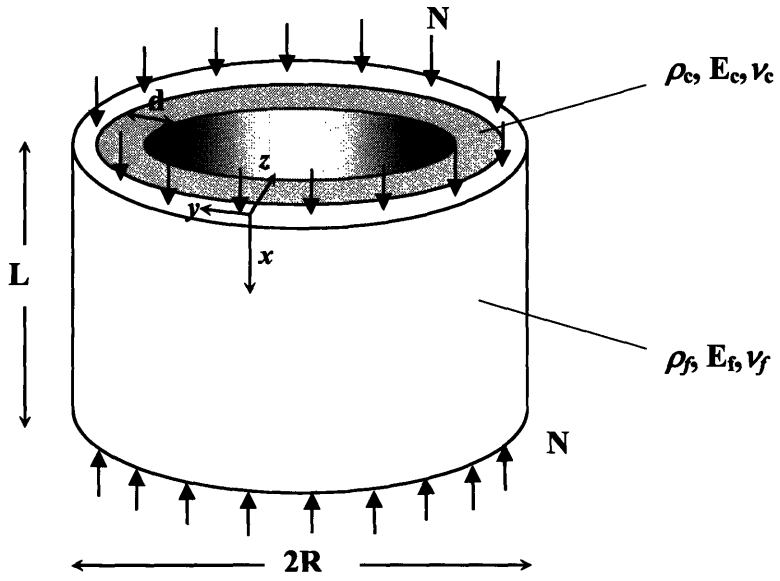

Figure 2.6: Thin walled cylindrical shell with a compliant elastic core.

The condition of global buckling, equation (2.4), continues to apply:

$$\frac{\sigma}{E_f} \le \frac{\sigma_1}{E_f} = \frac{\pi^2}{2}\left(\frac{R}{L}\right)^2 \quad \text{(Euler Buckling)}$$

Similarly to the case of the hollow shell, from $\sigma = P/(2\pi Rt)$ and equation (2.5), the Euler buckling condition can be expressed by equation (2.6), which is rewritten here for clarity:

$$\frac{\sigma}{E_f} \le \frac{\sigma_1}{E_f} = \frac{\sqrt{\pi}}{2}\left(\frac{R}{t}\right)^{\frac{1}{2}}\left(\frac{P}{E_f L^2}\right)^{\frac{1}{2}};$$

According to Karam, the local buckling condition is given by [20]:

$$\frac{\sigma}{E_f} \le \frac{\sigma_2}{E_f} = \frac{\gamma}{\sqrt{3\cdot(1-\nu_f^2)}}\frac{t}{R}\cdot f_1; \qquad (2.53)\ \text{(Local Buckling)}$$

where γ is still given by equation (2.8) [21]. For thin shells, f_1 can be approximated through the expression given by Seide [21]:

$$f_1 \approx \frac{3}{2}\cdot\frac{\left[12(1-\nu_f^2)\right]^{\frac{1}{6}}}{\left[4\left(1-\nu_c^2\right)\right]^{\frac{2}{3}}}\cdot\left[\frac{E_c}{E_f}\right]^{\frac{2}{3}}\cdot\left(\frac{R}{t}\right); \qquad (2.54)$$

where E_f is the Young's modulus of the shell, E_c is the Young's modulus of the core, ν is the Poisson ratio of the shell and ν_c is the Poisson ratio of the core. With this assumption, equation (2.53) can be simplified to

$$\frac{\sigma}{E_f} \le \frac{\sigma_2}{E_f} = \Gamma; \qquad (2.55)$$

where

$$\Gamma \approx \frac{3}{2}\cdot\frac{\gamma}{\sqrt{3(1-\nu^2)}}\cdot\frac{\left[12(1-\nu^2)\right]^{\frac{1}{6}}}{\left[4\left(1-\nu_c^2\right)\right]^{\frac{2}{3}}}\cdot\left[\frac{E_c}{E_f}\right]^{\frac{2}{3}}; \qquad (2.56)$$

The face yielding condition is given by:

$$\frac{\sigma}{E_f} \le \frac{\sigma_y}{E_f} = \varepsilon_y; \qquad (2.57)\ \text{(Plastic Yielding)}$$

Face wrinkling occurs if:

$$\frac{\sigma}{E_f} \le \frac{\sigma_{wrink}}{E_f} = M; \qquad (2.58)\ \text{(Face Wrinkling)}$$

where

$$M = B\left(\frac{E_c}{E_f}\right)^{\frac{2}{3}} \qquad (2.59)$$

and B is the Allen coefficient [19], equal to 0.58.

The optimum stress is therefore given by:

$$\frac{\sigma_{opt}}{E_f} = \min(\Gamma, \varepsilon_y, M); \qquad (2.60)$$

For thin wall shells, the weight can be approximated with the following expression:

$$W = \left[\rho_f \frac{P}{\sigma} + \rho_c \cdot 2\pi \cdot R \cdot d\right] L; \qquad (2.61)$$

It is convenient to put equation (2.61) in the following form:

$$\frac{W}{\rho_f L^3} = \frac{\left(\frac{P}{E_f L^2}\right)}{\left(\frac{\sigma}{E_f}\right)} + 2\pi \frac{\rho_c}{\rho_f} \cdot \left(\frac{d}{t}\right) \cdot \left(\frac{t}{R}\right) \cdot \left(\frac{R}{L}\right)^2; \qquad (2.62)$$

Karam and Gibson observed [20] that the normal σ_z and shear τ_{xz} stresses in the core decay along the radial direction from the wall to the center of the core (see Figure 2.6). Introducing the shell buckling parameter,

$$\lambda_{cr} = \left[\frac{(3-\nu_c)(1+\nu_c)}{12(1-\nu^2)}\right] \cdot \left[\frac{E_f}{E_c}\right]^{\frac{1}{3}} \cdot t; \qquad (2.63)$$

at a distance $z = 5 \cdot \lambda_{cr}$ from the wall the magnitude of normal σ_z and shear τ_{xz} stresses is about 5% of their maximum value [20]: this means that the core material at distances $z > 5 \cdot \lambda_{cr}$ does not contribute to the shell buckling resistance. Consequently, we can assume:

$$\left.\frac{d}{t}\right|_{opt} = \frac{5 \cdot \lambda_{cr}}{t}; \qquad (2.64)$$

Assuming $\Gamma < \varepsilon_y$, M and setting $\sigma_1 = \sigma_2 = \sigma_{opt}$ in accordance with the minimum weight criterion, from equations (2.4) and (2.55) we obtain:

$$\left(\frac{R}{L}\right)^2\Bigg|_{opt} = \frac{2}{\pi^2}\cdot\Gamma; \qquad (2.65)$$

Equations (2.6) and (2.55) give:

$$\frac{t}{R}\Bigg|_{opt} = \frac{\pi}{4\cdot\Gamma^2}\left(\frac{P}{E_f L^2}\right); \qquad (2.66)$$

Substituting equations (2.55), (2.64), (2.66) and (2.66) in equation (2.62), we obtain:

$$\frac{W_{\min}}{\rho_f L^3} = \Omega\left(\frac{P}{E_f L^2}\right); \quad (2.67) \quad \text{(Global + Local Buckling)}$$

where

$$\Omega = \frac{1}{\Gamma}\left[1+5\cdot\frac{\rho_c}{\rho_f}\cdot\left(\frac{\lambda_{cr}}{t}\right)\right]; \qquad (2.68)$$

Assuming $\varepsilon_y < \Gamma, \mathrm{M}$, equations (2.65-2.68) are still valid, with the only attention to substitute Γ with ε_y. Therefore:

$$\frac{W_{\min}}{\rho_f L^3} = \Lambda\left(\frac{P}{E_f L^2}\right); \quad (2.69) \quad \text{(Global Buckling + Face Yielding)}$$

where

$$\Lambda = \frac{1}{\varepsilon_y}\left[1+5\cdot\frac{\rho_c}{\rho_f}\cdot\left(\frac{\lambda_{cr}}{t}\right)\right]; \qquad (2.70)$$

Similarly, for $\mathrm{M} < \Gamma, \varepsilon_y$, the minimum weight index is

$$\frac{W_{\min}}{\rho_f L^3} = \Sigma\cdot\left(\frac{P}{E_f L^2}\right); \quad (2.71) \quad \text{(Global Buckling + Face Wrinkling)}$$

where

$$\Sigma = \frac{1}{M}\left[1+5\cdot\frac{\rho_c}{\rho_f}\cdot\left(\frac{\lambda_{cr}}{t}\right)\right]; \qquad (2.72)$$

2.2.5 Comparison of different form of constructions

The results for the minimum weight analysis are shown in Figures 2.7-2.9, for a typical high strength Aluminum alloy with $\varepsilon_y = 0.007, \nu = 1/3$ and considering small values of the load index $\left(P/E_f L^2 \approx 10^{-8}\right)$. Figures 2.7-2.9 have been obtained for different values of the knockdown factor: note that for small loads, the knockdown factor is pratically independedent from the load index and can be assumed constant for a given range of R/t. All the figures clearly show that hollow shells are outperformed by all the other forms of construction. Foam sandwich and Y-stiffened shells have basically the same performance, with the foam structures advantaged for lower load. The more efficient form of construction is the hollow shell with compliant core. However, this form of construction becomes less effective with increasing values of the load index.

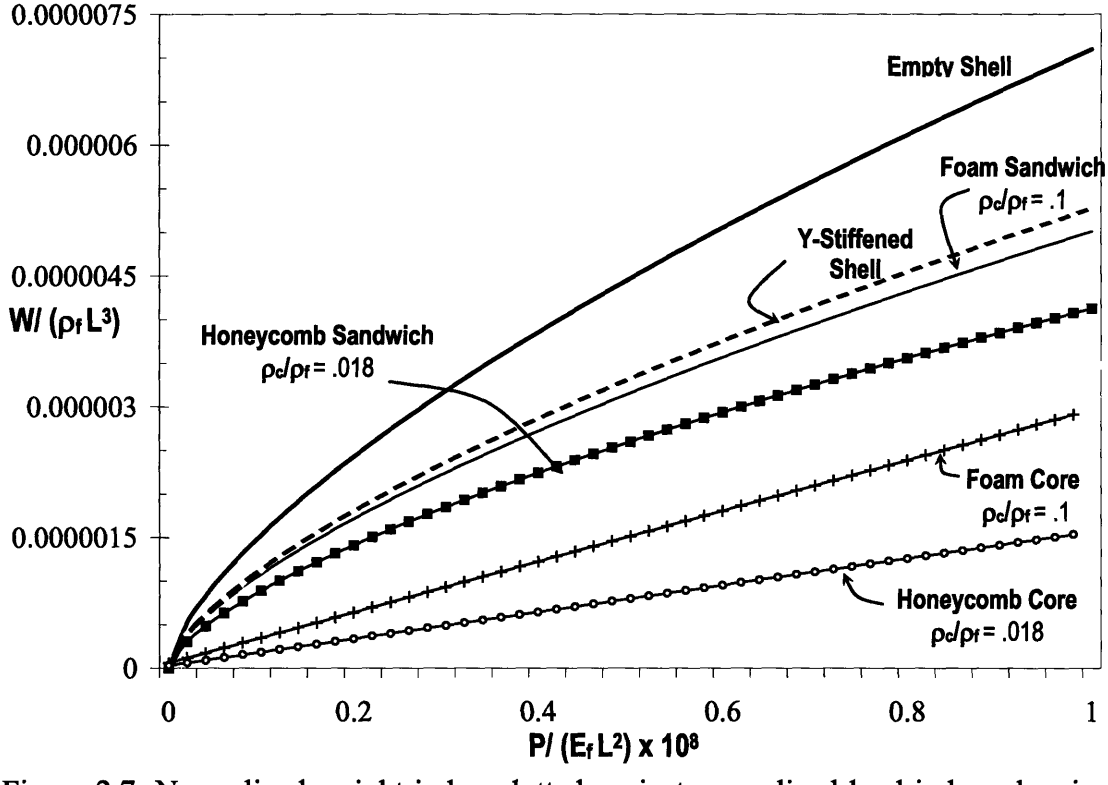

Figure 2.7: Normalized weight index plotted against normalized load index, showing curves for empty shell; longitudinal Y-stiffened shell; foam sandwich shell (with core density 10%); honeycomb sandwich shell (with core density of 1.8%); shell with foam core (with core density 10%); shell with honeycomb core (with core density 5%); $\gamma \approx 0.5, \varepsilon_y = 0.007, \nu = 1/3; \left(R/t < 50.\right)$.

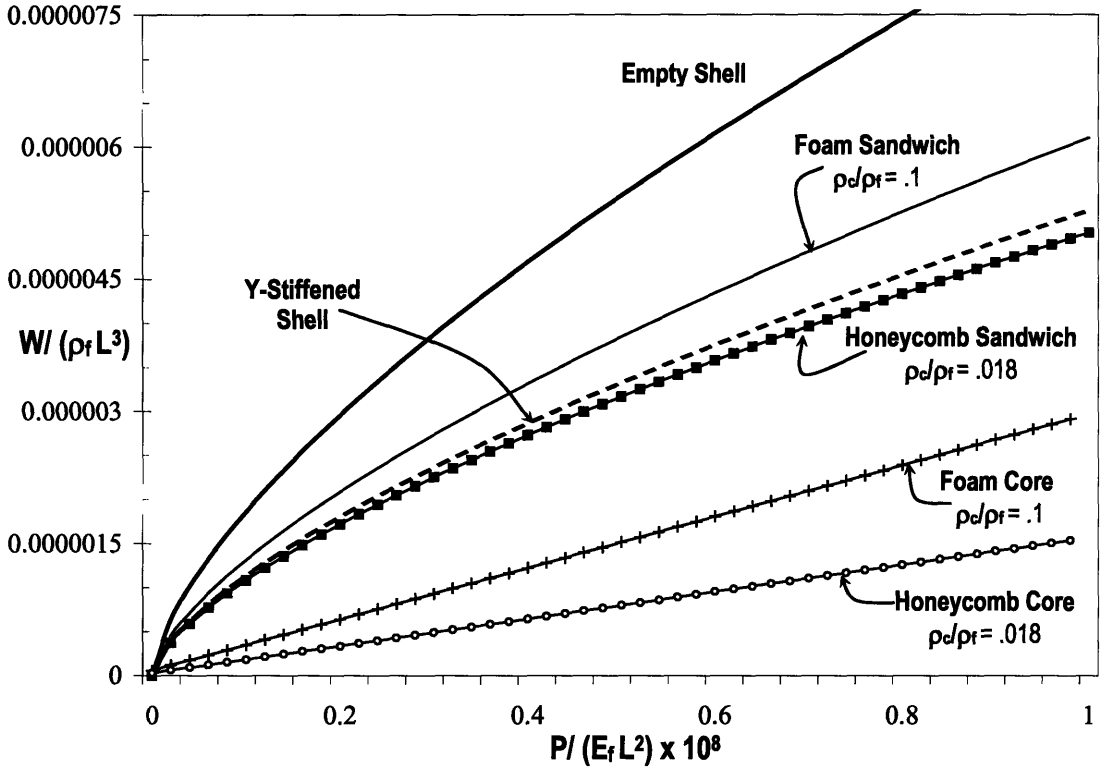

Figure 2.8: Normalized weight index plotted vs. load index. $\gamma \approx 0.3; (50 < R/t < 200)$

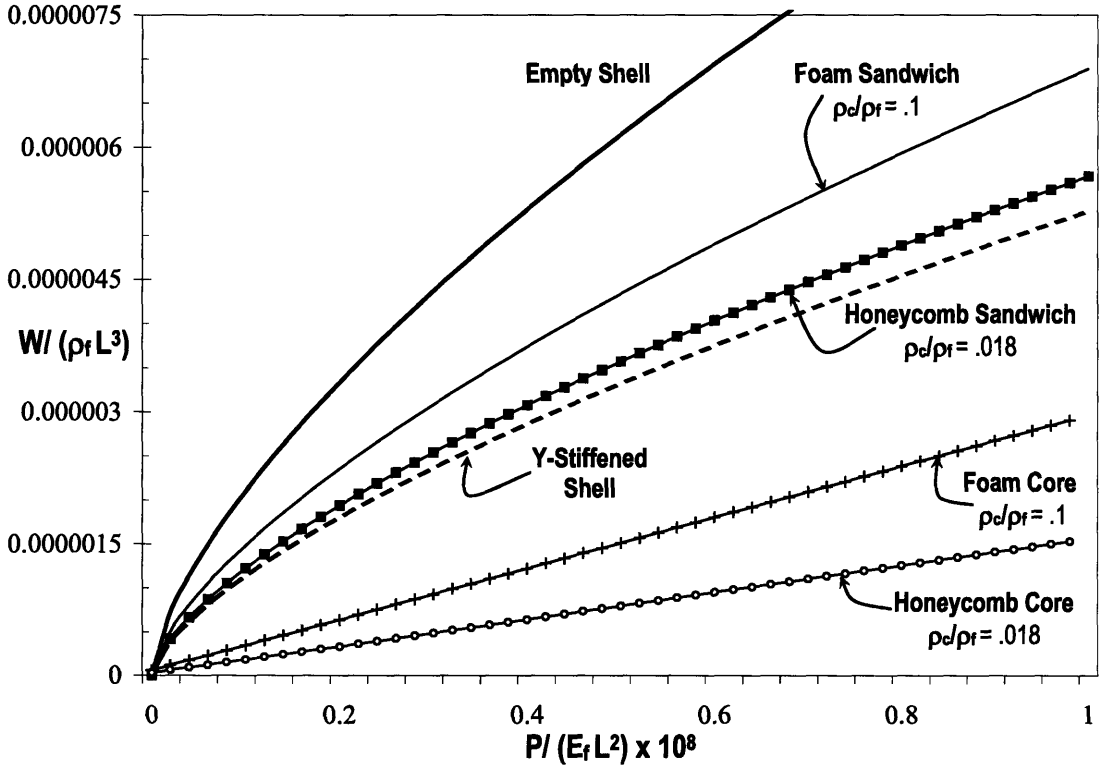

Figure 2.9: Normalized weight index plotted vs. load index. $\gamma \approx 0.2; (R/t > 200)$

2.2.6 Effect of Material

In Figures 2.7-2.9, we have compared compressive structures with different forms of construction assuming that they are composed of the same material, in particular aluminum. The second consideration involved in structural efficiency is concerned with the selection of the material as represented by the parameters ε_y, E,ν and ρ and the shape allowable. According to Ashby [21], materials used in minimum weight design for a given buckling stiffness, are characterized by the performance index:

$$M_1 = \frac{\left(E\phi_B^e\right)^{1/2}}{\rho} \qquad (2.73)$$

Where E = Young's Modulus;

ρ = Material's Density;

ϕ_B^e = Flexural Shape Factor.

Flexural shape factors vary for different sections. For hollow shells, $\phi_B^e = r/t$. In Table 2.2 [22], we have summarized values of the performance index for different materials, assuming the case of hollow shell construction. Note that in Table 2.2, Ashby refers to the shape factor for commercially available tubes, which are optimized for large values of the load index $P/\left(EL^2\right)$. The shape factor for small diameter CFRP tubes is limited by 10 for manufacturing constraints. Similarly, the shape factor for spruce is limited to two, due to fabrication difficulties.

Material	Modulus E (GPa)	Density ρ (Mg/m^3)	Shape factor ϕ_B^e	Index M_1 (GPa)$^{1/2}$/(Mg/m^3)	Price (US \$/kg)
Spruce	5.5	0.3	1-2	6.9-9.7	2-3
Steel (Mild)	210	7.9	1-30	1.8- 10.0	0.2-0.6
Fiberglass	40	1.84	1-10	3.4-10.8	24-35
Al Alloy	69	2.7	1-25	3.1-15.5	1.0-2.0
CFRP	120	1.8	1-10/20	6.1-19.2/27.3	45-56

Table 2.2: Materials for lightweight compression commercial hollow tubes [22].

In order to visualize different values of the performance index, we can refer to Figure 2.10, where density is plotted against the Young's modulus. Here, materials with modulus E and density ρ with different shapes are treated like new materials with modulus $E^* = E/\phi_B^e$ and density $\rho^* = \rho/\phi_B^e$ [22].

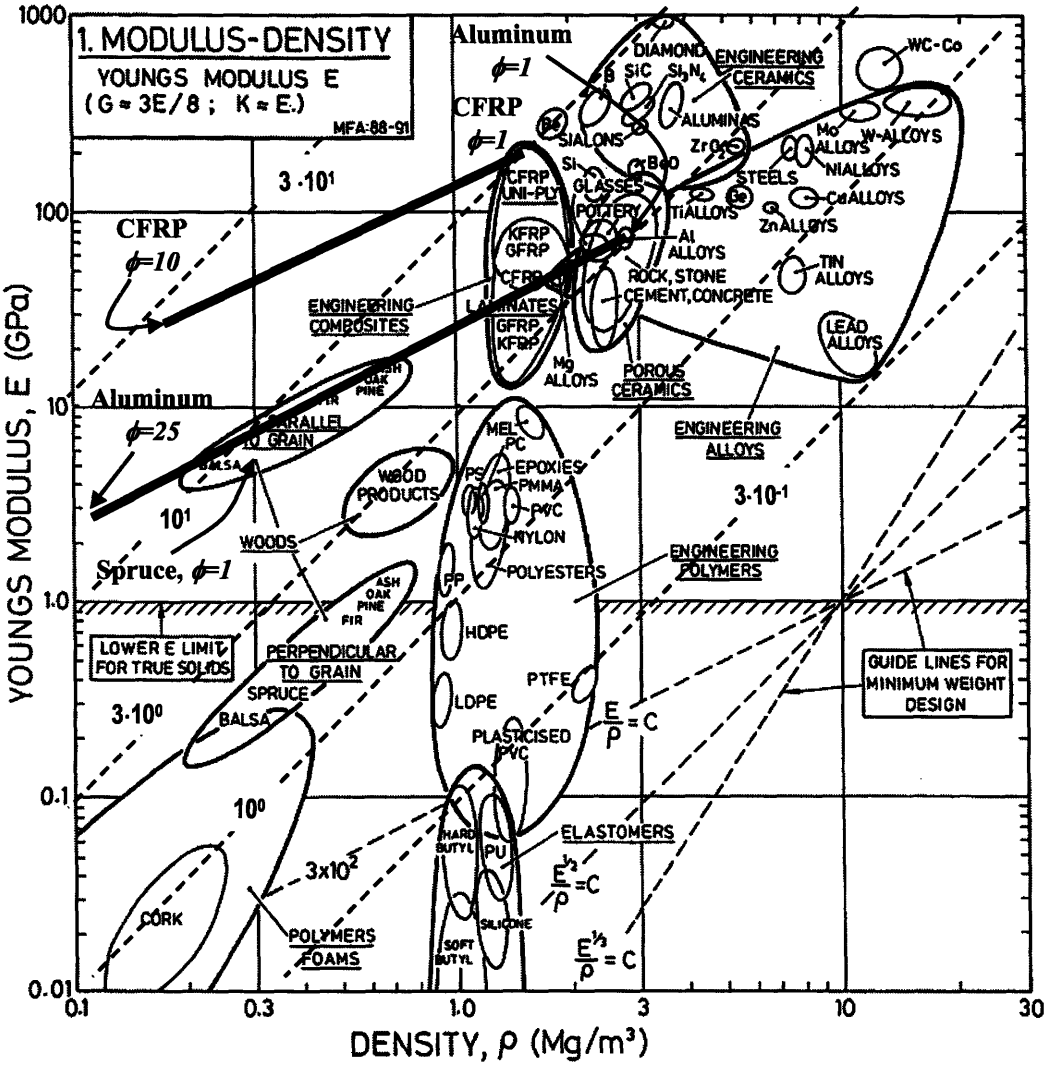

Figure 2.10: Material selection chart for commercial hollow tubes, plotted on the density-modulus chart. The Young's modulus E^* and the density ρ^* are defined as $E^* = E/\phi_B^e$ and $\rho^* = \rho/\phi_B^e$, where ϕ_B^e is the shape factor for hollow cylinder.

We want to evaluate the efficiency of aluminum Y-stiffened, honeycomb/foam sandwich and honeycomb/foam core shells, compared to aluminum or other materials hollow shells.

Considering the case of homogeneous materials, the shape factor is [21]:

$$\phi_e = \frac{4\pi I}{A^2}; \qquad (2.74)$$

In the case of column buckling $P = EI\pi^2 / L^2$: in this case, from $W = \rho AL$ we can write:

$$\phi_e = \frac{4}{\pi} \cdot \left(\frac{P}{EL^2}\right) \Big/ \left(\frac{W}{\rho L^3}\right)^2; \qquad (2.75)$$

For small values of the load index $P/(EL^2)$, the Euler relation is satisfied in all the cases considered. Consequently, in this region, Equation (2.75) can be used to calculate values of shape factors for all the types of construction: these values can then be substituted in Equation (2.73) in order to evaluate the performance index. Figure 2.11 shows plots of the shape factor for increasing load index for the different construction types, up to the limit corresponding to squashing failure for hollow shells.

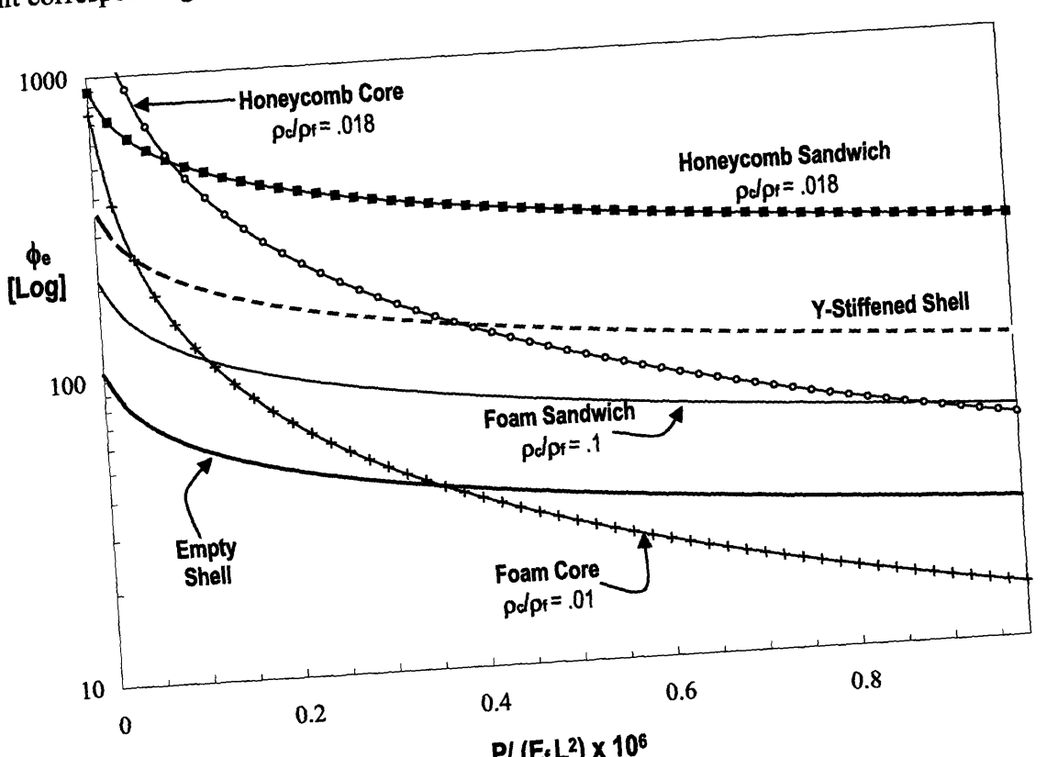

Figure 2.11: Shape factors for hollow, honeycomb- and foam-core shells.

Figure 2.11 shows that foam and honeycomb core shells are particularly efficient at low values of the load index, but their efficiency decays abruptly close to the hollow shell plastic failure region: in this part of the plot, sandwich constructions and stiffened shells seem to perform better. Figure 2.11 show also that constructions incorporating foam or honeycomb find natural application for low values of the load index. This result agrees with what found by Budiansky [8] for foam sandwich cylinders. Table 2.3 gives the performance index for the different types of constructions relative to $P/(EL^2) \approx 10^{-7}$ and $P/(EL^2) \approx 10^{-6}$, assuming $\varepsilon_y = 0.007$ and $\nu = 1/3$.

Construction Type Al Alloy	$P/(EL^2) \approx 10^{-7}$		$P/(EL^2) \approx 10^{-6}$	
	ϕ_B^e	Index M_1 $(\text{GPa})^{1/2}/(\text{Mg/m}^3)$	ϕ_B^e	Index M_1 $(\text{GPa})^{1/2}/(\text{Mg/m}^3)$
Hollow Tube	1-62	6.9-24.2	1-29	6.9-16.6
Y-Stiffened	1-212	6.9-44.8	1-99	6.9-30.6
Foam Sandwich $\rho_c / \rho_f = 0.1$	1-124	6.9-34.2	1-58	6.9-23.4
Honeycomb Sandwich $\rho_c / \rho_f = 0.018$	1-522	6.9-70.3	1-243	6.9-48.0
Honeycomb Sandwich $\rho_c / \rho_f = 0.05$	1-184	6.9-41.7	1-96	6.9-30.1
Foam Core $\rho_c / \rho_f = 0.1$	1-150	6.9-37.7	1-15	6.9-11.9
Honeycomb Core $\rho_c / \rho_f = 0.018$	1-540	6.9-71.5	1-54	6.9-22.6

Table 2.3: Different constructions for lightweight compression structures.

The advantage of aluminum honeycomb/foam core construction in lightweight compression structures is evidenced by comparing the performance indices in Table 2.3 with the ones in Table 2.2, relative to hollow tubes made of different materials.

2.3 Cost Estimation

In the previous paragraph, the performance of shells used in compression structures employing honeycomb or foam was discussed. In this paragraph, the cost of the same structures will be analyzed with the following assumptions:

- Aluminum foam or honeycomb are regarded as input materials and economies of scale associated with their purchase are neglected;
- Aluminum foam is obtained in hollow tubes produced through the powder route; this hypothesis is justified by the technical difficulty to manufacture hollow foam column by laser or water jet cutting;
- Only sandwich structures are considered.

Methods used to manufacture sandwich foam/honeycomb shells were discussed in the last chapter. Here we assume that the composite structure is formed in a one-step process through prepeg lay-up in an autoclave, where the inner and outer form tool have different coefficients of thermal expansion. We refer to the fabrication of a shell, characterized by the parameters listed in Table 2.4.The material cost is given in Table 2.5.

Geometrical Parameter	Honeycomb core	Foam core
External radius (m)	0.25	0.25
Length (m)	10	10
Core thickness (m)	0.0064	0.015
Face thickness (m)	0.0005	0.0005
Adhesive used [22]	Hexcel F-134	Hexcel F-134
Face sheet metal	Al Alloy 6061-T6	Al Alloy 6061-T6
Core metal	Al ¼"-5052-6.0	Alulight 0.32 (Mg/m^3)
Weight of the Face Metal (kg)	42.4	42.4
Weight of the Core (kg)	9.0	75.4
Weight of the Adhesive (kg) [23]	18.9	18.9
Total Weight (kg)	70.3	136.7

Table 2.4: Sandwich structures under investigation.

Parameter	Honeycomb core	Foam core
Unit cost of core ($/kg)	243 [24]	24 [23]
Unit cost of face sheets ($/kg)	6 [26]	6 [26]
Unit cost of resin ($/kg)	8 [27]	8 [27]
Cost of core ($)	2187	1809
Cost of face sheet ($)	255	255
Cost of resin ($)	151	151
Total material cost ($)	2593	2215

Table 2.5: Cost of materials.

The cost of tube is calculated according to the following formula [28]:

$$C = \left[\frac{\sum_i m_i C_{m,i}}{1-f}\right] + \left[\frac{C_t}{n}\right] + \left[\frac{\dot{C}_L}{\dot{n}}\right] + \left[\frac{\dot{P}C_e}{\dot{n}}\right] + \left[\frac{A\dot{C}_S}{\dot{n}}\right] + \left[\frac{\dot{C}_{ip}}{\dot{n}}\right] + \left[\frac{C_t}{t_t}\right] \quad (\$/unit) \qquad (2.76)$$

, where $C_{m,i}$ = cost of the material i ($/kg);

C_t = cost of tooling ($/unit);

$\dot{C}_L$ = overhead rate ($/hours);

C_e = cost of energy ($/(kW·h));

$\dot{C}_S$ = cost of space ($/(m^2·h));

$\dot{C}_{ip}$ = royalty payments, cost of intellectual properties;

m_i = mass of the material i (kg);

n = production volume (units);

$\dot{n}$ = production rate (units/h);

A = area (m^2);

$\dot{P}$ = power (kW);

f = total material utilization fraction.

t_t = tooling life (units);

The overhead rate in (2.76) can be calculated according to the formula:

$$\frac{\dot{C}_L}{\dot{n}} = \frac{1}{\dot{n}}\left\{\left[\dot{C}_{LO}\right] + \left[\frac{C_C}{t_c \cdot L_f} \cdot 24 \cdot 365\right]\right\} \quad (\$) \qquad (2.77)$$

, where t_c = capital write-off time (years);

L_f = load factor (fraction of time over which the equipment is used);

$\dot{C}_{LO}$ = basic overhead rate; e.g. given by the cost of the labor, maintenance, building, administrative, etc. ($/unit);

C_C = cost of capital ($);

Neglecting the energy, space, and IP cost, equation (2.75) can be rewritten as:

$$C = \left[\frac{\sum_i m_i C_{m,i}}{1-f}\right] + \frac{1}{n}\left[C_t\right] + \frac{1}{\dot{n}}\left[\dot{C}_L\right] + \frac{1}{t_t}\left[C_t\right] \quad (\$/unit) \qquad (2.78)$$

Values relative to our process were taken from the CES software and database [25] and are listed in Table 2.6.

$m_{honeycomb}$ (kg)	9.0	t_t (units)	1,000
m_{sheet} (kg)	42.4	C_t ($)	10,000
m_{resin} (kg)	18.9	C_C ($)	500,000
m_{foam} (kg)	75.5	$\dot{C}_{LO}$ ($/hour)	90
$C_{m,honeycomb}$ ($/kg)	243	t_c (year)	5
$C_{m,sheet}$ ($/kg)	6	$\dot{n}$ (unit/hour)	0.5
$C_{m,resin}$ ($/kg)	8	F	1
$C_{m,foam}$ ($/kg)	24	L	0.5

Table 2.6: Resources consumed in making composite honeycomb/foam core shell.

The variation of the unit cost with the production volume for both the honeycomb and foam sandwich structures is shown in Figures 2.12 and 2.13.

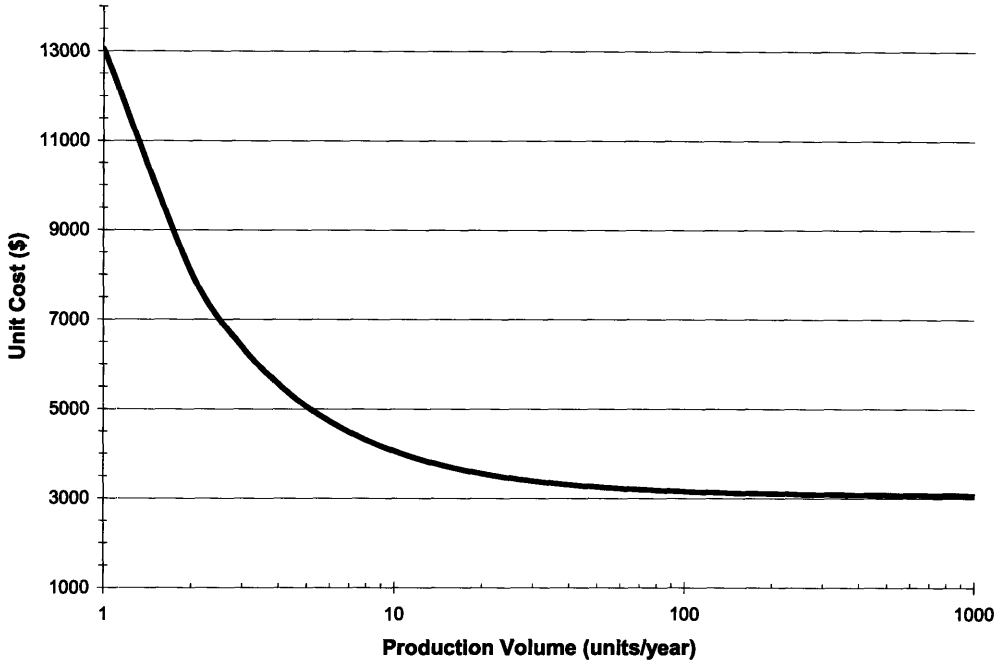

Figure 2.12: Unit cost plotted against production volume for honeycomb sandwich shell.

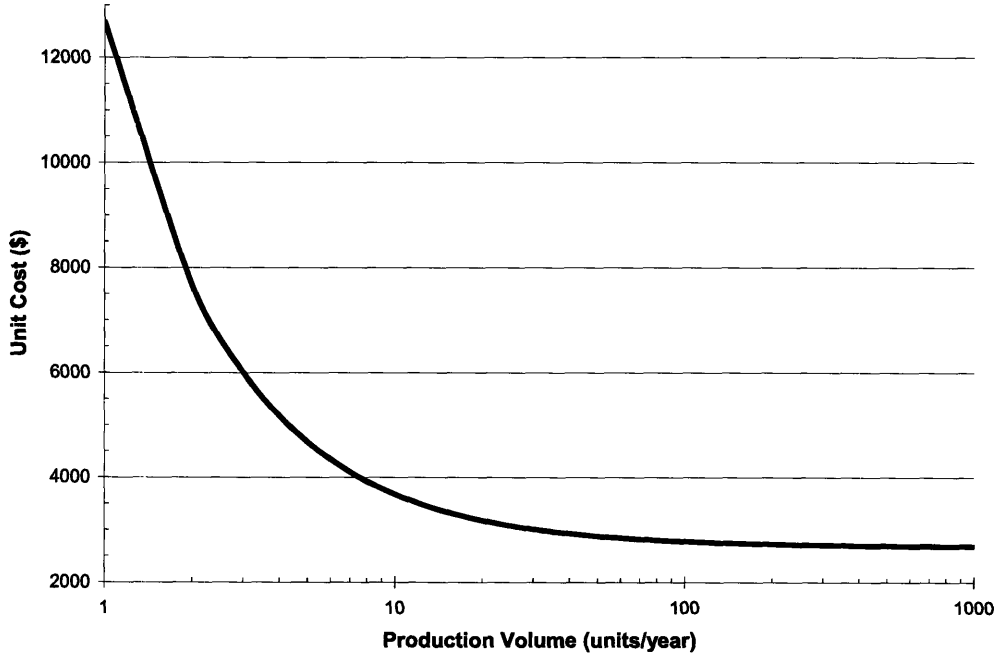

Figure 2.13:Unit cost plotted against production volume for foam sandwich shell

The results of these simplified cost analysis are:

1. The economic cost for the honeycomb and foam sandwich shells characterized by the properties given in Table 2.4 and 2.5 is respectively 3,100$ and 2,700$.
2. The economic cost is reached with a relatively small production volume; this indicates that economies of scale using this method of fabrication are not present.
3. The unit cost is dominated by the cost of the input materials.
4. Other main component of the manufacturing cost are the cost of the equipment, as the autoclave requires a high capital investment (see Table 2.6), and tooling costs, which are considerable due to strict resin cross-linking requirements.

In the next paragraph, results from the technical assessment and the cost estimation are used to discuss the value in the market of the foam/honeycomb filled tubes.

2.4 Value in the Market

The value in the market of either a new material can be assessed through a two-step analysis. In first place, the performance/cost of the new material has to be compared to existing materials. The information given by the performance-cost tradeoff plot is useful in order to scan different *potential markets*, where we can have advantages given by the parameters identified in the technical analysis. New materials characterized by best value in the market can still be not viable because the substitution time is large. For this reason, in the second place, barriers to entry for the new material have to be assessed.

In Figure 2.14, performances and costs for different lightweight compression cylindrical structures are represented. The prices are relative to common manufacturing techniques for tubes with a diameter of 500 mm and are obtained from the *CES* [25] or by the cost model described in the previous paragraph. Performance indices are taken by Table 2.2 and 2.3. Tubes with metal cellular core have performances comparable to CFRP, but represent a better cost alternative. This is mainly due to the substantial cost of the CFRP, which is about $50 per kilogram, as one can see in Table 2.2. On the other hand, shells with a metallic core have better performances than tubes produced with any other materials, but are more costly.

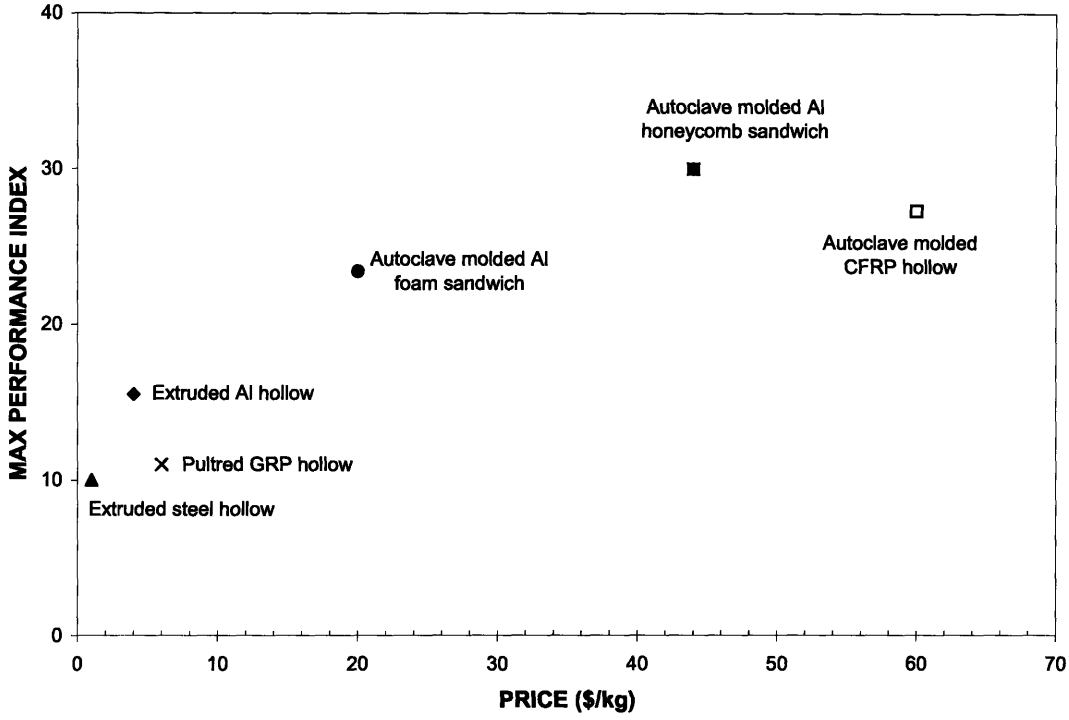

Figure 2.14: Performance-cost tradeoff for structural compression lightweight tubes.

The position of metal cellular core tubes in the price/performance plot suggests that the maximum utility for these structures lies in the transportation and sport industry, where rules the empirical law: "the faster a product moves, the more one will pay for a lower density material". In Table 2.7 is given the utility of weight saving in transport and sport systems, over the life of a vehicle [2].

Transport System	U (US $/kg)	High End Utility Requirement
Family Car (based on fuel saving)	0.5 – 1.5	Value of payload
Truck (based on payload)	5 – 10	Value of payload
Civil Aircraft (based on payload)	100 – 500	Power/weight ratio guarantee limit
Military Aircraft (based on payload)	500 – 2,000	Power/weight ratio guarantee limit
Space Vehicle (based on payload)	1,000 – 10,000	Value of payload
Bicycle (based on perceived performance)	1 – 1,000	Tour de France Standard

Table 2.7: Utility of Weight Saving in Transport Systems [2]

The utility of mass saving can be used together with the performance-cost tradeoff plot in order to understand the real value of the substitution (Figure 2.15).

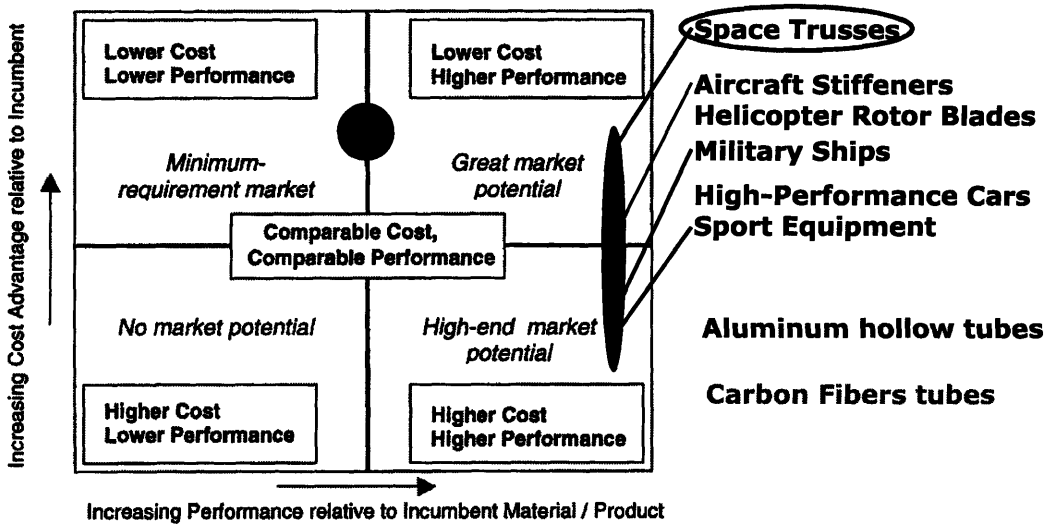

Figure 2.15: Types of Performance/Cost Substitution for cellular metal shells.

Two particular structures are studied for replacements: CFRP and aluminum hollow tubes. Substituting CFRP with aluminum foam-core shells is a viable option, even though the introduction of new materials characterized by comparable performances and lower price has proved to have a long penetration time [2]. On other hand, aluminum honeycomb-core sandwich shells are characterized by lower prices and higher performances than CFRP tubes and have great potential for replacement. The substitution of aluminum hollow tubes with both aluminum foam and honeycomb core tubes seems to be more attractive. The car industry is not the right sector due to the little utility in saving weight for load-bearing components at this time. The substitution in the sport industry depends on the perceived utility by customers. The aerospace market seems to be the more promising market, where we can get the highest value between cost and performance.

The second factor to be considered in order to assess the value in the market of a new material is the *time to substitution.* This is not typically a parameter, but a function of the relative penetration in the market with the time. Innovative materials are characterized by times to substitution difficult to forecast, but basic principles exist. In first place, it is

generally believed that the substitution period correlates with price and performance characteristics. Fisher-Pry [29] have calculated the time to substitution for 100% penetration for materials in general application with lower cost and higher performance in 20 years, lower cost and compatible performance 30 years, lower cost and lower performance 50 years, higher cost and higher performance 40 years. This is generally true if the substitution of a new material is in the same market. When we consider the introduction of new materials in different markets, e.g. the transportation and the sport market, and want to estimate the time to substitution, we have to refer to the concept of *value chain*. The value chain can help us to understand the forces and the constraints driving changes in the materials industry. The idea is based on the evidence that from the lab scale to the commercialization of a new material, different changes have to take place:

1. Changes in material attributes;
2. Changes in design requirements;
3. Changes in industry structure;
4. Changes in the organizational structure;
5. Changes in the level of risk needed to drive innovation;
6. Evolving customers needs/wants;
7. Changes in the perception of goods and services;

All of these changes are obstacles to the introduction of the new material and represents barriers slowing the process of replacement (see Figure 2.16).

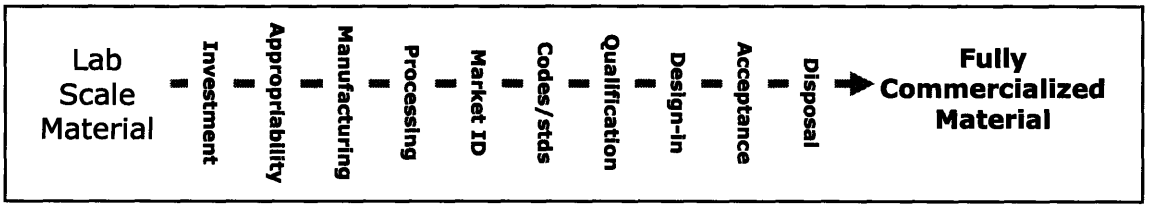

Figure 2.16: Value chain in material innovation.

Choosing applications where the barriers between the various steps in the value chain are minimized helps to reduce the time to market of a new product and consequently the investment risk. The concept can be extended to the application of cellular core shells in aircraft applications, as wing stiffeners or rotor blades: the substitution time is enlarged

by the design time, because safety tests 15 years long are required before the introduction of a new material in such structures. Thus, commercialization of foam/honeycomb core tubes in aerospace applications is not viable in short times. In the same way, aluminum foam tubes could be used in radically new designs, which would take advantage of the multi-dimensional attributes offered by metal foams, but even in this case these applications will be slowed down both by the lack of designer awareness or confidence in metal foams and by manufacturing difficulties.

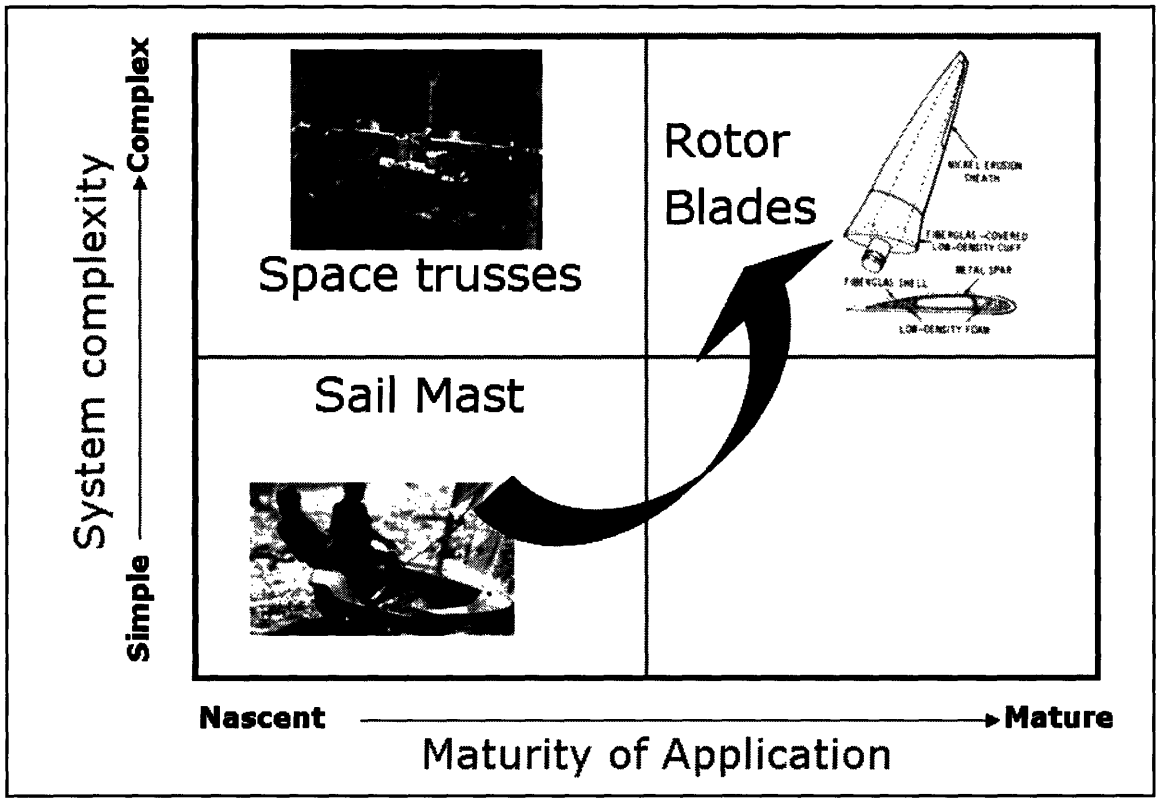

Figure 2.17: Market applications for maturity of application and system complexity.

The question how to speed-up the commercialization of a new material in the innovation pipe represented in Figure 2.16 has being analyzed by Musso [6]. He has identified two particularly sensible parameters: the complexity of design/application and the maturity of the applications where the new materials are used. Innovative materials characterized by rapid substitution times find generically the first application in products with low level of complexity (e.g. plastic in hoola-hoop). Subsequently they move to an area of short shift, where production volumes and numbers of applications increase but still have a low-level

of complexity (e.g. plastic in garbage can). Only in the end, when the materials properties and possible limitations are fully understood, applications in complex designs are sought. Businesses pursuing commercialization in the embryonic phase of the material in complex applications (super enablers) are distinguished by high capital commitment and risk, but if successful, are characterized by higher and quicker payback. Generally, this condition is to be sought for speculation and must be avoided if the objective is to establish a stable business. More often, this type of innovation is pursued by industry consortia, universities, and government agencies (the military, in particular, sponsors about 60 percent of Federal advanced structural composites research and development in the United States [3]).

In Figure 2.17 is represented a road map for a business based on tubular structure with foam/honeycomb core for structural purpose. Two applications have been identified in particular for quick substitution: space trusses and sporting equipment. The substitution of current aluminum space trusses with foam/honeycomb core tubes is feasible if supported by the military or some space agency, but the low production volume and the high system complexity does not justify entrepreneurial risks. Sport equipment is generally characterized by large market volume and short time to substitution. In particular, initial business applications should be represented by products like sail masts, where the technical advantages of the foam/honeycomb core are emphasized and we believe is possible to capture a good portion of the market, now represented by anodized extruded aluminum masts. In the next section, the sailboat market is analyzed in detail in order to understand the real need for the introduction of this innovation and forecast the market growth.

2.5 References

[1] H.-P. Degischer, B. Kriszt, *Handbook of Cellular Metals: Production, Processing, Applications,* Wiley-VCH Verlach, Weinheim, **2002.**

[2] E.M.A. Maine, "Innovation and Adoption of New Materials", University of Cambrige, U.K., *PhD. Dissertation,* **2000.**

[3] Congress of the United States, Office of Technology Assessment, *Advanced Materials by Design,* OTA-E-351, Washington, DC; U.S. Government Printing Office, **1988.**

[4] E.M.A. Maine, M.F. Ashby, "An investment methodology for materials. Part 1: the methodology", *Mater. Design,* Elsevier, **2002.**

[5] C.G.E. Mangin, R. De Neuville, F. Field, J. Clark, "Defining Markets for New Materials. Developing a Utility Methodology with Case Application.", *Resources Policy*, 21, p. 169-178, **1995.**

[6] K. Musso, "Beating the System: Breaking the Barriers of Commercialization of New Materials", Massachusetts Institute of Technology, *Ph.D. Dissertation,* **2004.**

[7] Gerard, G., *Minimum Weight Analysis of Compression Structures*, New York University Press, New York, **1956.**

[8] Budiansky, B., "On the Minimum Weight of Compression Structures", *International Journal of Solids and Structures,* 36, p. 3677-3708, **1999.**

[9] S.P. Timoshenko and J.M. Gere, *Theory of Elastic Stability*, 2nd edition, McGraw-Hill, New York, **1961.**

[10] Anon., *Buckling of Thin-Walled Circular Cylinder*, NASA Space Vehicle Design Criteria. NASA SP-8007, **1965** (revised **1968**).

[11] B. L. Agarwal, L.H. Sobel , "Weight Comparison of Optimally Stiffened, Unstiffened, and Sandwich Cylindrical Shells", *AIAA J.* 14, 1000-1008, **1977.**

[12] B. L. Agarwal, Davis, R.C., "Minimum Weight Designs for Hat-Stiffened Composite Panels Under Uniaxial Compression", NASA TN-D 7779, **1974.**

[13] Schuette, E.H., *Charts for the Minimum Design of 24S-T Aluminum Alloy Flat Compression Panels with Longitudinal Z-section Stiffeners.* NACA Technical Report 827, **1945.**

[14] Zahorski, A., "Effects of Material Distribution on Strength of Panels". *J. Aeronautical Sciences* 11, p. 247-253, **1944.**

[15] Farrar, D.J. "The Design of Compression Structures for Minimum Weight", *J. Royal Aeronautical Society* 53, p. 1041-1052, **1949.**

[16] Catchpole, E.J., "The Optimum Design of Compression Structures having Unflanged Integral Stiffeners", *J. Royal Aeronautical Society* 58, p. 765-768, **1954.**

[17] J.W. Hutchinson and M.Y. He, "Buckling of cylindrical sandwich shells with metal foam cores", *International J. of Solids and Structures* **2000**, *37*, p.6777-6794.

[18] Plantema, F.J., *Sandwich Construction*, John Wiley & Sons, Inc., New York, **1972.**

[19] Allen, H.G., *Analysis and Design of Structural Sandwich Panels*. Pergamon Press, Oxford, **1969.**

[20] G.N. Karam and L.J. Gibson, "Elastic buckling of cylindrical shells with elastic cores – I. Analysis" in *Int. J. Solids Structures*, **1995**, *32*, p. 1259-1283.

[21] P. Seide, "The Stability under Axial Compression and Lateral Pressure of Circular-Cylindrical Shells with a Soft Elastic Core", *J. Aerospace Sci. 32*, p. 641-650, **1962**

[22] M.F. Ashby, *Materials Selection in Mechanical Design*, Butterworth-Heinemann. Oxford **1992.**

[23] D. Zenkert, *The Handbook of Sandwich Construction,* EMAS, **2000.**

[24] T. Bitzer, *Honeycomb Technology,* Chapman & Hall, London, **1998.**

[25] CES, *The Cambridge Engineering Material Selector*, Granta Design Ltd, **1999.**

[26] United Aluminum Corporation, http://www.unitedaluminum.com, **2004.**

[27] Applied Vehicle Technology, http://www.avtcomposites.com/resins, **2004.**

[28] M.F. Ashby, A. G. Evans, N.A. Fleck, L.J. Gibson, J.W. Hutchinson, H.N.G. Wadley, *Metal Foams: a Design Guide*, Butterworth-Heinemann, Oxford **2000**.

[29] J.C. Fisher, R.H. Pry, "A Simple Substitution Model of Technical Change". Technical Forecasting and Social Change 3, pp.75-88, **1971.**

Chapter 3

Sailboat Masts with Cellular Metal Core

"When I saw her masts across the River rising queenly,
Built out of so much chaos Brought to law,
I learned the power of knowing How to draw,
Of beating through into the Perfect line:
I vowed to make that power of Beauty mine"

J. Masefield

3.1 Introduction

Masts, together with spreaders and stays, are designed as members to transfer/withstand the load generated in the sails to the hull. In this section, the application of cellular metallic materials in sailboat masts is discussed. The first part deals with the conventional mast designs. The load acting on the mast is mainly compressive. Consequently, masts need to have longitudinal and transverse moment of inertia large enough to prevent global buckling. In addition, masts have also to be as light as possible in order to lower the heeling moment acting on the sailboat. These requirements lead to elliptical tubes with thickness limited by local buckling and materials characterized by the maximum ratio between stiffness and density. In the second part, we compare conventional designs employing aluminum-extruded profiles with cellular aluminum-filled masts, focusing on the design of the mast of a 12-metres long yacht. This comparison is made as first approximation, considering masts characterized by a polar moment of inertia equal to the average of the longitudinal and transversal moments of inertia. In second approximation, we compare the extruded and cellular metal composite masts, considering the elliptical shape, but using a simplified analysis to evaluate the local buckling. Finally, the possibility of extending this technology to CFRP masts is discussed.

3.2 Mast Load System

In order to calculate the load acting on the mast, we start by introducing the various forces and moments acting on a sailing yacht (Figure 3.1) [1]. In equilibrium condition,

the driving force from the sail is balanced by the drag produced by the water. The force acting on the sails has also another component, which is balanced by a hydrodynamic side force. Considering the load system in the plane perpendicular to the direction of motion of the yacht, we will assume that the lateral component of the sail force (called heeling force) and the hydrodynamic force are applied at right angles to the mast in points called respectively center of effort of the sail (C.E.) and center of buoyancy (C.B.). The moment generated by the heeling force about the center of gravity, called heeling moment (H.M.), is balanced by the righting moment (R.M.), equal to the couple created by the weight and the buoyancy force with lever arm ψ (see Figure 3.1).

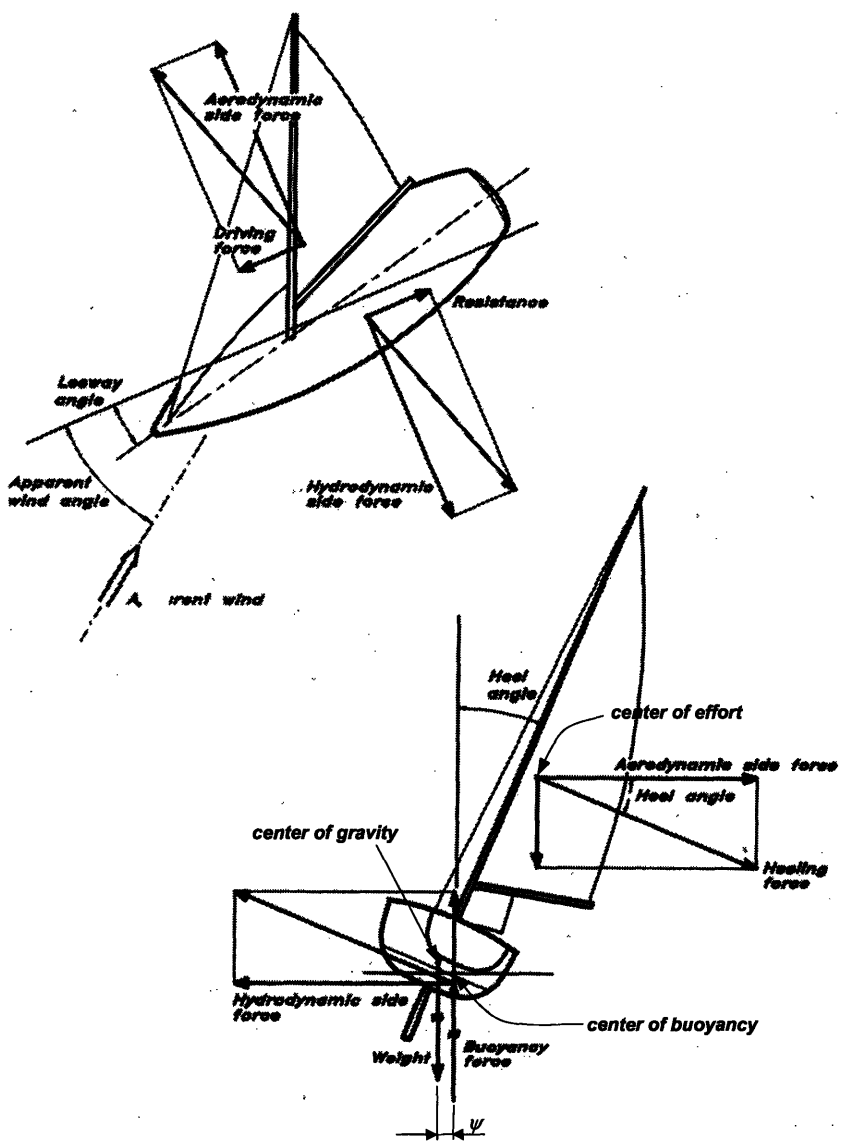

Figure 3.1: Forces on a sailing yacht [1].

The stress patterns in the sailcloth caused by the wind are represented in Figure 3.2.

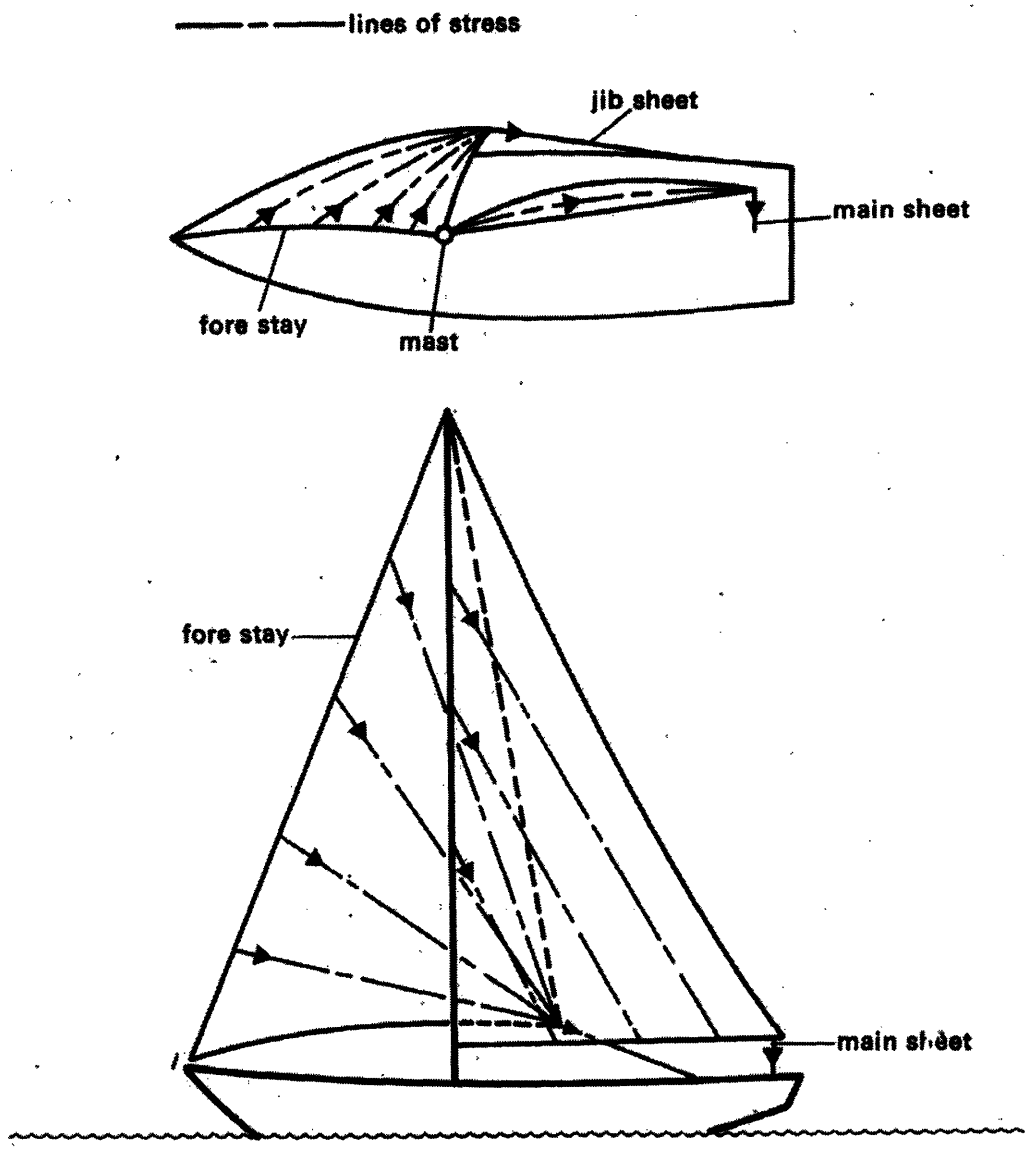

Figure 3.2: Sail loads on rigging [2].

The stress generated by the wind is carried mainly by the fore- and back-stay and the lateral shrouds, which are loaded in tension and is transferred to the mast as compressive load (see Figure 3.3) [3]. The mast is also bent by a lateral distributed force from the mainsail luff and a lateral point load from the boom [3]: as the entity of these forces is small, we will neglect their contribution.

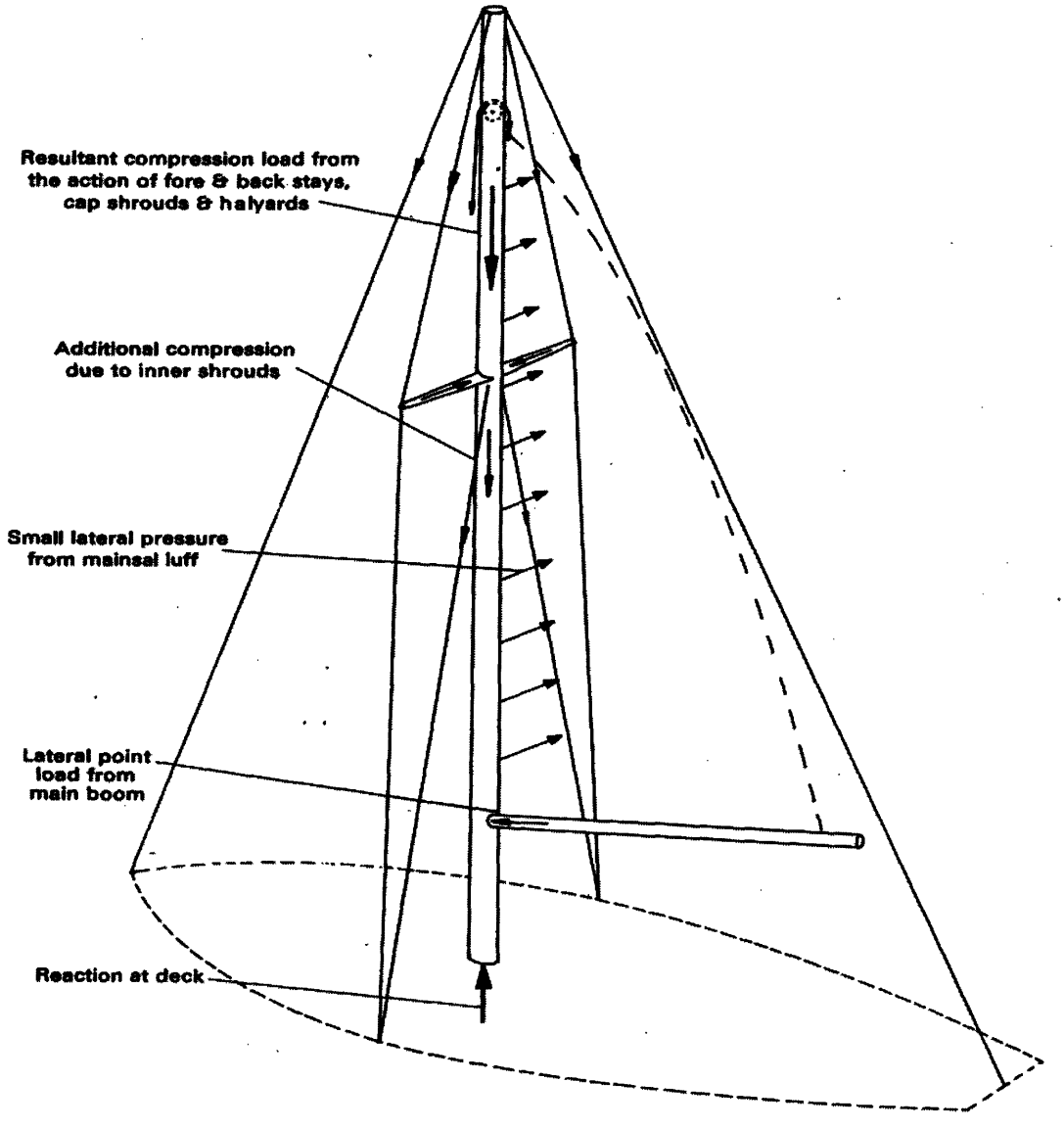

Figure 3.3: Mast load system [3].

Larsson and Eliasson [1] and Skene [4] use an approximate approach to estimate the compressive force acting on the mast, due to the tension in the shrouds and in the stays, considering the case in which the rig is loaded by a foresail only. In this case, the forces coming from the wind pressure are accounted through a transverse force T applied in the mast head, whose magnitude is simply the righting moment divided by the distance from the waterline to the uppermost shroud l (see Figure 3.4): it does not matter what kind of fractional rig is used. For simplicity, in Figure 3.4 we refer to a rig with no spreaders.

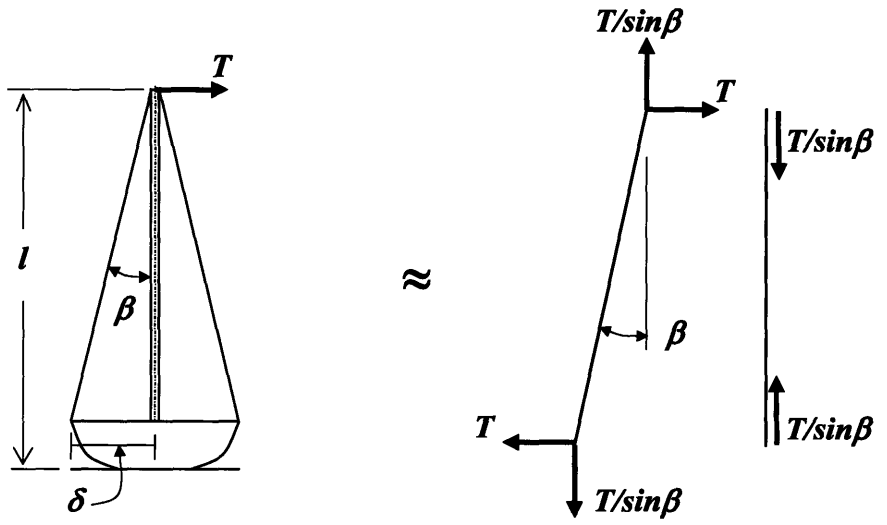

Figure 3.4: Mast compressive load calculation.

Defined F as the compressive force acting on the mast and β as the shroud angle (see Figure 3.4), then

$$F = \frac{T}{\sin\beta} = \frac{T \cdot l}{\sin\beta \cdot l} \approx \frac{R.M.}{\delta}[N] \qquad (3.1)$$

The compressive force, due to the weight of the mast itself, rigging, sails and boom and the pull of the halyards is not included in equation (3.1), but can be neglected [1].

When the yacht is heeled, the distance ψ between the weight and the force of buoyancy increases and so does the righting moment. Consequently, according to equation (3.1), the compressive force acting on the mast will also become larger with increasing heel angles. According to the literature [1-4], the maximum heel angle should not be larger than 30°: letting the boat heel more results in increased resistance (see Figure 3.1) and a slower yacht. With this assumption, the maximum allowable compressive force is:

$$F_{max} = \zeta \cdot \frac{R.M._{30}}{\delta}[N] \qquad (3.2)$$

where $R.M._{30}$ is the righting moment calculated at 30° of heel angle and ζ is a safety factor, which according to Skene [4] should be taken between 2.7 and 4.

3.3 Mast Design: Functional Requirements

In order to find practical use the mast needs to satisfy certain *functional requirements*, which are:

1. *Stiffness;*
2. *Minimum Weight;*
3. *Maximum Aerodynamic Efficiency;*
4. *Price;*
5. *Easy of Maintenance;*
6. *Reliability;*
7. *Resistance to Environmental Damages;*

In the next part, we discuss specifically how stiffness, minimum weight, and maximum aerodynamic efficiency are correlated with the mast material and design.
The final price of the mast and its lifetime are also correlated to the choice of the material, the shape chosen and the fabrication methodology and will be considered later in the discussion.

3.3.1 Stiffness

3.3.1.1 Global Buckling

The mast is basically a column loaded in compression that will fail by elastic buckling at a critical load F_{crit} given by Euler's formula [5]:

$$F_{crit} = \frac{n^2 \pi^2 EI}{l^2} [N] \qquad (3.3)$$

where l = length of the column (m);
I = moment of inertia (m^4);
E = Young's modulus (N/m^2);
n = half-wavelengths in buckled shape (this factor depends on the constraints applied at the ends of the column). [6]

Theoretical values of n are one for free-free, pinned-pinned, guided-guided, and fixed-guided b. c.; ½ for guided-free, guided-pinned, fixed-free b. c.; two for fixed-fixed b. c. and $\sqrt{2}$ for fixed-pinned boundary conditions. Values used in engineering applications are reduced for safety reasons. Generally, masts stepped on the keel can be considered as columns with one fixed end and one pinned end; while masts stepped on deck are regarded as columns with two pinned ends [4]. The value of n in equation (3.3) can be increased by bracing the mast, so that the unsupported sections are shortened. In the athwart ship direction, spreaders can be used to divide the mast in short sections. Rigs with increasing numbers of spreaders, which will be considered in this discussion are represented in Figure 3.5. The denomination M is for masthead rig, which means that the shrouds and the stays are fixed in the top of the mast, so that the whole mast is compressed. In the same way, F denotes fractional rig, which means that just a fraction of the total height of the mast (usually $^3/_4$ or $^7/_8$). In the fore- and aft-direction, it is more difficult to provide support to the mast. Different solutions are shown in Figure 3.6: lowers shrouds, runners, inner forestay, and checkstay can be used. It is an obvious extension that the more spreaders and shrouds used transversely and intermediate forestays and running backstays used longitudinally, the smaller the allowable mast section for same buckling load, but also the more the cost of the rig and the more the skill required to trim and tackle.

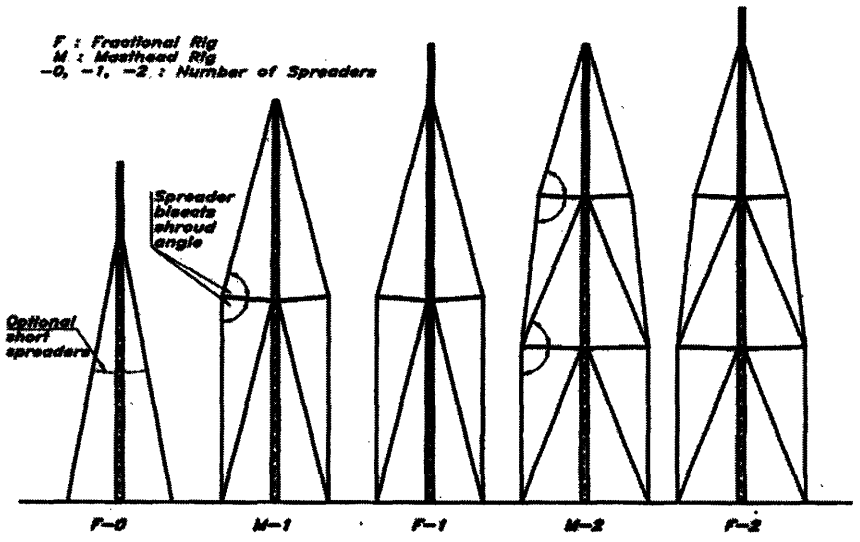

Figure 3.5: Types of rig considered in the study [1].

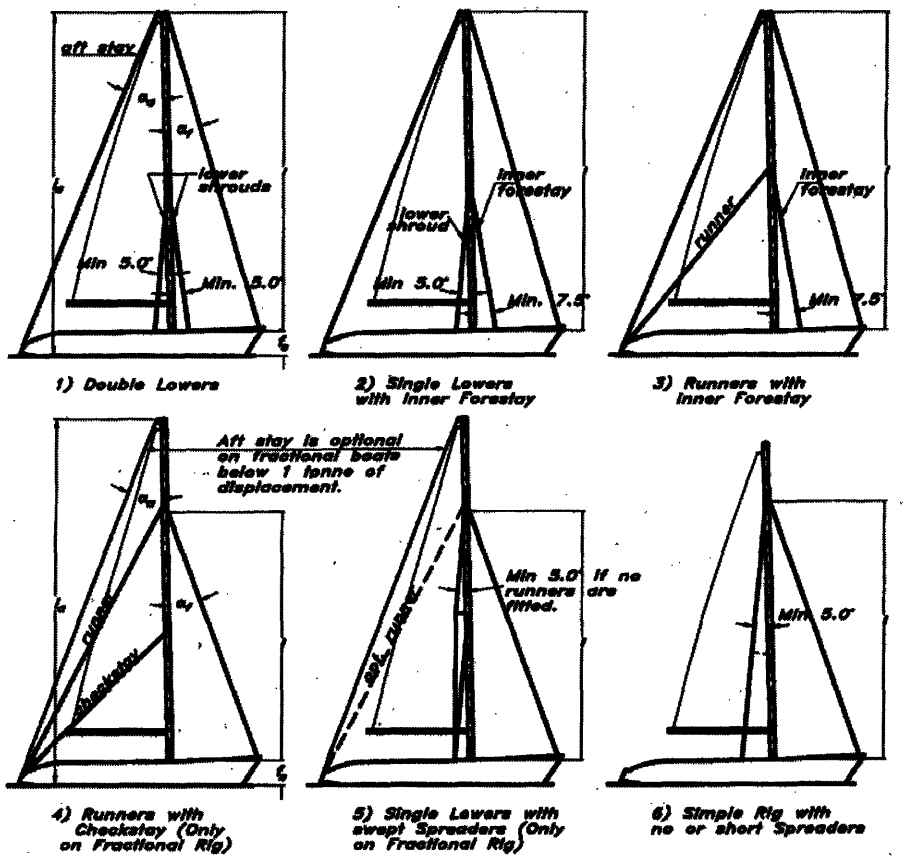

Figure 3.6: Types of staying [1].

In the following part, the transverse and longitudinal stability of the mast are discussed separately. The notation used is represented in Figure 3.7.

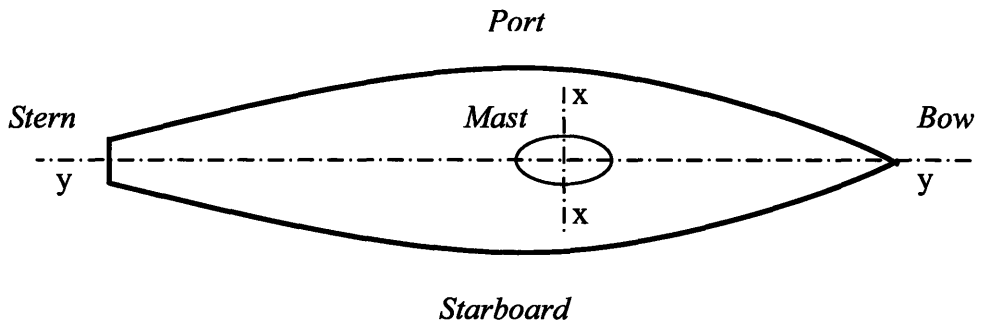

Figure 3.7: Reference system.

3.3.1.2 Transverse mast stiffness $E \cdot I_{yy}$

The transverse mast stiffness is calculated separately for each panel. From equation (3.3), defining p as the panel number (see Figure 3.8) then:

$$E \cdot I_{yy}(p) = \frac{F_{crit}(p) \cdot l(p)^2}{\pi^2 \cdot n_{yy}(p)^2} \quad [mm^4] \qquad (3.4)$$

where:

- $l(p)$ = actual panel length;
- $F_{crit}(p)$ = maximum compressive load acting on the mast. For panel 1 or F-0 rig, $F_{crit}(1)$ is still defined according to equation (3.2); for panel 2, $F_{crit}(2)$ is decreased by $\sigma_{s1} \cos\beta_1$; for panel 3, $F_{crit}(3)$ is decreased by $\sigma_{s1} \cos\beta_1 + \sigma_{s2} \cos\beta_2$; where β_1 and β_2 are angles defined in figure 3.8; σ_{s1} and σ_{s2} are the tensions respectively in the lower and intermediate shrouds. Methods used to calculate the tension in the shrouds, σ_{s1} and σ_{s2}, can be found in literature [1].
- $n_{yy}(p)$ = half- wavelength in buckled shape; for panel 1 or F-0 rig, $n_{yy}(1)$ = 1.13 for mast stepped in the keel (theoretical value of the buckling factor for fixed-pinned b. c. reduced by 20%) or $n_{yy}(1)$ = 0.8 for mast stepped in the deck (theoretical value of the buckling factor for pinned-pinned b. c. reduced by 20%) [4]. For other panels, for simplicity, we calculate $n_{yy}(p)$ assuming pinned-pinned conditions, but reducing the theoretical value of the buckling factor of 30% [1].

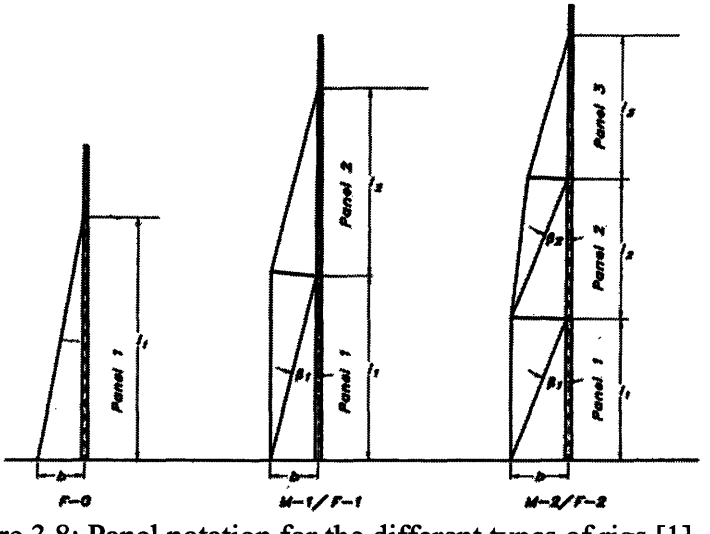

Figure 3.8: Panel notation for the different types of rigs [1].

3.3.1.2 Longitudinal mast stiffness $E \cdot I_{xx}$

The longitudinal mast stiffness (see Figure 3.7) is calculated according to equation (3.3):

$$E \cdot I_{xx} = \frac{F_{crit} \cdot h^2}{\pi^2 \cdot n_{xx}^{\ 2}} \quad [mm^4] \qquad (3.5)$$

where

- h = height above the deck to the highest sail carrying forestay;
- F_{crit}= maximum compressive load acting on the mast, as defined in equation (3.2).
- n_{xx} = half- wavelength in buckled shape, determined according to $n_{xx} = n_{xx,1} \cdot n_{xx,2}$, where $n_{xx,1}$ = 1.13 for mast stepped in the keel (theoretical value of the buckling factor for fixed-pinned conditions reduced by 20%) or $n_{xx,1}$ = 0.8 for mast stepped in the deck (theoretical value of the buckling factor for pinned-pinned conditions reduced by 20%). $n_{xx,2}$ is a factor, which takes into account the stiffness of the particular staying as shown in Figure 3.6 and is calculated according to Table 3.1.

Type of Staying	Staying Factor $n_{xx,2}$				
	F – 0	M – 1	F – 1	M – 2	F – 2
1) Double Lowers	-	1.08	1.12	1.05	1.08
2) Single Lowers	-	1.12	1.15	1.08	1.12
3) Runners & i.f.	-	-	1.08	-	1.12
4) Runners & c.s.	-	1.00	1.03	1.03	1.05
5)Swept spreaders	-	-	1.00	-	1.03
6a) Short spreaders	0.98	-	-	-	-
6b) No spreaders	0.71	-	-	-	-

Table 3.1: Calculation of the staying factor $n_{xx,2}$ (elaborated from [1]).

3.3.2 Minimum Weight

Minimum weight, consistent with stiffness, is particularly important to achieve in mast design. The reason lies in the balance of moments acting on a sailboat (see Figure 3.1).

The maximum velocity of a sailboat, given by the driving force represented in Figure 3.1, depends on the total sail area. If the force of wind is kept constant, increasing the sail plan will also cause a larger heeling moment. As the heeling moment is balanced by the righting moment, this will also determine a larger heel angle (see lower picture of Figure 3.1). We have already observed in the second paragraph that the maximum heel angle must be limited to 30° [1-4], as larger heel angles resolve in an augmented hydrodynamic resistance of the hull (the relation between drag and heel angle is exponential [1]) and in a reduction of the speed of the yacht. The equilibrium of a yacht is also dependent on the value of magnitude of the heeling and righting moment at 30°: if low, the yacht would be subjected to unproductive motions, like pitching, rolling, and yawing. These motions would degrade the performance of the boat, increase the wear on gear, and reduce the comfort of the crew.

A lightweight mast allows concentration of more weight near the center of buoyancy of the boat (roughly speaking, saving one kilogram above the deck is like adding 10 kilogram on the keel) , increasing the righting moment and therefore the stability of the boat. Keeping the maximum heel angle at 30°, the augmented righting moment allows a taller rig and then a larger sail plan, which means a larger speed of the boat.

The importance of a light, stiff, mast was known since ancient times: the best example is probably represented by the bamboo mast, used on Chinese junks since four thousands of years ago [4].

3.3.3 Maximum Aerodynamics Efficiency

Another requirement given in design of the rig is to reduce the interference of the mast to the mainsail. The sail is a wing, which virtually has no thickness, experiencing lift due to the pressure difference between the leeward and the windward side [1]. In Figure 3.9 is represented the distribution of the pressure along the windward and leeward sides of a sail with no mast: the area highlighted is the lift.

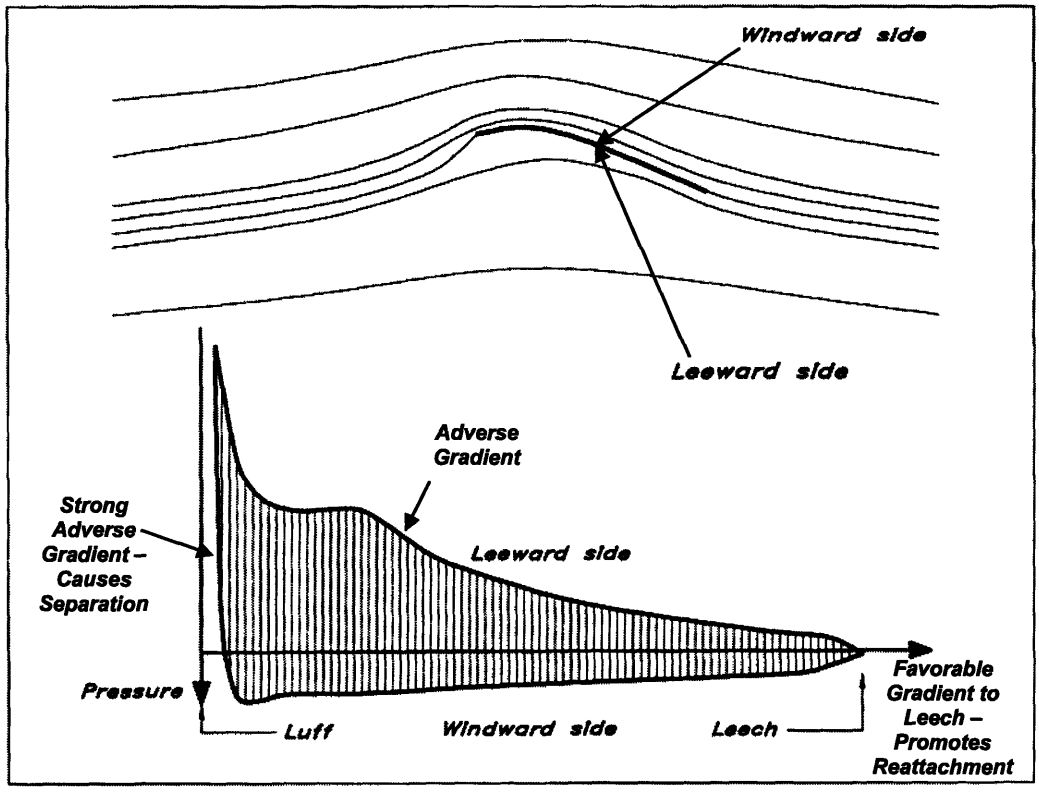

Figure 3.9: Pressure distribution along a sail. The pressure in the leeward side is generally larger than the one in the windward side. The velocity profiles follow the same trend [1].

The mast, necessary to sustain the sail, modifies the flow around the sail. This flow is shown schematically in Figure 3.10. Three zones of separation are present: two are immediately behind the mast, leeward and windward respectively, while the third is in the aft part of the leeward side. There are two main reasons that these separation zones have to be avoided. First, the pressure curves, represented in Figure 3.9, tend to overlap:

this causes a reduction in lift and driving force. Secondly, separation itself causes a drag increase. Experiments conducted by the Southampton University [1] showed that using a circular mast with a diameter of 7.5% of the total sail chord, leads to a reduction of the driving force of 20% respect to the case of sail without mast. Using a mast with double diameter, the driving force is almost halved.

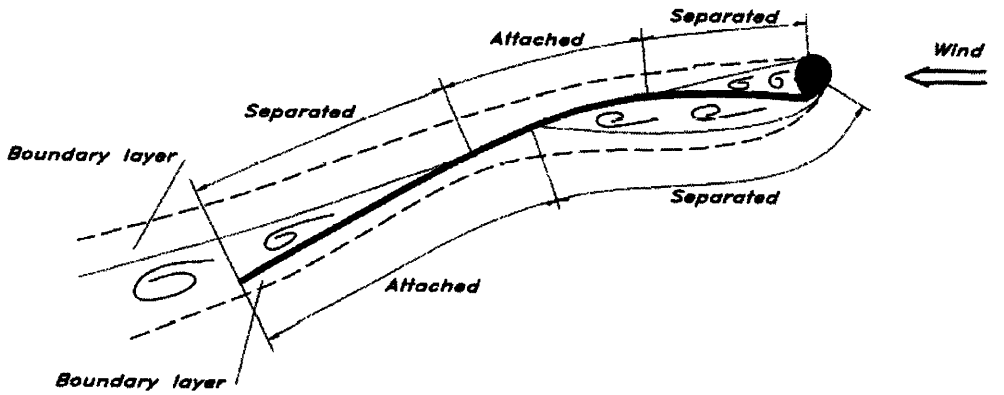

Figure 3.10: Flow around a mast/sail combination [1].

The separation behind the mast can be minimized by proper shaping of the mast section. The best way to do that is to design the mast and the sail together, starting from the pressure distribution needed [7]. If the shape of the mast and the sail is based on the profile of an existing airfoil (see Figure 3.11), the characteristic of the flow around the sail should approximate the flow around the same airfoil [7].

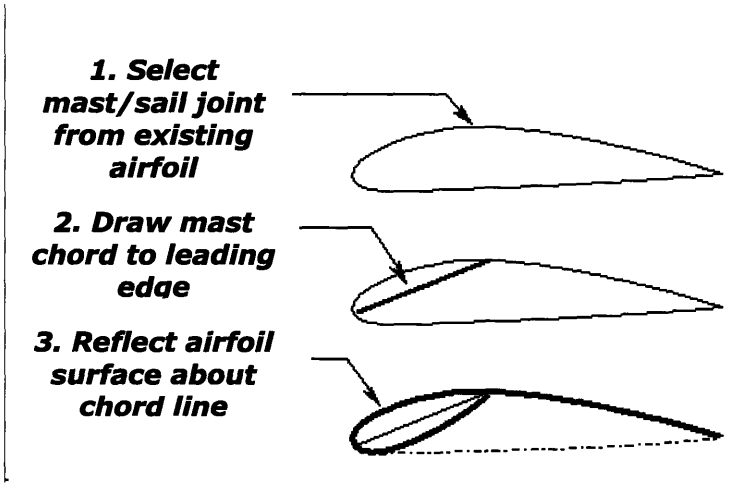

Figure 3.11: Wing-mast concept: creating a mast from an existing airfoil [7].

In order to understand how changing the dimension of an airfoil-shaped mast affects the overall performance, in Figure 3.12 we have represented different combinations mast-sail for a typical NACA profile, where dimension of the mast varies between 10% and 50% of the total chord dimension.

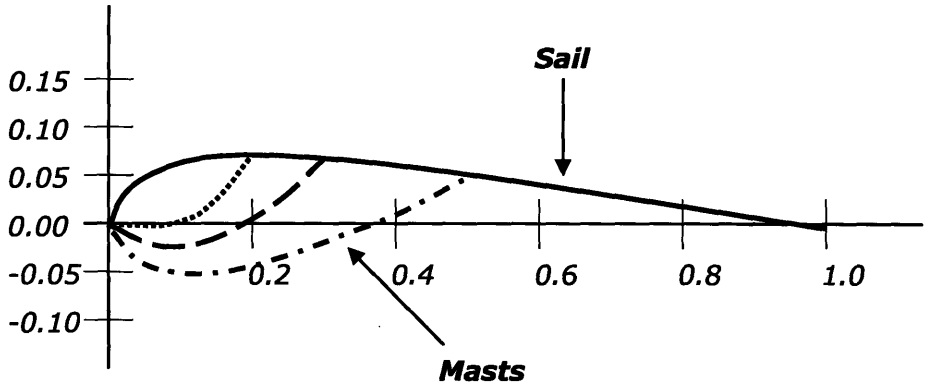

Figure 3.12: Profiles of masts of different dimension (measured in % of the total chord).

Results of computer simulations [7] proved that, keeping the angle of attack constant (the angle of attach is defined as the angle between the chord line and the wind direction), and employing masts of different dimensions, the profile of the pressure curve leeward (see Figure 3.9) does not change. This is not true for the pressure distribution windward: the amplitude of the suction peak and the adverse pressure gradient are consistently reduced [7]. Consequently, wing-masts of larger diameters are characterized by increased lift. This effect is emphasized for small angles of attack [7], while at large angles of attack the lift coefficient is about the same for both small and large masts. This means that the small and large masts have the same performances, but the smaller the mast the more restricted is the range of angles of attack where the sail is efficient.

3.4 Mast Design: Material Selection

3.4.1 Figures of Merit

We have seen in the previous paragraph, that the mast must be designed as a column to withstand a compression load with minimum weight. Consequently, *the optimum design is given by a material-and-shape combination that minimizes the weight for a given buckling stiffness*. For simplicity of comparison, we can assume the required second moment of inertia of the section equal to $I = (I_x + I_y)/2$; where I_x and I_y are the longitudinal and transverse moments of inertia, as calculated in (3.2) and (3.3). With this assumption, as seen in the previous chapter the performance index to be maximized is:

$$M_1 = \frac{(E\phi_B^e)^{1/2}}{\rho} \qquad (3.6)$$

The analysis of the previous chapter showed that commercial materials characterized by high values of the performance index, are wood (in particular oak and spruce), GRP, CFRP, steel and aluminum alloys. In fact, all of these materials are or have been used in sailboat masts. The other primary constraint in the selection of the material for the mast is represented by the *resistance to environmental conditions*, particularly the resistance to seawater and to UV radiation. A comparative ranking for different materials is given in Table 3.2. In the next part of the paragraph, the selected materials are considered individually.

Seawater Resistance				
U.V. Resistance	*Rank*	*Average*	*Good*	*Very Good*
	Good	Spruce	-	CFRP; GFRP
	Very Good	Steel (mild)	Aluminum	Stainless Steels

Table 3.2: Resistance to environmental conditions for materials employed in masts [5].

3.4.2 Wood

If a solid section has to be used (ϕ_B^e=1), wood, particularly spruce, is extraordinarily efficient and is the only practical material [2]. Wooden masts had been in use for many thousands of years and proved themselves as a reliable means of carrying sail. Major drawbacks of wood are [8]:

- Wood is particularly sensitive to seawater corrosion (see Table 3.3) and tends to rot if not treated and maintained properly;
- The length of masts is limited by the height of available trees.

3.4.3 Aluminum

Aluminum masts were first used in dinghies after the Second World War [8], when the technology of drawing thin-walled tubes improved [5] and there was a relatively cheap supply of aluminum foil sections from the aerospace industry [8]. At present, aluminum masts are the most common for most cruisers and a large number of racing classes [8]. Aluminum itself is stiffer than spruce, but it is also five times denser, making it less attractive as a solid. In any case, spruce anyway cannot be made practically in hollow sections, unlike aluminum: as one can see in Figure 2.7, an aluminum tube with a shape factor of $\phi_B^e = R/t = 10$ is good as solid spruce [5]. Aluminum tubes with higher shape factors outperform spruce [5]. The manufacturing method employed to build aluminum masts is determined by the size that needs to be constructed. For small or medium sailboats, the mast is obtained extruding a bar of solid aluminum alloy, generally 6061-T6, through a mould. The mast is then cut to its desired length and the fittings are attached [8]. When the diameter of the mast is considerable, the mast is obtained by forming a foil of aluminum [8]. This technique is also used for high-strength alloys, which cannot be extruded easily [8].

3.4.4 Steel and GRP

Steel and GRP have never been successful as materials for sailboat masts [8]. Stainless steel masts provide a reduced windage over the conventional aluminum alloy, due to the increased shape factor, but the performance index is lower due to the increase in weight.

In addition, the wall thickness for steel often becomes too thin, not even reaching the upper limit sets by local buckling, and indentation can be a problem. Fiberglass is poor because of its low elastic modulus and relatively high density.

3.4.5 CFRP

Despite the first carbon fiber was patented by Shindo in 1961, the first CFRP mast was used aboard Heath's *Condor* in the 1977-1978 World Race [9]. CFRP were at first considered "exotic" in racing circles and their use in masts was therefore prohibited [8]. For this reason, the first practical employment of CFRP in sailboat masts was in cruising yacht [8]. CFRP masts began to be used in competitions in the early 90's, initially in the America's cup and Admirals cup yachts [8]. In Figure 2.7, the performance index for aluminum and CFRP spars, with different shape factors, is shown: it is clearly demonstrated that CFRP spars outperform aluminum ones. Experiments conducted on same boat, but with different rigging, proved that the carbon-fiber-rigged boat gained 3 seconds per mile over an aluminum-rigged one in breeze wind condition [10]. In strong wind and wave conditions, this advantage was further increased [10]. CFRP masts are also proving to be more durable than aluminum ones [10].

In spite of these advantages, a carbon spar has its weaknesses. The most glaring problem is the price [9]: a CFRP mast costs between three or four times the price of an aluminum mast: this difference is mainly due to the unit cost of the materials (as one can see in Table 2.2) and to the production cycle time (2 weeks against 4 days) [10]. This cost can be justified for racers, but it is hard to justify for sailors, who do not pursue performance [8]. Further, CFRP masts remain structurally vulnerable to point loading and twisting, and are particularly prone to catastrophic failures, requiring a special care for installation and operation [9]. A recent famous accident happened in the America's Cup 2003 aboard of *Black Magic*: when the crew quickly released the runners for a jibe, the mast failed, literally exploding.

In the next paragraph, the application of cellular metals as core materials in sailboat masts is considered.

3.5 Application of Cellular Metals in Sail Masts: Circular Sections.

As seen in the previous chapter, the upper limit of the performance index M_1 for circular hollow Al shells, sets by the shape factor $\phi_B^e = R/t \approx 25$, can be increased using cellular metals. In the rest of this chapter, we consider the application of Al foam/honeycomb in the design of a mast for a medium-size yacht (Figure 3.13). The performance of these masts is compared with that of masts employing hollow aluminum sections.

The architecture of the yacht considered is shown in Figure 3.13 [1]. The YD-40 is a 12 meter ocean-going yacht, designed for a crew of four. The rig chosen is of the F-2 type, with double lower shrouds. The mast is keel stepped. The required stiffness of the mast is calculated in a few steps using the classical approach given by Skene [4].

Step 1- Calculate the R.M at 30° of the heeling angle [4]:

$$R.M._{30} = m \cdot g \cdot sf \qquad (3.7)$$

where g = 9.81 m/s^2, m = mass at total load = 9300 kg (given by the constructor), sf = traverse stability factor (consider the variance of the righting moment with the heeling angle) = 0.59 for this boat class [1] $\Rightarrow$ R.M.$_{30}$ = 53,000 N;

Step 2- The critical load is calculated from equation (3.2). From Figure 3.13, δ=1.300 m. Assuming a safety factor $\zeta = 3 \Rightarrow F_{crit}$ = 122,300 N;

Step 3- From equation (3.4), calculate the required $E \cdot I_{yy}(1)$ in the panel 1 (base of mast):

$$E \cdot I_{yy}(1) = \frac{F_{crit}(1) \cdot l(1)^2}{\pi^2 \cdot n_{yy}(1)^2} = \frac{122{,}300N \cdot (5{,}950mm)^2}{\pi^2 \cdot (1.13)^2} = 3.436 \cdot 10^{11} Nmm^2 \qquad (3.8)$$

By rule, the stiffness of the mast should be recalculated for the other panels reducing the critical load of a factor, given by the product of the shroud tensions times the shroud angle. For simplicity of construction, we will assume the mast stiffness constant all along the length of the rig.

Step 4- From equation (3.5), calculate the required $E \cdot I_y$:

$$E \cdot I_{xx} = \frac{F_{crit} \cdot h^2}{\pi^2 \cdot n_{xx,1}{}^2 \cdot n_{xx,2}{}^2} = \frac{122{,}300N \cdot (15{,}515mm)^2}{\pi^2 \cdot (1.13)^2 \cdot (1.08)^2} = 20.028 \cdot 10^{11} Nmm^2 \qquad (3.9)$$

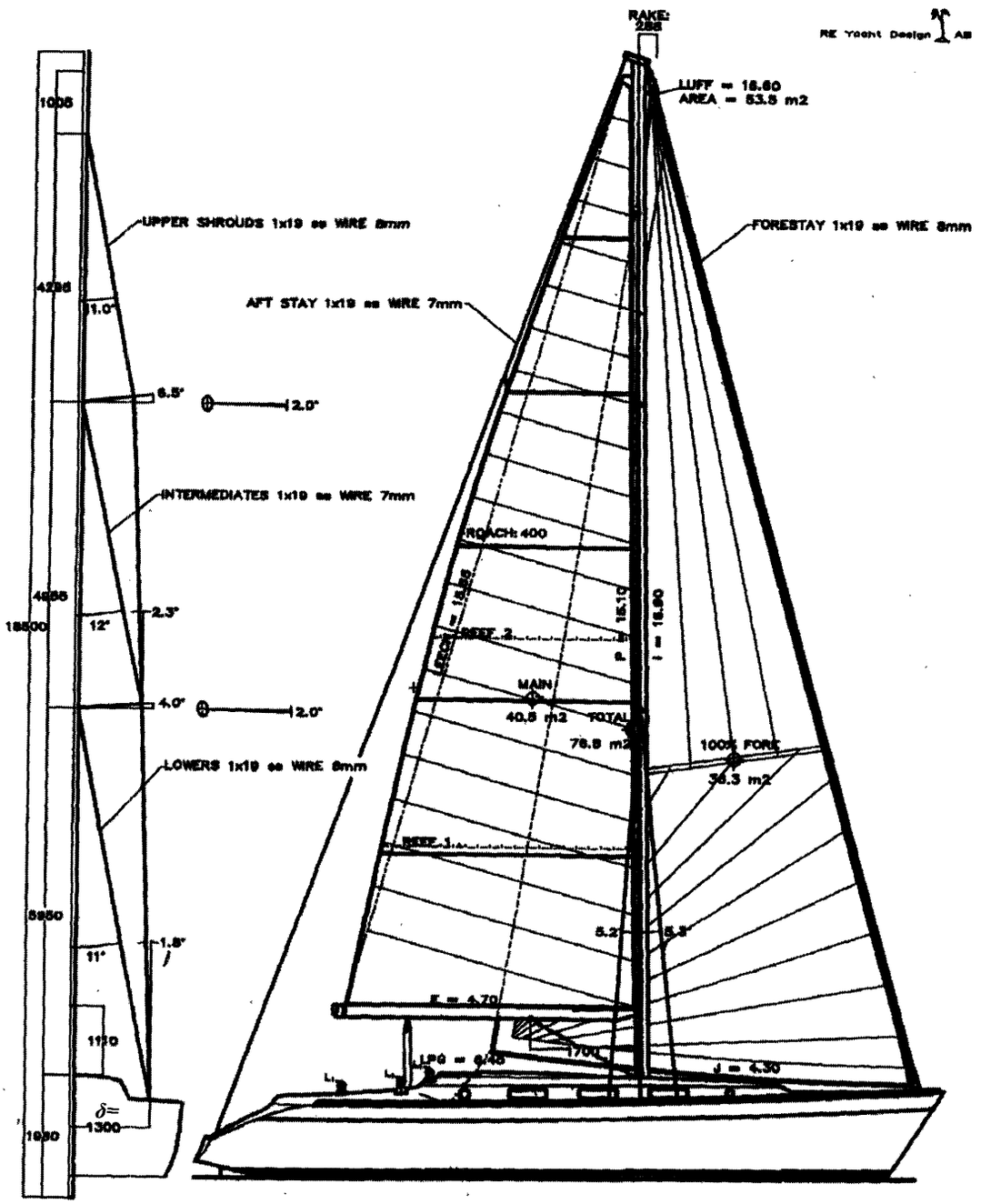

Figure 3.13: YD-40 rig [1].

In this paragraph, as a first approximation, we consider masts with circular sections, assuming $EI_{crit} = E\left(I_{xx} + I_{yy}\right)/2 = 11.732 \cdot 10^{11} Nmm^2$, where I_{xx} and I_{yy} are the transverse and longitudinal moments of inertia, as calculated in (3.8) and (3.9). The case of elliptical masts is discussed in the next paragraph. The theory of Chapter 2 was

developed for columns with pinned ends: in order to use the same theory, we have to assume that the mast has pinned-pinned boundary conditions. For this purpose, we introduce an equivalent length $l_{eqv} = 9.73m$ calculated form equation (3.3) with $n = 1$ and $F_{crit} = 122{,}300N$. The optimal design is determined according to the "minimum weight per given stiffness criterion" for the types of constructions discussed in the second chapter: circular hollow shells, honeycomb/foam core shells and honeycomb/foam core sandwich shells. As the typical mast diameter ranges from 10 to 50 cm, stiffened shells are impractical for this application and are not considered here.

Unlike the second chapter, the optimization is not carried on for a range of design loads, but for the critical load given by equation (3.2). In the third paragraph, we have seen that if the mast is not shaped properly, the negative interference of the mast on the mainsail flow put a superior limit to the ratio of the mast diameter with the sail chord length, where the maximum ratio is generally fixed to 6-8% [11]. In order to take into account this effect, minimum weight designs are obtained for different values of the mast diameters. Other functional requirements like cost, maintainability, reliability, environmental resistance requirements of the masts will not be considered here.

3.5.1 Circular Cylindrical Aluminum Extruded Tube

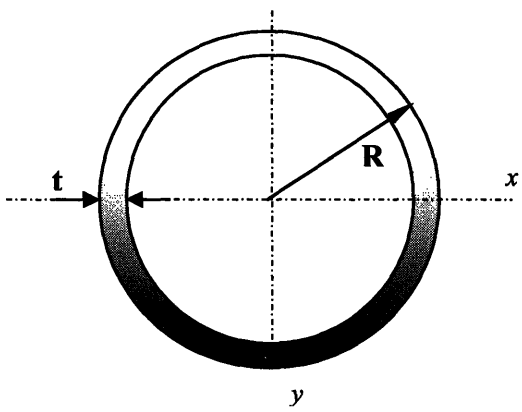

Figure 3.14: Circular cylindrical hollow section.

Considering a typical Al-alloy used for extrusion, like Al 6061-T91:

$$E_f = 69{,}000 Nmm^{-2}; \varepsilon_{y,f} = 0.0057;$$
$$\rho_f = 2.7 \cdot 10^3 kgm^{-3}; \nu_f = \tfrac{1}{3};$$

With the notation of Figure 3.14, the stress in the wall σ_z is given by $\sigma_z = F_{crit}/(2\cdot\pi\cdot R\cdot t)$.

Fixing the shell radius R arbitrarily, the allowable wall thickness t, which corresponds to the minimum weight, is determined according to the constraint

$$\sigma_z = \min(\sigma_1, \sigma_2, \sigma_{y,f}); \qquad (3.10)$$

where σ_1 is the global buckling stress, σ_2 is the local buckling stress and $\sigma_{y,f}$ is the wall yielding stress.

Observing that $A \approx 2\pi\cdot R\cdot t$ and $I \approx \pi\cdot R^3\cdot t$, then $A \cong 2I/R^2$ and the global buckling stress can be expressed as

$$\sigma_1 = \frac{F_{crit}}{A_{crit}} = \frac{F_{crit}\cdot R^2}{2I_{crit}}. \qquad (3.11)$$

The local buckling stress is given by Equation (2.7):

$$\sigma_2 = \frac{E_f\cdot\gamma}{\sqrt{3\cdot(1-\nu_f^2)}}\cdot\left(\frac{t}{R}\right); \qquad (3.12)$$

where γ is the knockdown factor, assumed conservatively to be 0.20 [12]. For uniaxial load, yield occurs when:

$$\sigma_{y,f} = E_f\cdot\varepsilon_{y,f}. \qquad (3.13)$$

From equations (3.10), (3.11), (3.12) and (3.13), we find that

$$t = \max\left[\frac{I_{crit}}{(\pi\cdot R^3)}; \sqrt{\frac{F_{crit}\cdot\sqrt{3\cdot(1-\nu^2)}}{E_f\cdot\gamma\cdot 2\pi}}; \frac{F_{crit}}{2\pi\cdot R\cdot E_f\cdot\varepsilon_{y,f}}\right]_R. \qquad (3.14)$$

The weight per unit length is then given by:

$$\frac{W}{L}(R) = \rho_f\cdot 2\pi\cdot R\cdot t_{\min} \qquad (3.15)$$

Figure 3.15 shows the plot of the weight per unit length against the radius. The minimum weight corresponds to $\sigma_1 = \sigma_2 \Rightarrow t = 1.5mm, R = 153mm, \left(W/l_{eqv}\right)_{\min} = 3.9\frac{kg}{m}$. Note that for F_{crit} = 122,300 N; squash-load design never takes over.

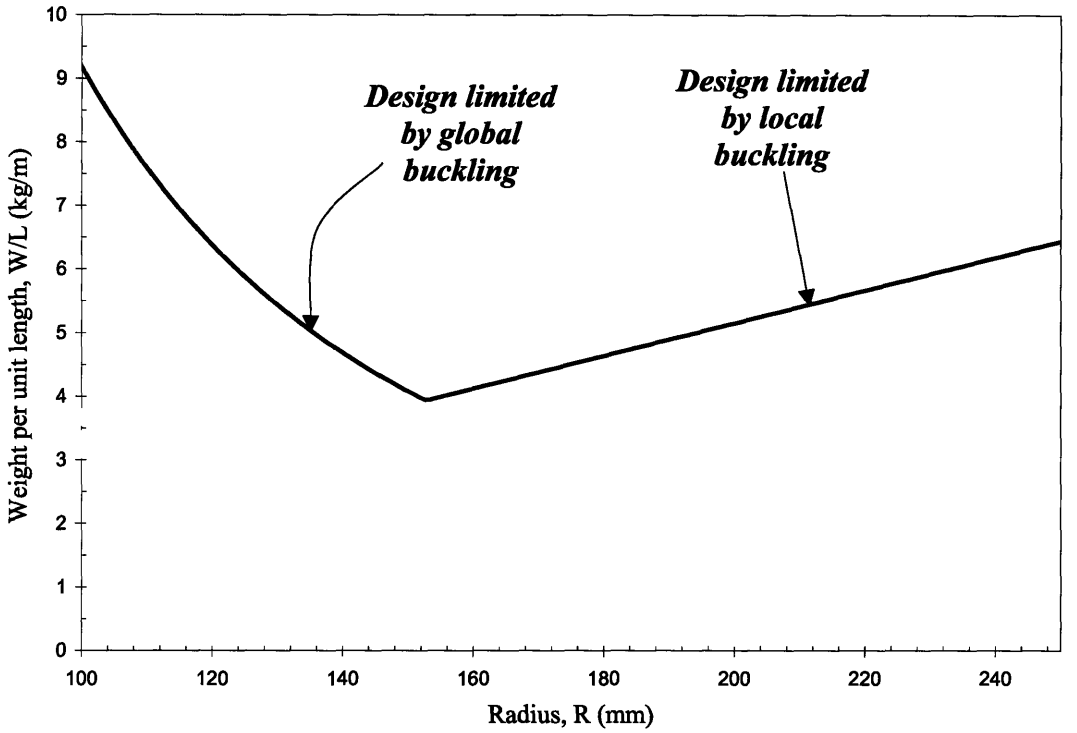

Figure 3.15: Weight per unit length plotted against the radius for hollow circular shell.

3.5.2 Aluminum Circular Cylindrical Sandwich with Foam Core

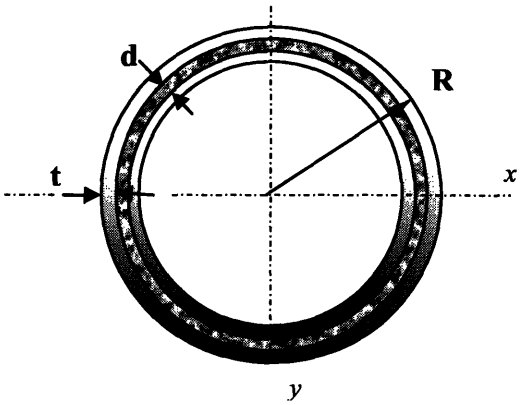

Figure 3.16: Circular sandwich shell section with foam core.

Consider sandwich shells with inner foam core of three prescribed relative densities:

$$\eta_1 = \frac{\rho_{c,1}}{\rho_{s,1}} = 0.05;\ \eta_2 = \frac{\rho_{c,2}}{\rho_{s,2}} = 0.1;\ \eta_3 = \frac{\rho_{c,3}}{\rho_{s,3}} = 0.2;$$

where $\rho_{c,i}$ = density of core; $\rho_{s,i}$ = density of core parent material; assume $\rho_{s,i} = \rho_f, \forall i$. With the notation of Figure 3.16, the stress in the wall σ_z is now given by $\sigma_z = F_{crit}/(4 \cdot \pi \cdot R \cdot t)$. Fixed again the shell radius R arbitrarily, the allowable wall thickness t and the core thickness c, which corresponds to the minimum weight, is determined according to the relation

$$\sigma_z = \min(\sigma_1, \sigma_2, \sigma_{y,f}, \sigma_{wr}); \qquad (3.16)$$

where σ_1 is the global buckling stress, σ_2 is the local buckling stress, $\sigma_{y,f}$ is the wall yielding stress, and σ_{wr} is the wrinkling stress. According to equation (2.34), the values of the relative densities considered exclude face wrinkling. According to equation (2.35), $F_{crit}/(E_f L^2) \geq \left|F_{crit}/(E_f L^2)\right|_y \forall \eta_i$, and face yielding is also excluded. The global buckling stress is still given by equation (3.11), while the local buckling stress is now given by equation (2.36). For simplicity, we assume conservatively $\gamma = 0.20$. With this assumption the core thickness is determined by

$$d = \max\left[d_1 = R \cdot \sqrt[3]{\frac{k_1 \left(\frac{F_{crit}}{E_f l_{eqv}^2} \right)}{2 \cdot k_2}}; d_2 = 20mm \right]; \qquad (3.17)$$

where k_1 and k_2 are still defined by equation (2.39) and d_2 is the minimum core thickness allowable. Note that for this particular case, the value of d_1 calculated with equation (3.17) has been found less than 5% different from the analogous value given by Hutchison and He.

The face thickness is given by:

$$t = \max\left[t_1 = \frac{I_{crit}}{(2 \cdot \pi \cdot R^3)}; t_2 = \frac{F_{crit} \cdot \sqrt{1-\nu^2}}{4\pi \cdot \gamma \cdot E_f \cdot d}; t_3 = (1/64)" \right]_R . \qquad (3.18)$$

where t_1 is the value required from global buckling, t_2 is the value required from local buckling and t_3 is the minimum face thickness. Considering the mast will receive rough treatment, a facing thickness of 0.016 in. (0.40 mm) is required. Then the weight per unit length is given by:

$$\frac{W}{L} = \left[4\pi\rho_f \cdot R \cdot t + 2\pi\rho_c \cdot R \cdot (d-t) \right] \qquad (3.19)$$

In Figure 3.17 are represented plots of the weight per unit length against the radius for different foam relative densities.

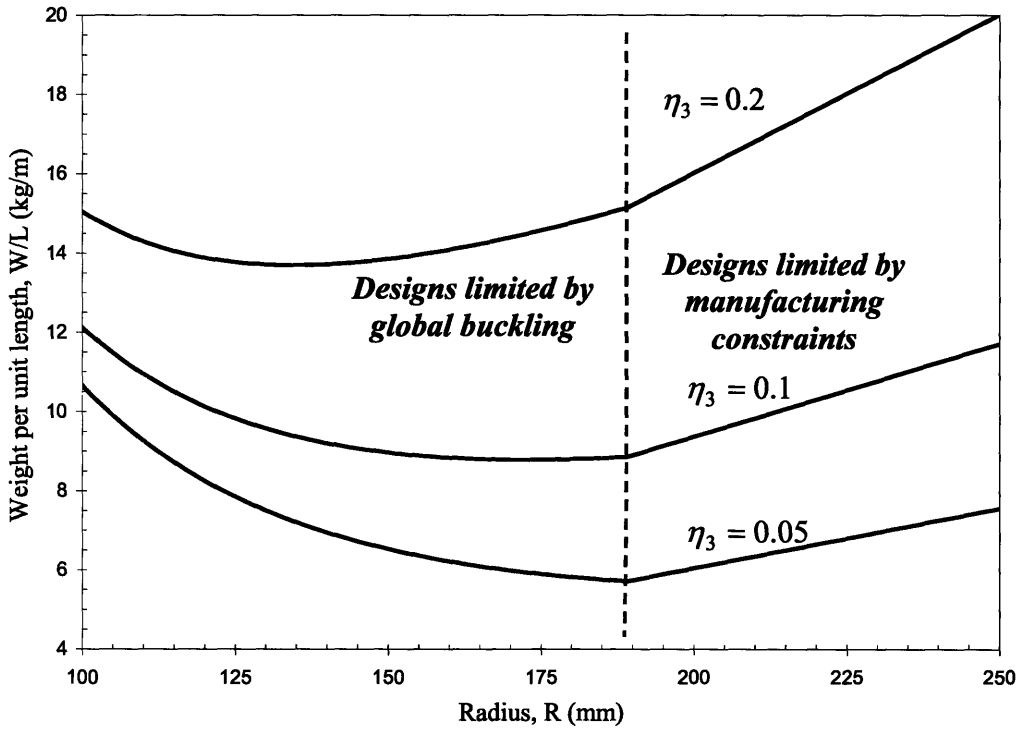

Figure 3.17: Weight per unit length plotted against the radius for foam core sandwich shells with different relative densities.

3.5.3 Aluminum Circular Cylindrical Sandwich with Honeycomb Core

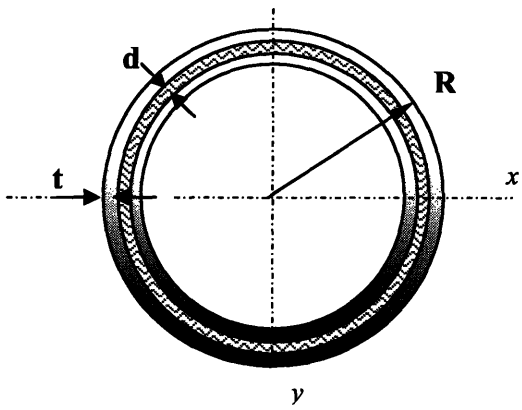

Figure 3.18: Circular sandwich shell section with honeycomb core

Consider sandwich shells with 5052 Hexweb® Aluminum high-grade hexagonal honeycomb core with three prescribed cell sizes and relative densities:

$$c_1 = \frac{1}{16}",\eta_1 = \frac{\rho_{c,1}}{\rho_{s,1}} = 0.05;\ c_2 = \frac{1}{8}",\eta_2 = \frac{\rho_{c,2}}{\rho_{s,2}} = 0.025;\ c_3 = \frac{3}{8}",\eta_3 = \frac{\rho_{c,3}}{\rho_{s,3}} = 0.01;$$

where c_i is the cell size, defined as the distance from one node to the other node along the W direction [13]; $\rho_{c,i}$ = density of core; $\rho_{s,i}$ = density of core parent material; assume $\rho_{s,i} = \rho_f, \forall i$. Defined E_c as the Young modulus of the core, for honeycomb core $E_c/E_f = \rho_c/\rho_f$ [14]. Fixed again the shell radius R arbitrarily, the allowable wall thickness t and the core thickness d, which corresponds to the minimum weight, is determined according to the relation

$$\sigma_z = \min\{\sigma_1, \sigma_2, \sigma_{y,f}, \sigma_{wr}, \sigma_{dm}\} \qquad (3.20)$$

where σ_1 is the global buckling stress, σ_2 is the local buckling stress, $\sigma_{y,f}$ is the wall yielding stress, σ_{wr} is the wrinkling stress and σ_{dm} is the face dimpling stress. Analogously to the previous case, $\sigma_z = F_{crit}/(4 \cdot \pi \cdot R \cdot t)$, σ_1 is given by equation (3.11), σ_2 is given by equation (2.36), σ_{wr} is given by equation (2.49). For the face dimpling stress, we can use the following estimation [15]:

$$\sigma_{dm} = \frac{1}{3} \cdot E_f \cdot \left(\frac{2 \cdot t}{c_i} \right)^{1.5}; \qquad (3.21)$$

As in the previous case, face yielding and wrinkling are excluded and we assume conservatively $\gamma = 0.20$. The core thickness is still determined by equation (3.17), but the manufacturing constraint here is $d_2 = (1/16)"$. The face thickness is given by:

$$t = \max\left[t_1 = \frac{I_{crit}}{2\pi \cdot R^3}; t_2 = \frac{F_{crit}\sqrt{1-\nu^2}}{4\pi \cdot \gamma \cdot E_f d}; t_3 = \sqrt[3]{\frac{F_{crit} \cdot \left(1-\nu^2\right) \cdot c_i^2}{16\pi \cdot R \cdot E}}; t_4 = \frac{1}{64}" \right]_a . \qquad (3.22)$$

where t_1 is the thickness from the global buckling requirement, t_2 from the local buckling one, t_3 from the face dimpling one and t_4 is the minimum thickness allowable. The weight per unit length is still given by equation (3.19). Figure 3.19 shows the plot of the weight per unit length against the radius for different 11honeycomb densities.

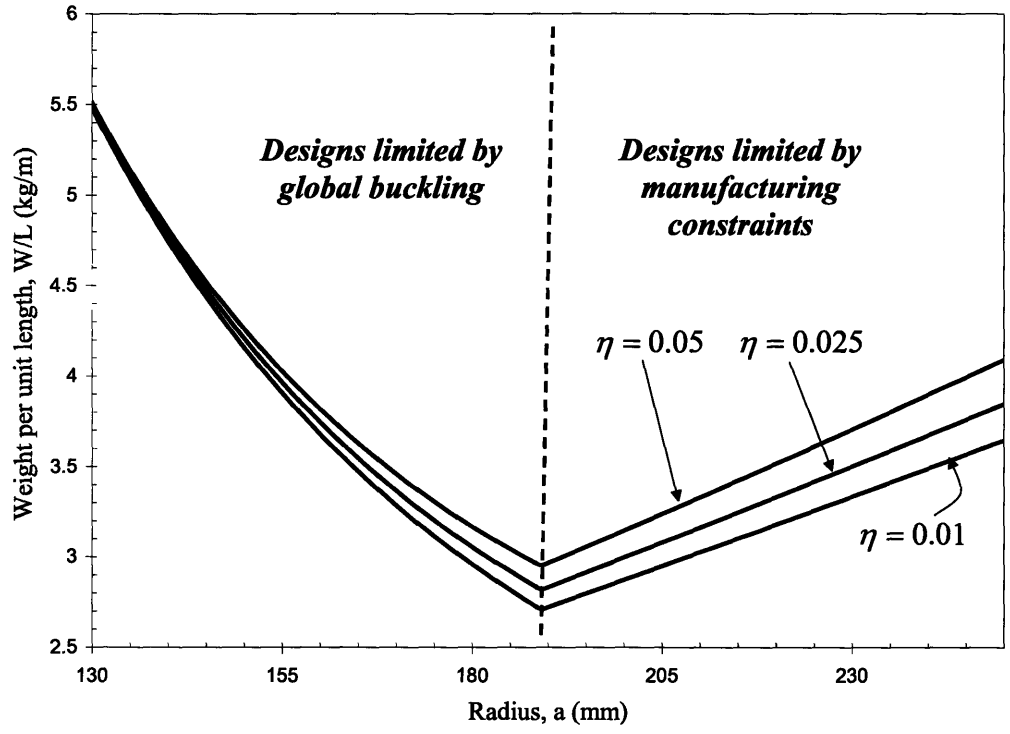

Figure 3.19: Weight per unit length plotted against the radius for honeycomb-core sandwich shells with different relative densities.

3.5.4 Aluminum Circular Cylindrical Shell with Foam Core

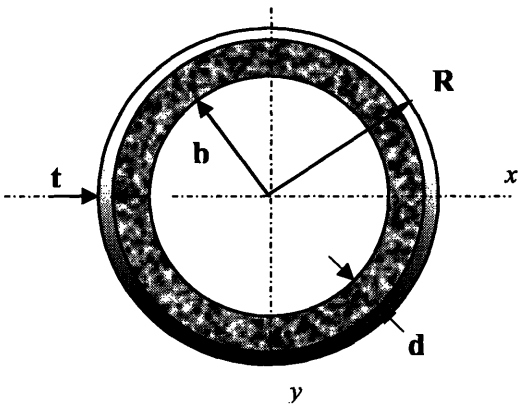

Figure 3.20: Circular cylindrical hollow section with foam core.

Analogously to section 3.5.2, consider foam core of three prescribed relative densities:

$$\eta_1 = \frac{\rho_{c,1}}{\rho_{s,1}} = 0.05;\ \eta_2 = \frac{\rho_{c,2}}{\rho_{s,2}} = 0.1;\ \eta_3 = \frac{\rho_{c,3}}{\rho_{s,3}} = 0.2;$$

where $\rho_{c,i}$ = density of core; $\rho_{s,i}$ = density of core parent material; assume $\rho_{s,i} = \rho_f, \forall i$ and $E_c/E_f = (\rho_c/\rho_f)^2$. Referring to Figure 3.20, fixed R arbitrarily, the minimum weight configuration is the one minimizing the wall stress:

$$\sigma_z = \min(\sigma_1, \sigma_2, \sigma_{y,f}, \sigma_{wr}); \qquad (3.23)$$

where $\sigma_z = F_{crit}/(2\cdot\pi\cdot R\cdot t)$; σ_1 is the global buckling stress, given by equation (3.11); σ_2 is the local buckling stress, given by equation (2.53) assuming $\gamma = 0.20$, $\sigma_{y,f}$ is the wall yielding stress and σ_{wr} is the wrinkling stress, given by equation (2.58). The face thickness is then determined by;

$$t = \max\left[\begin{array}{c} t_1 = \frac{I_{crit}}{\pi\cdot a^3}; t_2 = \frac{F_{crit}}{2\pi\cdot R\cdot\Gamma\cdot E_f}; \\ t_3 = \frac{F_{crit}}{2\pi\cdot R\cdot E_f\cdot\varepsilon_{y,f}}; t_4 = \frac{F_{crit}}{2\pi\cdot R\cdot B\cdot E_f}\cdot\left(\frac{E_c}{E_f}\right)^{-\frac{2}{3}}, t_5 = \frac{1}{64}" \end{array}\right]_R . \qquad (3.24)$$

where t_1 is the thickness from the global buckling requirement, t_2 from the local buckling requirement, t_3 from the face yielding condition, t_4 from the face wrinkling and t_5 is the minimum thickness. The core thickness is determined trough equations (2.64). Consequently:

$$d = \max[d_1 = 5\lambda; d_2 = 20mm]; \qquad (3.25)$$

where d_2 is fixed by manufacturing constraints. The weight per unit length is

$$\frac{W}{L} = \left[2\pi\rho_f \cdot R \cdot t + \pi\rho_c \cdot (2R + 2t - d) \cdot d\right] \qquad (3.26)$$

Figure 3.21 shows the plot of the weight per unit length against the radius for different foam densities.

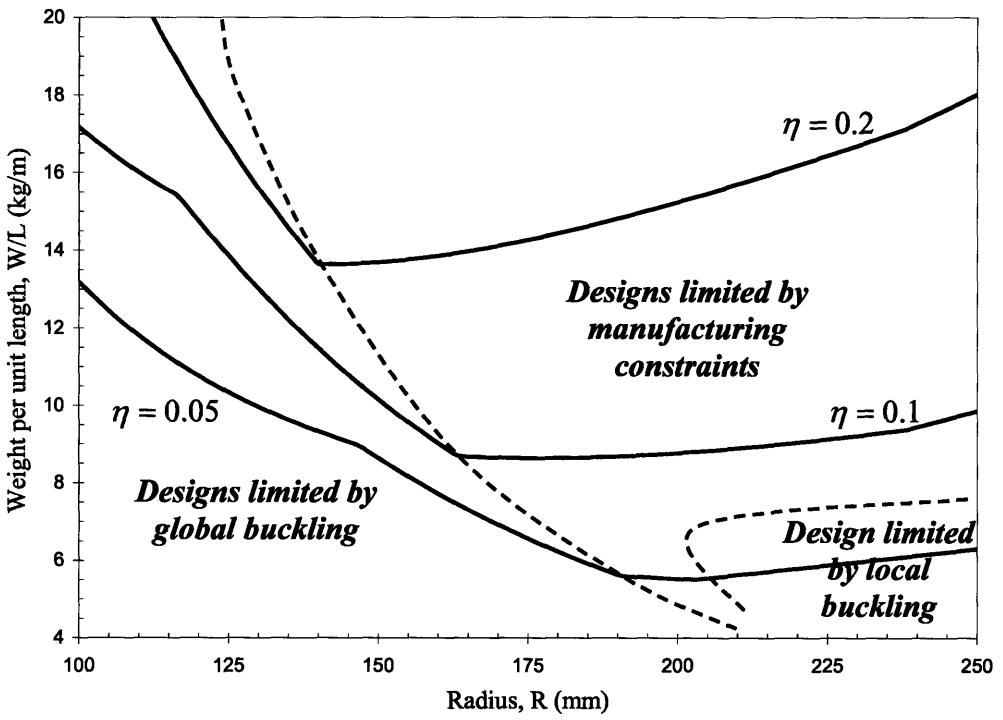

Figure 3.21: Weight per unit length plotted against the radius for foam core shells with different relative densities.

3.5.5 Aluminum Circular Cylindrical Shell with Honeycomb Core

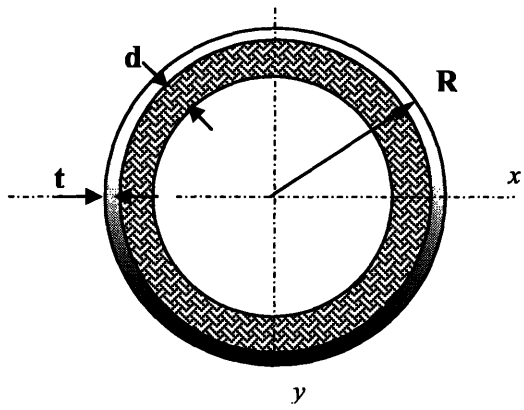

Figure 3.22: Circular cylindrical hollow section with honeycomb core.

Consider shells with 5052 Hexweb® Aluminum OX® honeycomb core with three prescribed cell sizes and relative densities:

$$c_1 = \frac{1}{16}",\eta_1 = \frac{\rho_{c,1}}{\rho_{s,1}} = 0.05;\ c_2 = \frac{1}{8}",\eta_2 = \frac{\rho_{c,2}}{\rho_{s,2}} = 0.025;\ c_3 = \frac{3}{8}",\eta_3 = \frac{\rho_{c,3}}{\rho_{s,3}} = 0.01;$$

where c_i is the cell size, defined as the distance from one node to the other node along the W direction [13] and $E_c/E_f = \rho_c/\rho_f$. Referring to Fig. 3.22, for given R, the minimum weight configuration is the one minimizing the wall stress:

$$\sigma_z = \min\{\sigma_1, \sigma_2, \sigma_{y,f}, \sigma_{wr}, \sigma_{dm}\}; \qquad (3.27)$$

where $\sigma_z = F_{crit}/(2\cdot\pi\cdot R\cdot t)$; σ_1 is the global buckling stress, given by equation (3.11); σ_2 is the local buckling stress, given by equation (2.53); $\sigma_{y,f}$ is the wall yielding stress; σ_{wr} is the wrinkling stress, given by equation (2.58), and σ_{dm} is the face dimpling stress. Assuming the case of square-cells, σ_{dm} can be approximated by [15]:

$$\sigma_{dm} = 2.5\cdot E_f\cdot\left(\frac{t}{c_i}\right)^2; \qquad (3.28)$$

We assume that the core stabilizes the outer shell against local buckling. The face thickness is then determined by:

$$t = \max\left[\begin{array}{l} t_1 = \dfrac{I_{crit}}{\pi \cdot R^3}; t_2 = \dfrac{F_{crit}}{2\pi \cdot R \cdot \Gamma \cdot E_f}; t_3 = \dfrac{F_{crit}}{2\pi \cdot R \cdot E_f \cdot \varepsilon_{y,f}}; \\ t_4 = \dfrac{F_{crit}}{2\pi \cdot R \cdot B \cdot E_f} \cdot \left(\dfrac{E_c}{E_f}\right)^{-\frac{2}{3}}; t_5 = \sqrt[3]{\dfrac{F_{crit} \cdot c_i^2}{5E_f \cdot \pi \cdot R}}; t_6 = \dfrac{1}{64}"; \end{array}\right]_a \quad (3.29)$$

where t_1 is the thickness from the global buckling requirement, t_2 from local buckling, t_3 the face yielding condition, t_4 from the face wrinkling, t_5 from face dimpling and t_6 is the minimum thickness. The core thickness is still determined through equation (2.64), then

$$d = \max\left[d_1 = 5\lambda; d_2 = \frac{1}{16}"\right]; \quad (3.30)$$

where d_2 is fixed by manufacturing constraints. The weight per unit length for different mast radius and honeycomb densities is given by equation (3.26) and shown in Fig. 3.23.

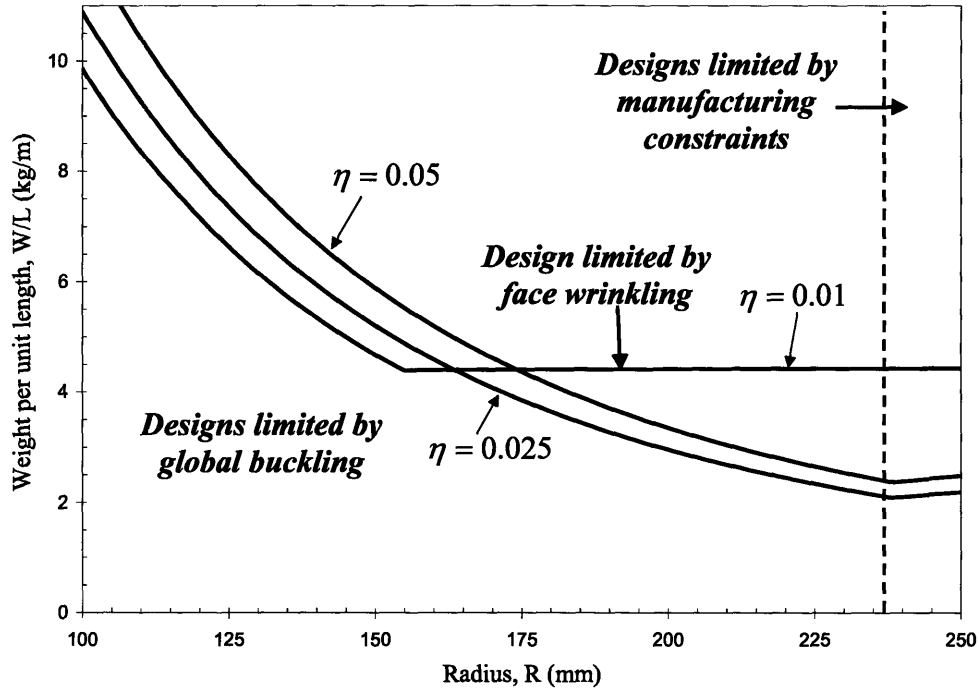

Figure 3.23: Weight per unit length plotted against the radius for honeycomb core shells with different relative densities.

3.6 Application of Cellular Metals in Sail Masts: Elliptical Sections.

3.6.1 Estimation of the Local Buckling Stress

The comparison of masts employing different materials has been performed until this point considering circular cylindrical shells. This assumption was simplifying the real problem, because the required longitudinal and transversal stiffness of the mast is different and mast sections are elliptical. The local buckling behavior of elliptical cylindrical sections is needed for a more accurate design. Figure 3.24 shows the geometry considered in this analysis.

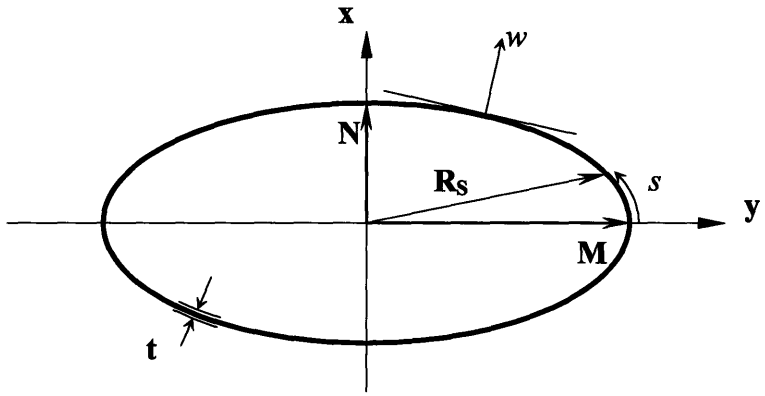

Figure 3.24: Geometry of elliptical cylindrical shell.

According to Figure 3.24, the locus of the points on the surface of the shell is defined by:

$$\left(\frac{y}{M}\right)^2+\left(\frac{x}{N}\right)^2=1 \qquad (3.31)$$

Introduced a circumferential coordinate s, the radius of curvature of the surface can be expressed as:

$$R_s=\frac{M}{N^2}\left\{1+\left[\left(\frac{N}{M}\right)^2-1\right]\cdot\left(\frac{y}{M}\right)^2\right\}^{3/2} \qquad (3.32)$$

The elastic stability of elliptical cylindrical shells was studied by Kempner and Chen [16] and later by Hutchinson [17] using the Ritz's method. The basic relations used in all these

analyses are equivalent to the ones used by Donnell [18] for studying the elastic stability of circular cylindrical shells. Both Kempner [19] and Hutchison [17] showed that for an oval cylinder, buckling initiates in the region of minimum curvature at the ends of the minor axis of the ellipse, as one would expect. The buckling stress approaches that of a circular cylinder whose curvature is the same as occurs locally at the ends of the minor axis of the oval shell; i.e., with reference to equations (2.7) and (3.32), [17]:

$$\sigma_{crit,ell} = \frac{\gamma \cdot E}{\sqrt{3(1-\nu^2)}} \cdot \frac{t}{R_N}; \quad R_N = \frac{M^2}{N}; \qquad (3.33)$$

According to Tennyson [20], the effect of the cylinder ellipticity on reducing the initial buckling load below the equivalent circular cylindrical value is given by the ratio:

$$\sigma_{crit,ell} / \sigma_{crit,circle} = R_0 / R_N; \qquad (3.34)$$

where R_0 is the radius of the circle with exactly the same perimeter of the ellipse, i.e.,

$$R_0 = \frac{perimeter}{2\pi} = \frac{2M}{\pi} \int_0^{\frac{\pi}{2}} \left\{ 1 + \left[\left(\frac{N}{M} \right)^2 - 1 \right] \sin^2 \psi \right\}^{\frac{1}{2}} d\psi = (N \cdot M)^{\frac{1}{2}} \qquad (3.35)$$

and $\sigma_{crit,circle}$ is the classical buckling stress for the circular cylinder of radius R_0. Hutchinson [17] has shown that for

$$\left[12 \cdot \left(1-\nu^2 \right) \right]^{\frac{1}{2}} \cdot \left(R_0 / t \right) \geq 625 \qquad (3.36)$$

the critical buckling load for an elliptical cylinder differs from the value given equation (3.33) by less than 5% for $N/M \geq 0.20$. Thus, for the range of elliptical shells considered in this investigation, equation (3.33) will be used to predict the local buckling loads.

3.6.2 Elliptical Cylindrical Aluminum Extruded Tube

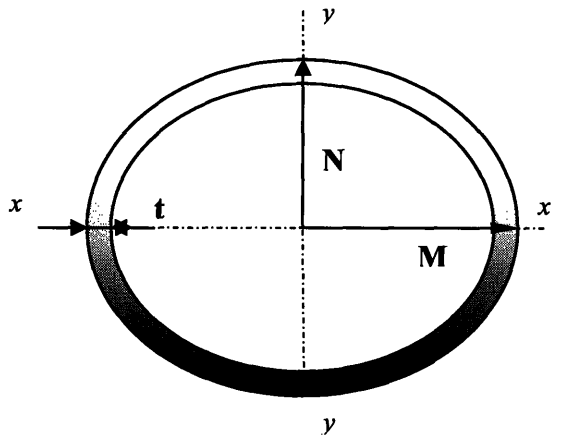

Figure 3.25: Elliptical cylindrical hollow section.

In this part, we discuss the optimal design for an extruded aluminum tube including the condition of different transverse and longitudinal stiffness. The shape of the section, minimizing the weight per unit length of the mast, is elliptical. With reference to Figure 3.25, equations (3.8) and (3.9) can respectively be rewritten as:

$$\frac{\pi}{4} MN^3 t \cdot \left(\frac{1}{M} + \frac{3}{N}\right) = 498 \cdot 10^4 mm^4 = I_{yy} \qquad (3.37)$$

$$\frac{\pi}{4} NM^3 t \cdot \left(\frac{1}{N} + \frac{3}{M}\right) = 2902 \cdot 10^4 mm^4 = I_{xx} \qquad (3.38)$$

Considering an elliptical shape, it is more convenient to express equation (3.37) and (3.38) as:

$$I_{yy} \cdot \xi^3 + 3 \cdot I_{yy} \cdot \xi^2 - 3 \cdot I_{xx} \cdot \xi - I_{xx} = 0 \qquad (3.39)$$

$$\frac{\pi}{4} N^3 \cdot t \cdot (1 + 3\xi) = I_{yy} \qquad (3.40)$$

where $\xi = M/N$. Substituting equations (3.37) and (3.38) in equation (3.39) $\Rightarrow$ $\xi \cong 3.145$. Like in the previous paragraph, the optimum design is the one minimizing the wall stress and equation (3.10) still holds with $\sigma_z = F_{crit}/(2\pi \cdot t \cdot R_o)$. The wall thickness is therefore calculated through:

$$t = \max\left[t_1 = \frac{4 \cdot I_{yy}}{\pi \cdot (1+3\xi) \cdot N^3}; t_2 = \sqrt{\frac{F_{crit} \cdot R_N \cdot \sqrt{3 \cdot (1-\nu^2)}}{\gamma E_f \cdot 2\pi R_0}}; t_3 = \frac{F_{crit}}{2\pi R_0 E_f \varepsilon_{y,f}} \right] \qquad (3.41)$$

, where t_1 is the value required by the global buckling condition (3.40); t_2 is the one required by the local buckling condition (3.33) and t_3 is the value of the thickness required by the face yielding condition. Finally, the weight per unit length is given by:

$$\frac{W}{L} = \rho_f \cdot 2\pi \cdot R_0 \cdot t; \qquad (3.42)$$

Figure 3.26 shows the plot of the weight per unit length against the radius. The minimum weight corresponds to $\sigma_1 = \sigma_2 \Rightarrow t = 3.58mm, R_0 = 98mm, (W/L)_{\min} = 6.0\frac{kg}{m}$. Similarly to the hollow circular shell, even in this case, squash-load design never takes over.

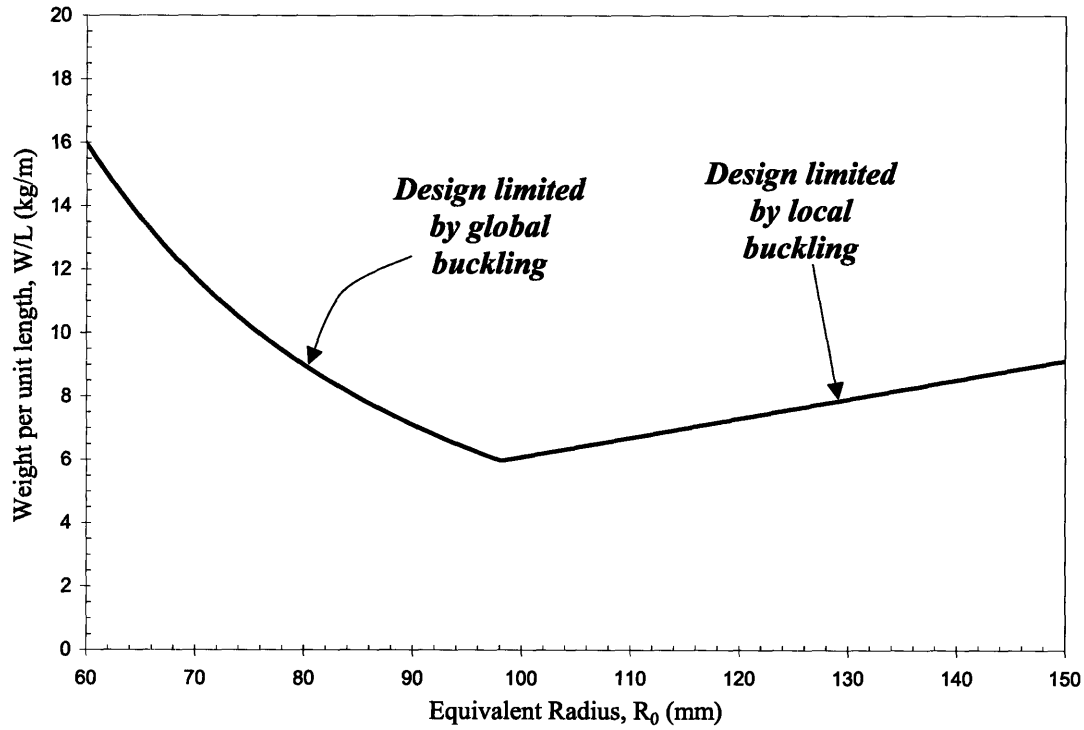

Figure 3.26: Weight per unit length plotted against the equivalent radius for elliptical cylindrical hollow shell.

3.6.3 Aluminum Elliptical Cylindrical Sandwich with Foam Core

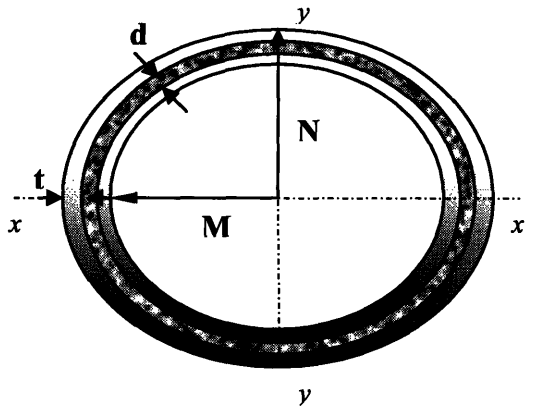

Figure 3.27: Elliptical sandwich shell section with honeycomb core.

The optimization of the elliptical sandwich shells is done following the same procedure followed for the circular ones. In particular, we will consider the same materials and choose the optimal design according to the minimum wall stress criterion, equation (3.16), where now $\sigma_z = F_{crit}/(4\pi \cdot t \cdot R_o)$. According to section 3.6.1 and referring to Figure 3.27, the local buckling condition can be rewritten:

$$\sigma_2 = \frac{\gamma \cdot E_f}{\sqrt{1-\nu^2}} \cdot \frac{d}{R_N} \qquad (3.43)$$

, where γ is assumed conservatively 0.20. Like in the case of circular mast, for this value of the design load, face yielding and wrinkling never intervene. Consequently, the core thickness is determined according to equation (2.41)

$$d = \max\left[d_1 = R_N \cdot \sqrt[3]{\frac{k_1\left(\frac{F_{crit}}{E_f \cdot l_{eqv,1}^2}\right)}{2 \cdot k_2}}; d_2 = R_N \cdot \sqrt[3]{\frac{k_1\left(\frac{F_{crit}}{E_f \cdot l_{eqv,2}^2}\right)}{2 \cdot k_2}}; d_3 = 20mm \right]; \qquad (3.44)$$

, where $l_{eqv,1} = \pi\sqrt{E_f \cdot I_{xx}/F_{crit}}$ and $l_{eqv,2} = \pi\sqrt{E_f \cdot I_{yy}/F_{crit}}$ are the supported length of the mast supposing pinned-ends condition.

The wall thickness is then given by:

$$t = \max\left[t_1 = \frac{2 \cdot I_{yy}}{\pi \cdot (1+3\xi) \cdot N^3}; t_2 = \frac{R_N}{R_0} \cdot \frac{F_{crit}}{4\pi \cdot d} \cdot \frac{\sqrt{1-\nu^2}}{\gamma \cdot E_f}; t_3 = \frac{1}{64}" \right] \qquad (3.45)$$

, where t_1 is the thickness required by the global buckling condition; t_2 is the one derived by the local buckling stress, equation (3.43); t_3 is the minimum value required by manufacturing constraints. Finally, the weight per unit length is given by:

$$\frac{W}{L} = \left[4\pi\rho_f \cdot R_0 \cdot t + 2\pi\rho_c \cdot R_0 \cdot (d-t) \right] \qquad (3.46)$$

Figure 3.28 shows the plot of the weight per unit length against the radius for different foam densities.

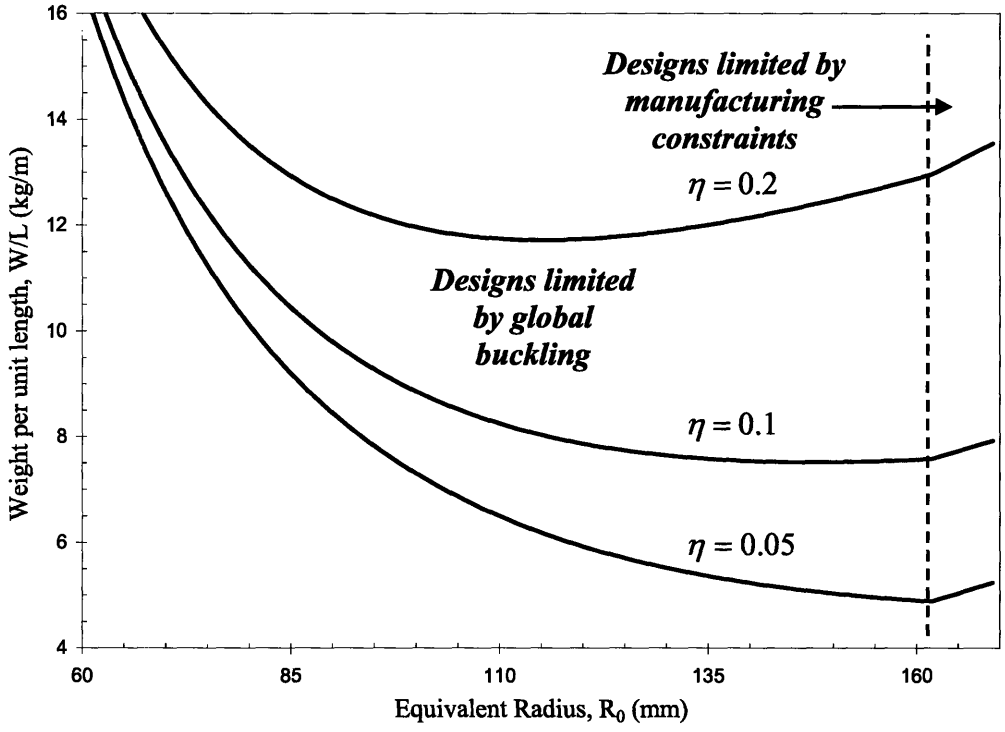

Figure 3.28: Weight per unit length plotted against the radius for elliptical foam- core sandwich shells with different relative densities.

3.6.4 Aluminum Elliptical Cylindrical Sandwich with Honeycomb Core

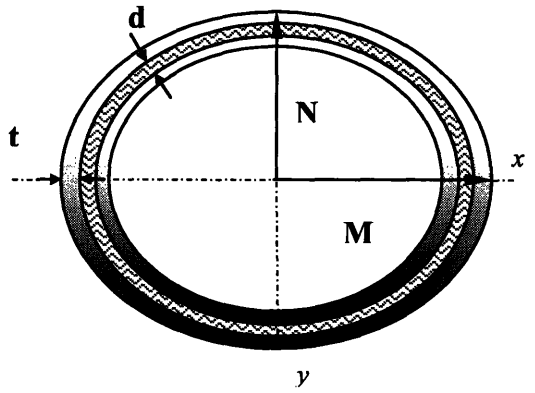

Figure 3.29: Elliptical sandwich shell section with honeycomb core.

The optimal design for honeycomb-core sandwich elliptical mast is performed with the same approach followed in the last section for the foam-core sandwich shell. Due to the small radius of curvature in the points $(\pm M,0)$, the honeycomb types considered in this analysis are over-expanded, in the same fashion of section 3.5.5. The minimum weight configuration is found minimizing the wall stress $\sigma_z = F_{crit}/(4\pi \cdot t \cdot R_o)$ and equation (3.20) still holds. Equation (3.28) is used to determine the face dimpling stress. Similarly to the case of circular section, face yielding and wrinkling never intervene. The core thickness is still defined by equation (3.44), but the manufacturing constraint here is $d_3 = (1/16)"$. The face thickness is given by:

$$t = \max\left[t_1 = \frac{2 \cdot I_{yy}}{\pi \cdot (1+3\xi) \cdot N^3}; t_2 = \frac{R_N \cdot F_{crit} \cdot \sqrt{1-\nu^2}}{4\pi R_0 \cdot d \cdot \gamma \cdot E_f}; t_3 = \sqrt[3]{\frac{F_{crit} \cdot c_i^2}{5\pi R_0 \cdot E_f}}; t_4 = \frac{1}{64}" \right]_a \quad (3.47)$$

, where t_1 is the thickness required by the global buckling condition; t_2 is the one derived by the local buckling stress; t_3 is the value determined by the face dimpling stress and t_4 is still the minimum face thickness required. The weight per unit length is still calculated through equation (3.46). Figure 3.30 shows the plot of the weight per unit length against the radius for different foam densities.

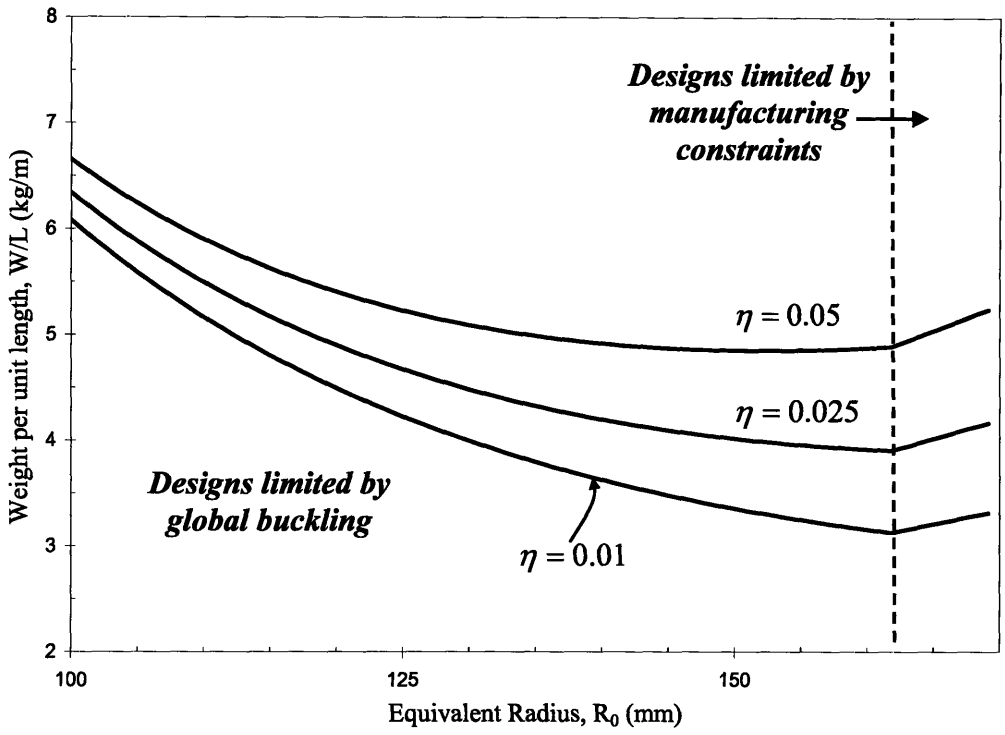

Figure 3.30: Weight per unit length plotted against the radius for elliptical honeycomb-core sandwich shells with different relative densities.

3.6.5 Aluminum Elliptical Cylindrical Shell with Foam Core

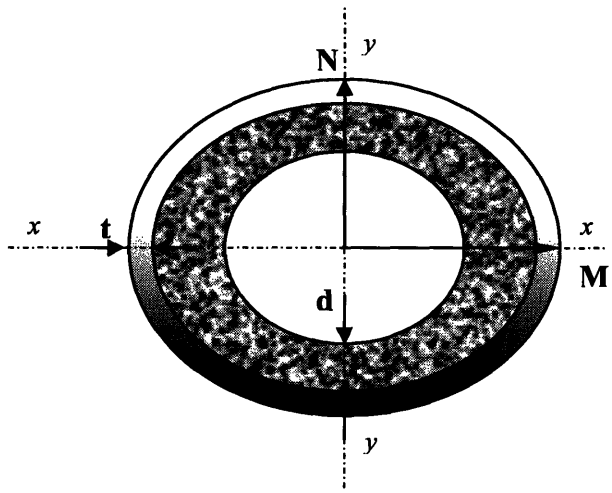

Figure 3.31: Elliptical cylindrical hollow section with foam core.

In this section, we want to define the optimum design for an elliptical cylindrical shell with a foam core of the type represented in Figure 3.31. The foam densities are the same considered in section 3.5.4 and the same assumptions on the material are made.

Substituting R with R_0, the condition for the wall stress $\sigma_z = F_{crit}/(2\pi \cdot t \cdot R_o)$ is still given by equation (3.23). Consequently, the face thickness is determined by:

$$t = \max\left[\begin{array}{c} t_1 = \frac{I_{crit}}{\pi \cdot R_0^3}; t_2 = \frac{F_{crit}}{2\pi \cdot R_0 \cdot \Gamma \cdot E_f}; \\ t_3 = \frac{F_{crit}}{2\pi \cdot R_0 \cdot E_f \cdot \varepsilon_{y,f}}; t_4 = \frac{F_{crit}}{2\pi \cdot R_0 \cdot B \cdot E_f} \cdot \left(\frac{E_c}{E_f}\right)^{-\frac{2}{3}}, t_5 = \frac{1}{64}" \end{array}\right] \quad (3.48)$$

where t_1 is the thickness from global buckling , t_2 from the local buckling , t_3 from the face yielding , t_4 from the face wrinkling and t_5 is the minimum thickness. The core thickness is still determined through equation (2.64). In the case in which the value calculated through equation (2.64) is too high, we suppose that the mast is completely filled with foam. Finally, the weight per unit length is given by equation (3.26), substituting R with R_0. Figure 3.32 shows the plot of the weight per unit length against the radius for different foam densities.

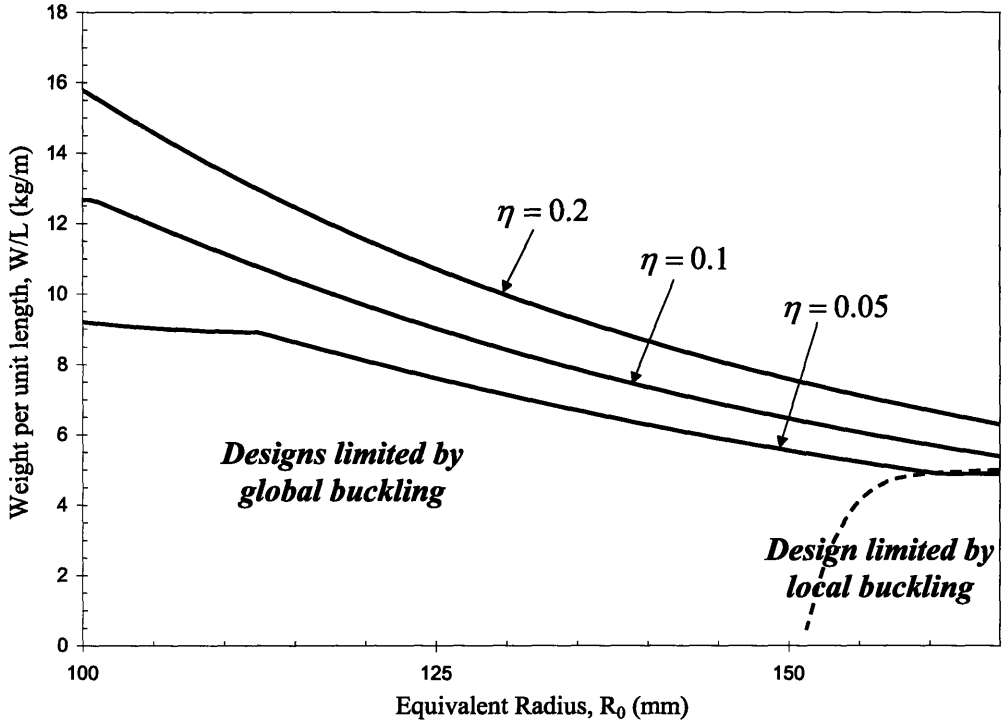

Figure 3.32: Weight per unit length plotted against the radius for elliptical foam-core shells with different relative densities.

3.6.6 Aluminum Elliptical Cylindrical Sandwich with Honeycomb Core

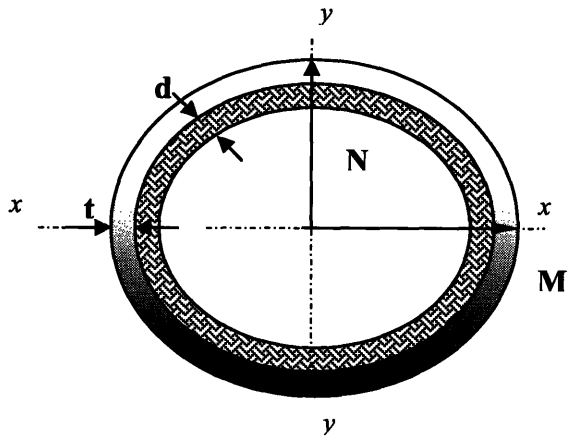

Figure 3.33: Elliptical cylindrical hollow section with honeycomb core.

The last design considered in this analysis is the honeycomb-filled elliptical shell represented in Figure 3.33. The honeycomb type and densities are the same assumed in Section 3.5.4. Defined the wall stress as $\sigma_z = F_{crit}/(2\pi \cdot t \cdot R_o)$, the minimum weight configuration is found using the same approach followed in Section 3.5.4. In particular, the condition for the stresses, Equation (3.27), is still valid. Substituting R with R_0, the shell thickness is found according to

$$t = \max\left[\begin{array}{l} t_1 = \dfrac{I_{crit}}{\pi \cdot R_0^3}; t_2 = \dfrac{F_{crit}}{2\pi \cdot R_0 \cdot \Gamma \cdot E_f}; t_3 = \dfrac{F_{crit}}{2\pi \cdot R_0 \cdot E_f \cdot \varepsilon_{y,f}}; \\ t_4 = \dfrac{F_{crit}}{2\pi \cdot R_0 \cdot B \cdot E_f} \cdot \left(\dfrac{E_c}{E_f}\right)^{-\frac{2}{3}}; t_5 = \sqrt[3]{\dfrac{F_{crit} \cdot c_i^2}{5E_f \cdot \pi \cdot R_0}}; t_6 = \dfrac{1}{64}"; \end{array}\right] \quad (3.49)$$

where t_1 is the thickness from the global buckling requirement, t_2 from local buckling, t_3 the face yielding condition, t_4 from the face wrinkling, t_5 from face dimpling and t_6 is the minimum thickness. The core thickness is determined through equation (2.64). In the calculation of the core thickness, the geometric constraint $d > (N - t)$ (see Figure 3.33), has to be added. Substituting R with R_0, the weight per unit length is then given by Equation (3.26). Figure 3.32 shows the plot of the weight per unit length against the radius for different honeycomb densities.

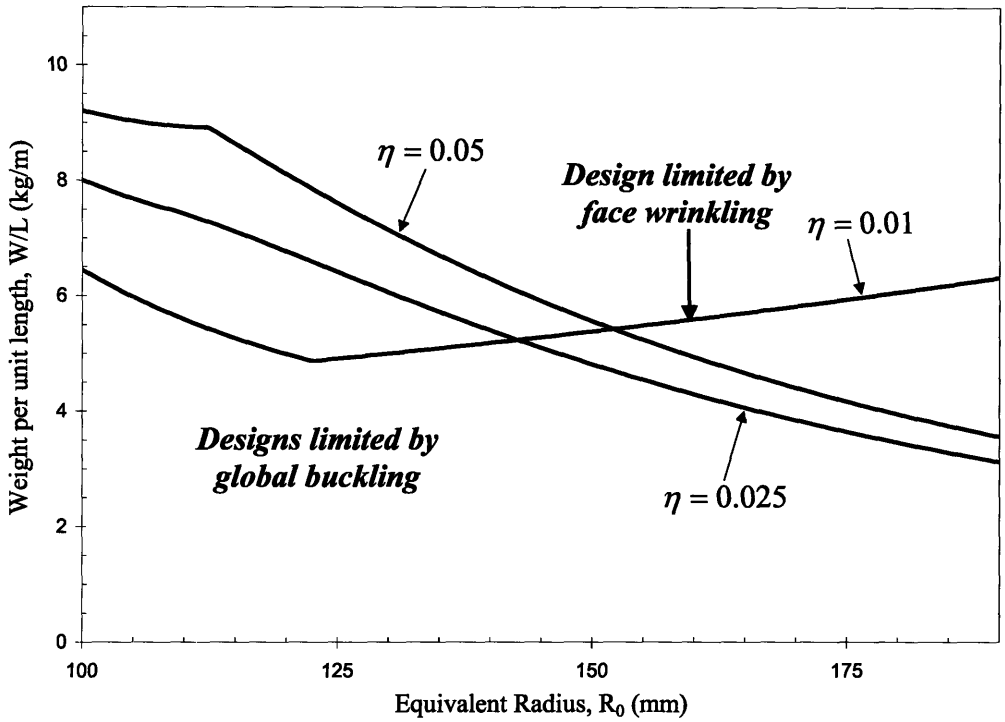

Figure 3.34: Weight per unit length plotted against the radius for elliptical honeycomb-core shells with different relative densities.

3.7 Application of Cellular Metal in Sailboat Masts: Discussion

In the previous paragraphs, we have observed that the mast is a column, designed to be as stiff and as light as possible. The designer has two groups of variables with which she/he can optimize the performance: the shape of the section and the materials properties. Five different combinations of sections and materials were analyzed for the design of the mast of a typical 12-meter yacht: hollow shell, sandwich shell with foam core, sandwich shell with honeycomb core, hollow shell with foam core and hollow shell with honeycomb core. For each construction type, we determined the design geometry minimizing the weight; this was done fixing the mast external dimension arbitrarily and considering different section types: circular in the first approximation and elliptical, in this case using a simplified theory to estimate the local buckling stress. Figures 3.35 shows plots of the weight per unit length against the radius for each mast construction type, assuming circular section. Figure 3.36 represents analogous plots for elliptical section.

As already observed in the last sections, the optimum geometry for hollow thin-walled masts subjected to a typical design load, corresponds to the simultaneous local and column buckling; in both Figures 3.35 and 3.36, the value of the radius R or equivalent radius R_0 relative to this condition has been indicated with $\Re_{opt,1}$. Elliptical sections, which are more sensitive to local buckling than circular ones, are characterized by a lower value of $\Re_{opt,1}$. For $R, R_0 \leq \Re_{opt,1}$, empty shells represent the best design; for $R, R_0 > \Re_{opt,1}$, shells integrating honeycomb, both in the sandwich and reinforced construction, are lighter than the hollow tubes counterpart, while foam-core shells do not perform particularly well compared to any other design.

Considering Figure 2.9 and taking $F_{crit}/\left(E_f l_{eqv}^2\right) \approx 10^{-8}$, which corresponds to the load index of our case of study, we would find that honeycomb- and foam-core reinforced shells represent the best design, followed by the sandwich constructions and at last by the empty shell. This points out a limit of the analysis of the second Chapter, in which optimal designs are obtained neglecting any manufacturing constraint.

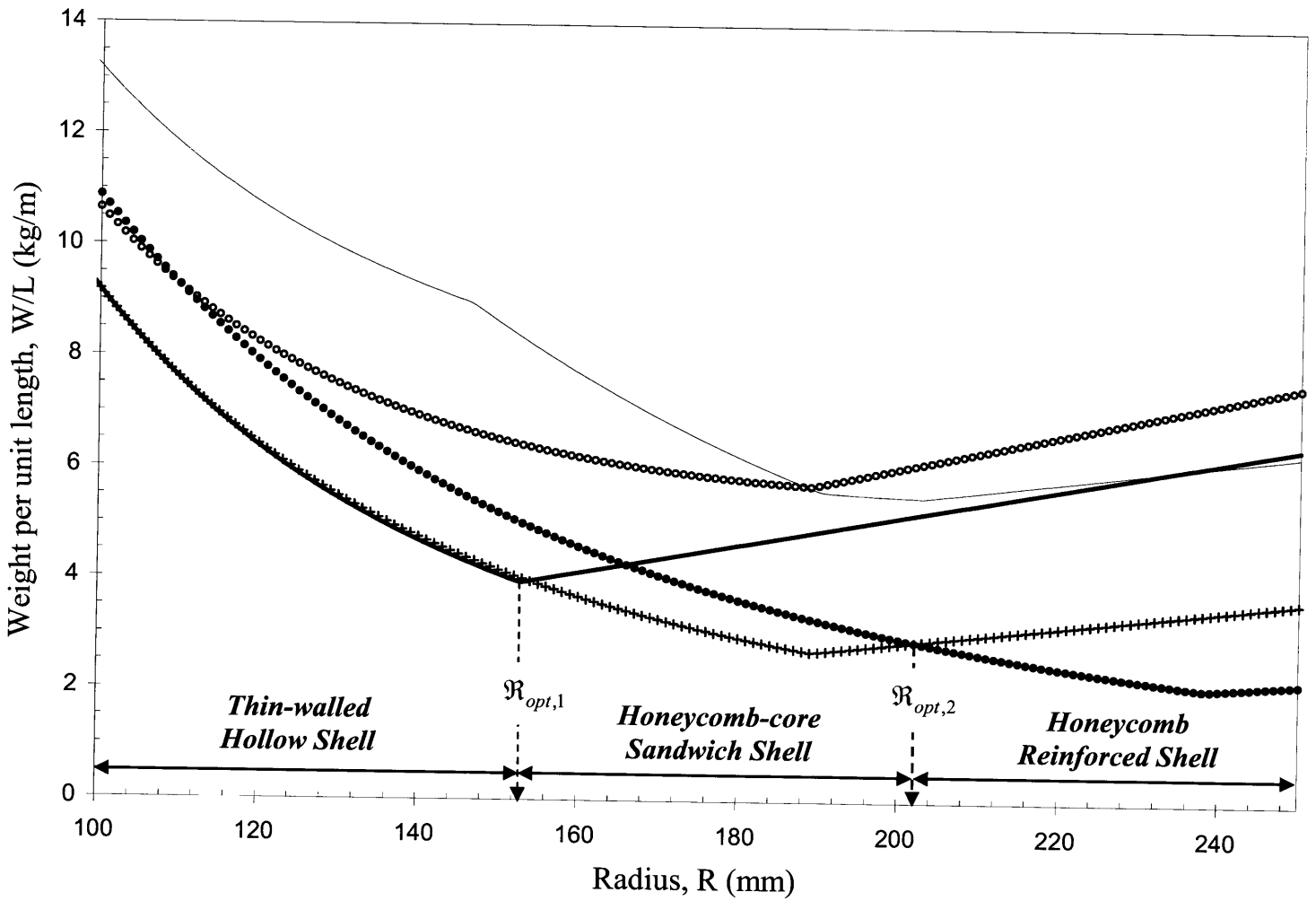

Figure 3.35: Weight per unit length plotted against the radius for hollow circular shell (—), foam-core sandwich shell $\eta = 0.05$ (○○), foam reinforced hollow shell $\eta = 0.05$ (—), honeycomb-core sandwich shell $\eta = 0.01$ (++), honeycomb reinforced hollow shell $\eta = 0.025$ (••).

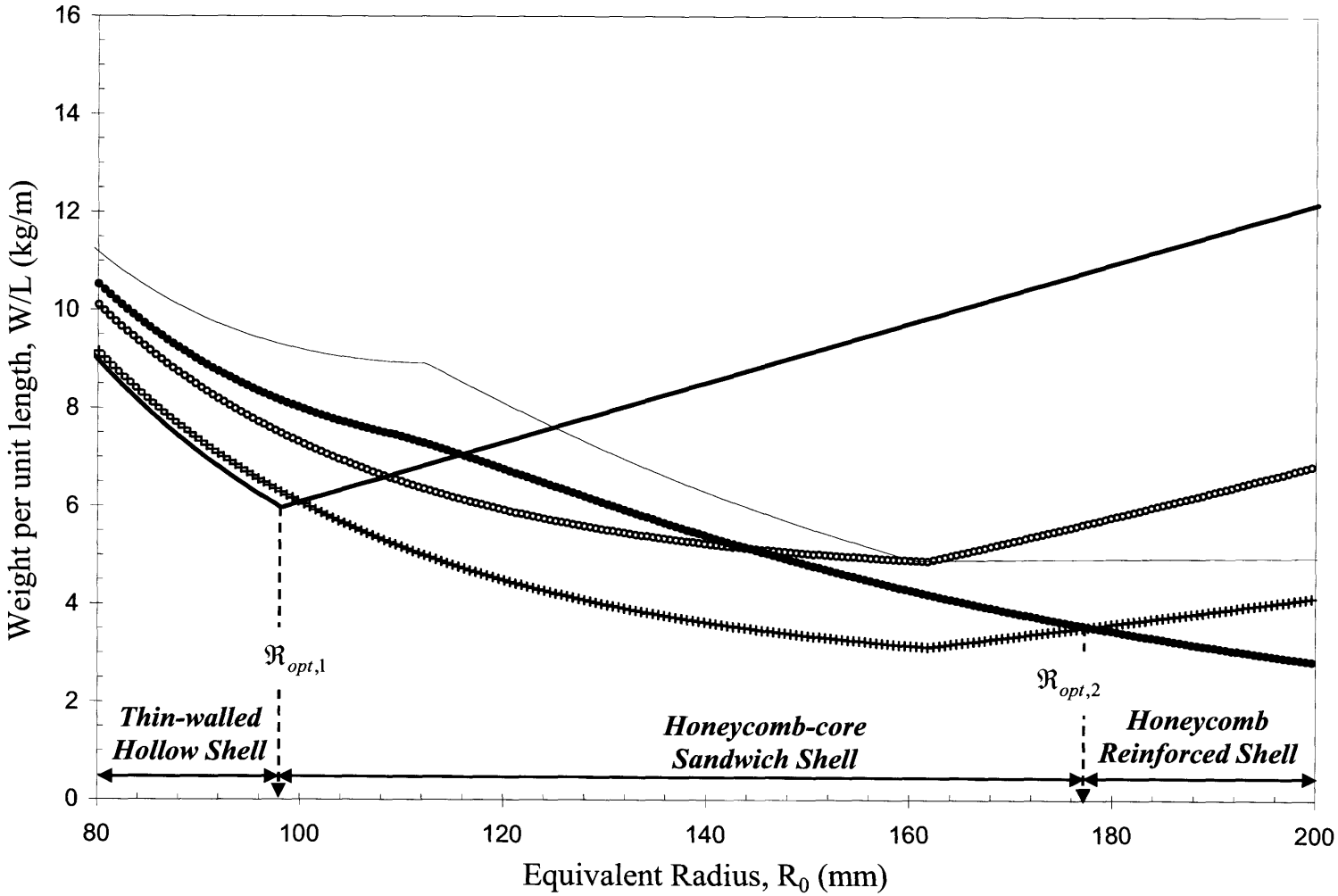

Figure 3.35: Weight per unit length plotted against the radius for hollow elliptical shell (—), foam-core sandwich shell $\eta = 0.05$ (○○), foam reinforced hollow shell $\eta = 0.05$ (—), honeycomb-core sandwich shell $\eta = 0.01$ (++), honeycomb reinforced hollow shell $\eta = 0.025$ (••).

In the foam-core shells, the irregularity of the foam microstructure (see Chapter 1) sets a lower limit to the core thickness. Consequently, the geometric parameters for these shells are significantly far from the optimum values. The case of honeycomb-core shells is different: the availability of core layers with a thickness of 1/16" or more makes possible to reach values of $R/t(R_0/t)$ near the optimum condition, where global and local buckling occur simultaneously.

Honeycomb reinforced hollow shells are impractical for small values of R or R_0. The reason is that, even using cells with special geometries, e.g. rectangular, the required core thickness would make impossible to bend the honeycomb layer up to the radius of curvature needed. However, in the optimum range of application of this design, i.e. for $R, R_0 \geq \Re_{opt,2}$ (see Figures 3.35 and 3.36), the corresponding core thickness is small and fabrication of this tubular structure is feasible.

Aluminum sailboat masts currently have an elliptical hollow section and, for boats of small dimensions, are designed against Euler buckling, while for medium-large boats are designed against local buckling and have an equivalent radius $R_0 \approx \Re_{opt,1}$ [22]. *The analysis of this Chapter proved that (Figure 3.36) in designs limited by local buckling the application of honeycomb as core material can lead to a significant reduction of the mast weight with a limited increment of the mast equivalent radius* R_0.

Future investigations should analyze also the effect of a bending moment applied to the mast and the possibility to extend the design to orthotropic materials, in particular CFRP shells and carbon honeycomb. In the next Chapter, business opportunities based on this application are discussed.

3.8 References

[1] L. Larson, R. Eliasson, *Principle of Yacht Design,* London, **2003.**

[2] Hammit, *Technical Yacht Design*, New York, **1975.**

[3] D. Gannel, *Modern Development in Yacht Design,* **1977.**

[4] N. L. Skene, *Elements of Yacht Design,* **1963.**

[5] M.F. Ashby, *Materials Selection in Mechanical Design*, Butterworth-H. Oxford. **1992.**

[6] S. P. Timoshenko, J. M. Gere, *Theory of Elastic Stability*, N.Y., **1996.**

[7] T. Speer, http://home1.gte.net/tspeer/Index.html, **2004.**

[8] J. Gilliam, "History of Sailing Yacht Masts, Rigging, Sails: 1900- Present Days", http://boatdesign.net/articles/mast-materials/, **2004.**

[9] *Cruising World,*, p.52, December **1998**.

[10] *Sail,* p.60, April **2000**.

[11] C. Cairoli, *private communication*, Department of Ocean Engineering, Massachusetts Institute of Technology, Cambridge, June **2004.**

[12] Gerard, G., *Minimum Weight Analysis of Compression Structures*, New York University Press, New York, **1956.**

[13] T. Bitzer, *Honeycomb Technology*, Chapman & Hall, London, **1998**

[14] L.J. Gibson and M.F. Ashby, *Cellular Solids: Structure and Properties*, 2nd ed., Cambridge University Press, Cambridge **1997.**

[15] F. Plantema, *Sandwich Construction,* John Wiley & Sons Inc., New York, **1972.**

[16] J. Kemper and Y.N. Chen, "Buckling and Post-Buckling of an Axially Compressed Oval Cylindrical Shell." *Proceedings, Symposium on the Theory of Shells to Honor Lloyd Hamilton Donnell,* Univ. of Houston, McCutchan Publishing Corp., pp. 141-183, **1962.**

[17] Hutchinson J.W. "Buckling and Initial Post-Buckling Behavior of Oval Cylindrical Shell under Axial Compression", *J. Applied Mechanics* **1968;** *35*, p. 66-72

[18] Donnell L. H. "A New Theory for the Buckling of Thin Cylindrical Shells Under Axial Compression and Bending" *Trans. ASME,* 56, **1934**, p. 795-806.

[19] Kemper J. "Some Results on Buckling and Post-Buckling of Cylindrical Shells", in *Collected Papers on Instabilities of Shell Structures*, NASA TND-1510, **1962**, p.173-86

[20] Tennyson R. C., Booton M., Caswell R.D., "Buckling of Imperfect Elliptical Cylindrical Shells under Axial Compression". *Am. Inst. Aereonat. Astronaut. J.* **1971;** *9*; p. 250-5.

[21] J.W. Hutchinson and M.Y. He, "Buckling of cylindrical sandwich shells with metal foam cores", *International J. of Solids and Structures* **2000**, *37*, p.6777-6794

[22] H.I.S.W.A., 10th International Symposium on Developments of Interest in Yacht Design and Yacht Building, , **1988.**

Chapter 4

Investment Assessment for Sailboat Masts with Cellular Core

"Measure what is measurable, and make measurable what is not so"

Galileo Galilei

4.1 Introduction

In Chapter 2, we have discussed the potential viability of cellular metals as materials in composite for load bearing structures. In Chapter 3, we have shown how cellular metals can be applied in the sailboat industry for the manufacture of high performance masts. This Chapter discusses investment opportunities for a Company producing masts with metallic foam/honeycomb cores. The organization of the Chapter is shown in Figure 4.1.

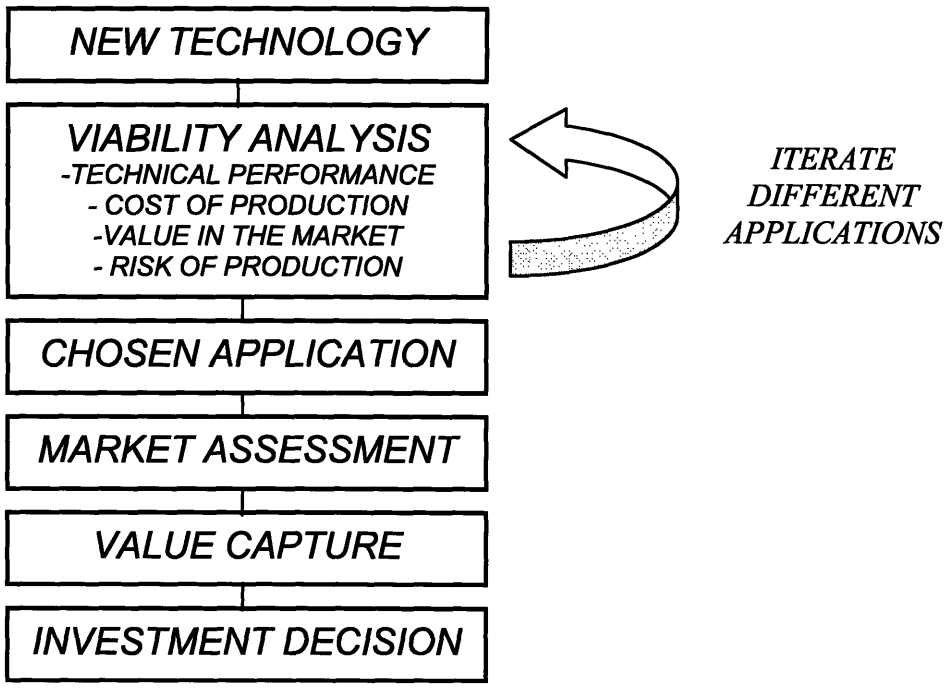

Figure 4.1: Investment assessment.

The investment assessment is divided in two parts. In the first part, we analyze the *potential market for our product.* The end user is described in terms of type of sailor and certain factors affecting the purchase decision. The companies producing masts are listed and the projected market for masts is estimated. At this time there are almost 30 principal companies producing aluminum and carbon fibers masts in the United States. Data on the mast market are somewhat scattered and incomplete, but good estimations can be done based on the behavior of the general sailboat market. The basic assumption here is that mast market growth is intimately related to sailboat sales, which is generally true with the only difference that the sailboat market is more sensitive to changes in the macroeconomic parameters than the mast market, where the demand is more stable. The demand of the products offered by the Company in the market is forecast, considering the penetration rate of products with similar degree of innovation and value in the sailboat market. A marketing strategy is also discussed. In the sailboat market the word-of-mouth is still the best way to promote products, so every action has to be focused on how to build-up the Company's credibility. This activity should also consider the channel chosen for the distribution, because the real customers of the Company are not end-users, but intermediate stakeholders.

In the second part, the *probability of value capture* is discussed. Viability assessment and market assessment may demonstrate that the materials innovation under consideration has the potential to create enormous value. However a Company may be not persuaded of this assessment and still decide not to invest. In order to invest, a Company must be convinced that they will be able to capture a significant portion of the value created by the innovation. The concepts of appropriability, industry structure, competitive advantage, and organizational structures are utilized to predict the likelihood of capturing value.

Finally, information from the market and value capture assessments is used as input to determine the best investment decision.

4.2 Market Assessment

4.2.1 Generality

The market assessment involves both the technical inputs of performance metrics and the market inputs of customer requirements and emerging opportunities. Desired inputs include: further information to direct the technical development effort, such as, suitable markets on which to concentrate development, and exchange constants for utility analysis; and information to guide financial decisions down-stream, such as, segments of markets which are more attractive, market projections, marketing, and customers and competitors analyses (see figure 4.2) [1].

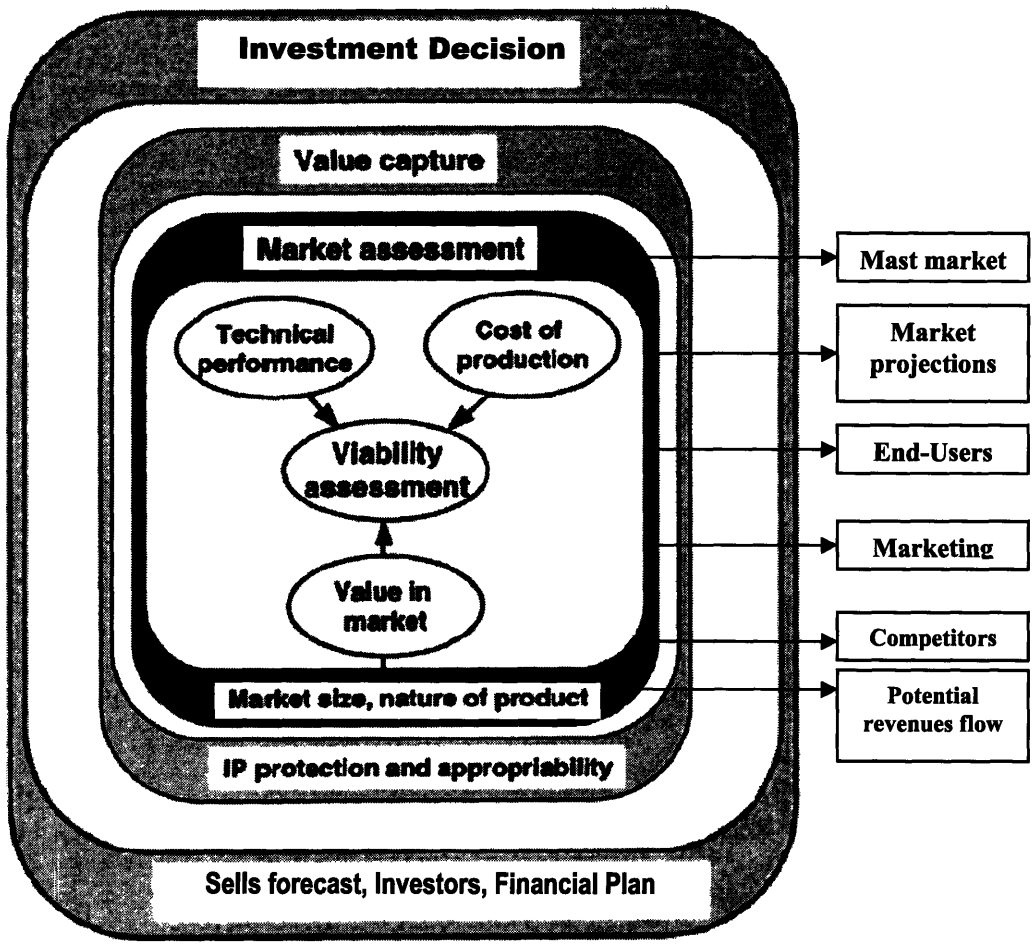

Figure 4.2: Market assessment.

4.2.2 Mast Market

We have seen that the mast market can represent an opportunity to capitalize on the principle of using cellular metals in load bearing components, where weight, strength, buckling resistance, and bend characteristics are key performance metrics. Another factor influencing the mast market choice is the ability of this market to accept rapidly design improvements, once proven. The market is extremely performance conscious and responds well to new products that offer significant increases in performance. However, nothing up to this point has been said about the market size. Table 4.1 shows estimates of the mast market for the year 2000:

Geographic Location	**Units**	**$(Million)**	**%**
United States	3,000	60	14.3
Europe	16,000	320	76.2
Other	2,000	40	9.5
TOTAL	21,000	420	100.0

Table 4.1: Mast market (2000).

The estimates were based on data given by *Cruising World* [2] and *Sailing World* [3] magazines, and discussion with the director of the MIT Sailing Club. Unit sales in Europe were based on the sailboat sales in Europe. The U.S. and European markets were assumed about 90% of the total world market of masts, with the Australian market leading the rest of the world. The average price of $2,000 for masts was used. The European market [4] is much larger than the United States. France and the British Islands are the leaders of the market with 20% each. Italy and Greece together have a 15% of share, followed by Spain and Portugal with 12%. Sweden, Norway, Denmark, and the Benelux have 10% of share respectively, while Austria, Germany, and Swiss represents 9% of the total sail market. Consequently, assuming that the Company is based in the United States, we still cannot ignore the European market as an export market.

Present market estimates would be incomplete, if historical and future trends were not considered: this can be particularly difficult, because information dealing specifically

with the mast market is difficult to find. For this reason, the general sailboat market will be considered: we assume that the masts and the sailboats sales are directly related.

However, a considerable difference has to be underlined: the mast market, as every accessory market, is less sensitive to economic fluctuations – in particular economic recessions – as the mast is cheaper to upscale than the boat and yet it has a significant impact on performance.

4.2.3 Sailboat Market Projections

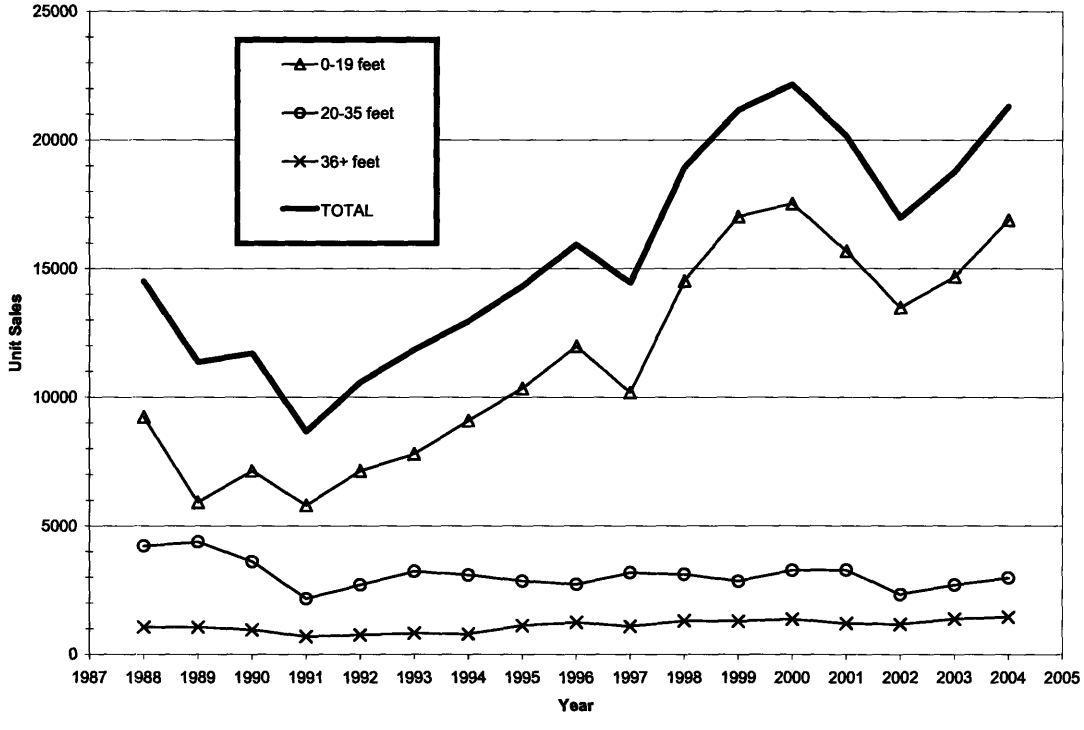

Figure 4.3: Sailboat sells in the United States by category.

Figure 4.3 shows the sailboat sales in the past 20 years, subdivided in each boat category. The information about the sales was obtained through the Annual Sailing Business Reports by the New York Times Magazine Group Resource Research Center [5]. The first relevant information is represented by the segmentation of the market. The Mid-size (20 to 35 feet in length) and large-size (36 feet in length and above) boat categories represent a stable portion of the market, while the small boat segment is extremely sensitive to the general national economy, as consumers of these relatively inexpensive

boats are the first to feel the squeeze of an economic turndown. The most influential parameter is cost of the petrol [6]: when the cost of the petrol falls, the demand of motor-power boats increases attracting new customers from the sailboat market. This phenomenon was at the base of the sales drop in the early 90s. In 2001, the recession caused again a cut in recreational spending, resulting in a built-up of sailboat inventory and thus a slowdown in boats manufactured [7]. Again, the sector of the industry to receive the most significant drop in production was the category of the boats 0-19 feet in length. This decrease in the sales is not worrying, as the retail value of this category is marginal in the total sailboat market (table 4.2).

Looking forward to the next five years, two factors are likely to improve sailboat production. The effect of *Sail America's initiative* [8] to increase participation in sailing started in the early 90s, made a difference for the first time in 2003 and is growing over time, including increased sales of sailboat of all sizes, as well as sailing products and services. A 2001 national survey by the National Sporting Goods Associations (NSGA) [9] already indicated that sailing was among the top 5 fastest growing sports in United States, with a participation of 2.7 million people and a 9.9 percent annual rise, compared to 2000. In addition, following the events of *September 11, 2001*, the sailboat industry is seeing an increased numbers of customers willing to spend time with friends and family close to home. For those with a passion for sailing, this means a greater dedication to spend time on their sailboat and likely a larger investment in sailing as activity.

Boat Length	Units sold	Unit Cost ($)	Retail Value ($)	%
0-8'	8001	2,000	16,002,000	**9.9**
8'-19'	9531	6,000	57,186,000	
20'-29'	2217	30,000	66,510,000	**26.2**
30'-35'	1052	121,000	127,292,000	
36'-40'	740	222,500	164,650,000	**63.9**
41'-45'	424	377,000	159,848,000	
46'-59'	181	660,000	119,460,000	
60'+	17	1,700,000	28,900,000	
Total	22,164	-	**739,848,000**	**100**

Table 4.2: Sailboat retail value in the United States (2000).

4.2.4 End-Users

Although the customers of the Company are sailboat manufacturers and sail dealers, the ultimate customers are the end-users, i.e. the sailors. Since the Company's products are high performance, the ultimate purchaser would be a professional sailor or the serious sailors with a desire for increased performance, and thus a reasonably sophisticated consumer of sailing products. In particular, the Company will target professionals with carbon fiber or aluminum core (in the categories were carbon fibers are forbidden) masts and attract the massive bulk of sailors, who desire increased performances but that now cannot affort the expensive carbon fibers masts, with traditional aluminum hollow masts. The typical consumer will gather information prior to purchase through trade journals and word-of-mouth. This sophisticated consumer would also be influenced by professionals' use patterns.

Consequently, we can identify three segments where we can introduce our new products:

1. Professional racing, where sailors want the best in the market and there is a strong need for increased performance;
2. High-performance recreation or sail cruising, where sophisticated sailors seek the best in the market but are more price sensitive;
3. High-performance recreation or sail cruising, where sailors want an innovative products but for an affordable price;

Ideally, the Company should try to place one product line for each of these segments. To accommodate the refined tastes of the high-end sailors, the Company should also develop a line of accessories for the mast and a boom line. In addition, the possibility to customize the bend characteristic of the mast, according to the end users' desires, should be taken into consideration.

4.2.5 Overall Marketing Strategy

The *overall marketing strategy* of the Company is to create a market demand-pull through building credibility and a reputation for its products as the state-of-art equipment. Various studies showed that professional promotion activities are crucial elements to the marketing plan of high-end sail products [10]. In order to generate visibility of the Company products, prototypes have to be supplied to key professionals on the sailing

circuits. In addition, advertising, trade press and online releases have to be placed, following major victories of these professionals. Specifically, these advertisements have to be concentrated from April to August of each year, in order to take into account of the summer selling peak.

The sales efforts will be focused on three primary *channels of distribution*: direct sales to dealers, sales to sailboat manufactures, and coventures with major sail makers on the possibility of supplying custom masts for tailor-made sails. Dealers represent the most common distribution channel for small size sailboat masts. The typical dealer has a shop dedicated to sailing equipment, carrying a full line of accessory equipment and sells directly to end-users.

Collaboration with sailboat manufacturers is essential when the mast has to be included in the boat overall design, as for medium-large sail cruiser. Typically, this collaboration is based on commissioned jobs and the margins of profits are predictably high compared to direct sales to dealers, due to high degree of specialization. As the benefits offered by the product sold by the Company are larger for large boats and cruisers, this channel of distribution is privileged. Another potential distribution strategy of the Company is represented by mast and boom OEMs, by allowing these companies to market the product under their own labels. This policy is advantageous on short-term cash flow, but may expose the Company to the risks involved in selling directly to competitors.

Coventure with sail makers for designing masts with bend characteristics tailored to a specific sail, is a fundamental prerequisite to become involved in top sail competitions like the America's Cup. In fact, the performance of a particular sail is directly dependent on the bend characteristic of a mast. The coventure may offer many advantages, like mutual exchange of expertise and joint promotion activities.

4.2.6 Competition

As mentioned already, the competition for sailboat masts is extremely fragmented: in the United States there are almost 30 companies producing masts for boat [11]. Some of these companies specialize in the production of spars for sailboat; others have a wide range of marine accessories. The main players are listed in table 4.3. The Company will compete primarily against carbon-fiber mast producers. The primary competitors are

represented by [12] Composite Solutions Inc., Forespars Products, GMT Composites and Hall Inc. Internationally the carbon fibers mast manufacturers, which export to the United States, are Marten Spars and Southern Spars.

The most direct individual competitor of our Company is Hall Inc. [12] Hall Spars & Rigging was founded in 1980 by Eric Hall and Phil Garland. Now Hall employs 63 People in Bristol and another 25 in Holland. The centerpiece of Hall's composite department is a 19 meter, purpose-built, aerospace grade autoclave, curing carbon fiber products at 85 pounds per spare inch of pressure at 250 °F. This high-pressure curing process eliminates voids, maximizes fiber straightness, assuring products of excellent quality. Hall equips the winner of the 2003 edition of America's Cup. Hall's share is estimated to be approximately 8% to 15% of the U.S. market.

Name	Employees	Est. Sales (Million $)	Product
Selden Masts	10 to 19	2.5 to 5	Aluminum
Sail One Design	1 to 4	0.5 to 1	Aluminum
Nance & Underwood	10 to 19	1 to 2.5	Aluminum
Hall Spars	50 to 99	20 to 30	CFRP
Charleston Spars	20 to 49	2.5 to 5	Aluminum
Dwyer Aluminum Masts	10 to 19	1 to 2.5	Aluminum
Florida Rigging	10 to 19	2.5 to 5	Aluminum
Zephyr	20 to 49	2.5 to 5	Aluminum
Metal Masts Marine	10 to 19	1 to 2.5	Aluminum
Composite Solutions	5 to 9	1 to 2.5	CFRP
Composite Engineering	5 to 9	1 to 2.5	CFRP
Forespar	1 to 4	1 to 2.5	CFRP
Chesapeake	10 to 19	1 to 2.5	Aluminum
GMT Composites	10 to 19	1 to 2.5	CFRP
New England Rigging	5 to 9	0.5 to 1	Aluminum
Others	-	less than 0.5	Aluminum

Table 4.3: U.S. sailboat masts producers

4.2.7 Potential Revenue Flows

Forecasting the demand for a product just introduced into the marketplace is a difficult matter. The approach we follow has been adopted by Elicia Maine [1] and is based on the Clark's and Abernathy transilience map [13]. The first thing to estimate is the *time of substitution,* defined as the period between the first commercialization and 100% substitution into an established application (full maturity) [13]. Substitution curves are modeled as error functions; this is because it always takes a certain amount of time for any new technology to take off [13]. When (and if) it does catch on, the technology usually sweeps through an industry quickly, because companies do not want to be left behind [1]. The technology reaches a plateau when most of the companies that planned to adopt the new technology have done so. Maine [1] points out that the substitution period correlates with price and performance characteristics, i.e. the substitution time for a product of lower cost and higher performance can be about 20 years, while a product of lower cost but lower performance can take 50 years for full substitution [1]. The method of comparison with historical substitutions, as substitution-time forecasts, is justified only if applied in the same market: obviously, it is not possible to compare electric shave blades with aluminum alloy rims, even if they belong to the same category in the transience map cost/performance.

In order to calculate the time of substitution for cellular metal masts, we can refer to the diffusion curve of CFRP hulls in the boat industry represented in Figure 4.4.

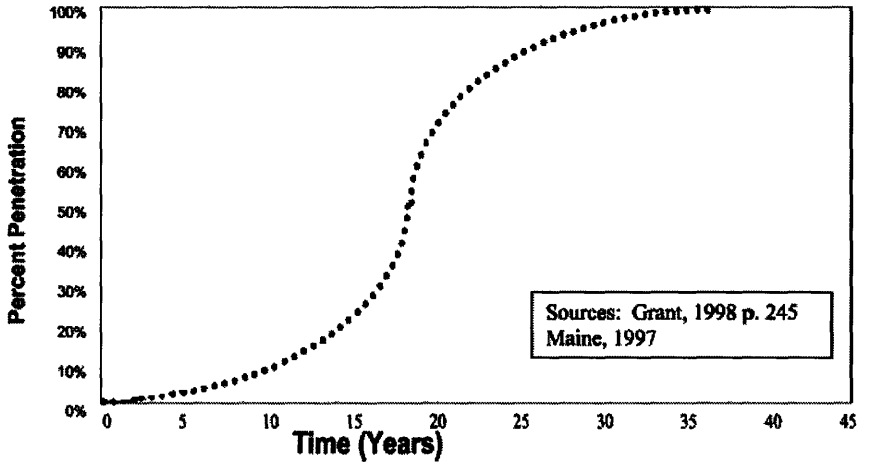

Figure 4.4: Market penetration of CFRP in boats' hulls [1].

The market, where we target introduction of the new product, is the U.S. high-end market; in particular masts for large cruiser sailboat and high-level recreation. This market is estimated to be about 45 M$. Based on these considerations, the gross revenues on sales can be forecast in 1.125 M$ in 5 years and 4.5 M$ in 10 years. Obviously, this analysis assumes that no company will use the same technology to produce masts. In the next paragraph, we will analyze the probability to defend this value.

4.3 Value Capture

4.3.1 Generality

The viability and market assessment indicate a strong likelihood of a future market in the sail industry for aluminum foam and honeycomb as substitute for aluminum and carbon fiber mast in excess of ~$5M annum in 10 years, with the medium term possibility of capturing other sport applications and the long-term possibility to capture aerospace applications. It remains to be seen, however, whether a small company starting a business based on this kind of innovation, is in strong position or not to capture the value created. In this section, tools to assess industry attractiveness, appropriability, and organizational structures are utilized to predict the likelihood of capturing value.

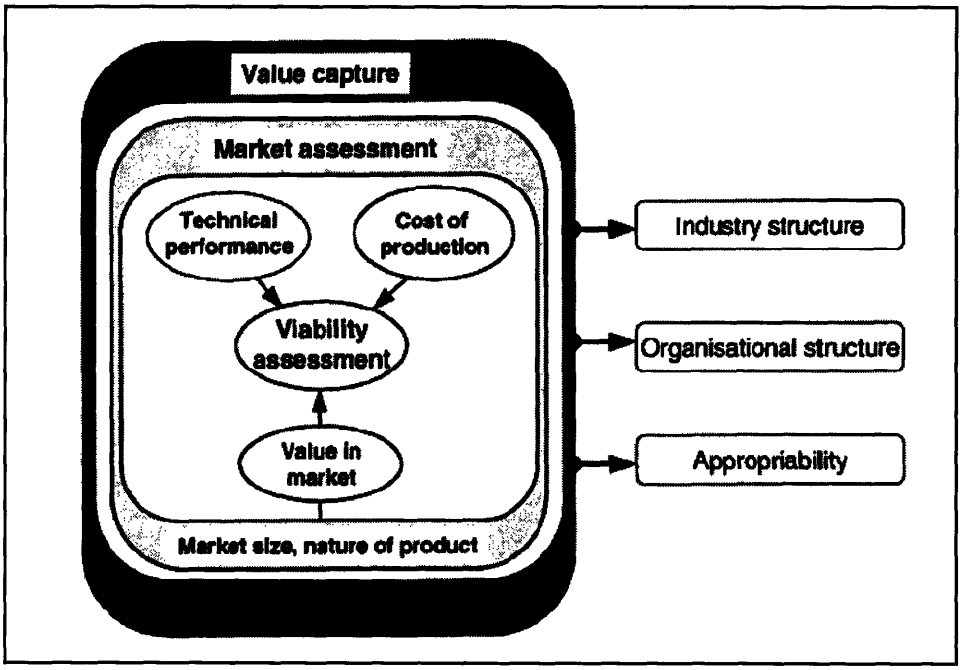

Figure 4.5: Value capture assessment.

4.3.2 IP Asset and Defence

No current licence exists for load-bearing honeycomb/foam core shells in any application: the objective of this section is to understand if the sailboat industry allows the defence of IP. Aluminium and CFRP masts producers have different IP management policies. The former, who manufacture a product that is easily replicable, protect special mast designs by patenting their products [14-19]. On the other side, CFRP mast producers keep most of their processing techniques as trade secrets [20], although particular fabrication methods are protected [21], as well as special composite lay-up designs [22-23]. Hence, the structure of the sail industry allows for defence of IP. On the other side, the possibility of a specialized asset does not seem feasible, as a CFRP mast producer can assemble the process in autoclave without excessive difficulties. In addition, product and customer linkages are not overturned and the product cycle time is comparable with the manufacture of CFRP masts.

Consequently, a Company starting to produce honeycomb/foam core masts would be at moderate appropriability regime.

4.3.3. Industry Structure

Industry attractiveness for businesses based on innovative materials, in particular aluminium foam, is described by Maine [1]. The methodology used, derived by Porter [24], directs attention to the competitive thread given by different stakeholders. In particular, Porter analyses the influence of potential entrants/substitutes and buyer/supplier, which might reduce value-capture by the innovating firm [24]. In the present context, we find that several companies producing masts for sailboat, some of them using CFRP and other aluminum of different performances and qualities. The number of substitutes is therefore considerable, especially in the high-end market. The company may suffer also by the pressure exerted by end-users. In addition, potential entrants, deciding to produce masts using the same technology the Company will pursue, may be advantaged by the moderate IP protection of the manufacturing process.

Summarizing, the industry attractiveness for this technology is low.

4.3.4. Organizational Structure

The most attractive innovation opportunity can be squandered if a company has not a proper organizational structure. According to Maine [1], entrepreneurial experience of management, presence of visionary dealmakers, flexibility of the organization, effective knowledge acquisition and management, and operational efficiency are all important ingredients for successful innovation. The small size of companies producing masts (many of them have 10-20 employees) represents a competitive advantage when introducing innovation, due to their flexibility and opportunistic approach to their decision making. In Table 4.4, it is represented the management efficiency for both a typical CFRP (Hall Spars Inc.) and extruded aluminium mast company (Selden Mast Company) [27].

Management Efficiency	**Aluminum**	**CFRP**
Income/Employee	6,000 ($/employee)	8,000 ($/employee)
Revenue/Employee	170,000 ($/employee)	273,000 ($/employee)
Receivable Turnover	6.8 %	6.1 %
Inventory Turnover	5.8 %	10.8 %
Asset Turnover	0.7 %	1.5 %

Table 4.4: Management efficiency [27].

Most CFRP mast producers are characterized by the presence of an engineering team (Hall Spars has the largest group with 7 engineers and several CAD designers) and high profile management. Eric Hall [25] the founder of Hall Spars graduated in 1966 from University of Michigan, Ann Arbor, MI with a BS in aeronautical engineering and naval architecture. He gained work experience working for Grumman Aircraft in Bethpage, NY and Union Mast in Bremen, Germany. Before becoming president of Hall Inc. he was department manager for Schaefer Marine. Peter Quigley [26] who is president and founder of Fiberspar, a company producing masts and booms for the sailboard market, is also responsible for the Engineering and Research & Development department, using his expertise and knowledge of composites gained while a student at M.I.T. Aluminium mast companies seems to lack visionary dealmakers.

4.3.5 Probability of Value Capture Summary

The chances of value capture for a Company, producing masts employing cellular metals, are medium. Good opportunities are represented by the lack of a large, established manufacturer. Difficulties might arise by the many substitutes and the moderate ability to defend the intellectual properties. Enlarging the production to aeronautical structural tubular components may even lower the probability to capture values, because will expose the Company to the strong power of the suppliers and buyers.

4.4 Investment Decision

In this section, using information from the market and value capture assessment, we discuss the investment system for the technology under consideration. Figure 4.6 shows the market-size/value capture of a Company producing cellular metal masts ten years after the beginning of the business.

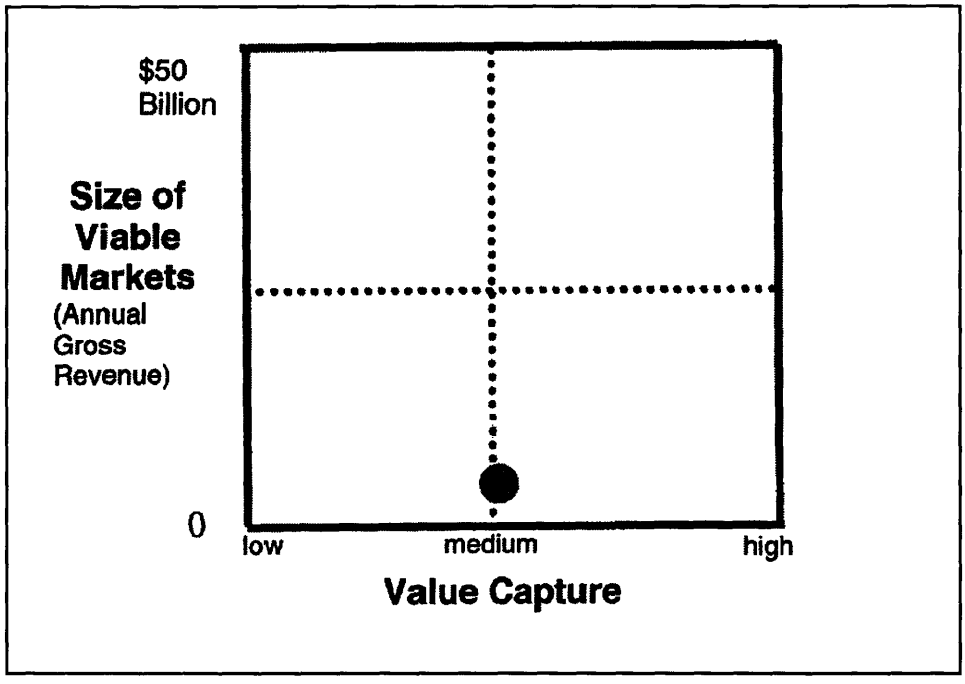

Figure 4.6: Value created by the technology under investigation.

It is clear from Figure 4.10 that the size of the market is too low to justify the risk of starting a new business specialized in producing cellular metal masts. This consideration is reinforced by the high start-up costs derived by the acquisition of an autoclave (an autoclave 40" long can cost 250,000$ [20]) and the competition of CFRP mast producers. The opportunity to apply the same technology in other market niches, e.g. the aerospace market, is weakened by absence of a killer application.

Starting a Company producing cellular metal together with traditional CFRP masts seems more promising: the reason is that the Company could take advantage of the growing sailboat market and, in the same time, acquiring experience in the field. The problem of starting a Company can be financial. Making some rough calculations, we can estimate the cost of the equipment and facility to be about 1.5M$. Being the expected revenues of 25$M in ten years time and set a marginal profit of 20% per mast sold, we can expect to break even in 6-10 year time: this makes difficult to raise venture capital.

Another option is to licensee the technology to an already existing CFRP sailboat mast Company. This possibility seems the best as CFRP mast manufactures already own autoclaves and are always interested in product of superior technical performances. Table 4.5 summarizes the different financial options.

Investment Strategy	**Attractiveness**
Start-up specialized in the fabrication of honeycomb/foam core aluminum or CFRP masts and looking to expand in other markets, e.g. aerospace	*Low*
Start-up producing honeycomb/foam core aluminum or CFRP masts together with a line of CFRP masts	*Medium/Low*
Licensee the technology to existing CFRP mast manufacturer	*High*

Table 4.5: Attractiveness of different investment strategies

4.5 References

[1] E.M.A. Maine, "Innovation and Adoption of New Materials", University of Cambrige, U.K., *PhD. Dissertation,* **2000**

[2] *Cruising World Magazine* **2000**, *3*

[3] *Sail Magazine* **2001**, *1*

[4] Interconnection Consulting, "European Boating Industry", **2003**, *2*

[5] New York Times Magazine Group Resource Research Center, *Annual Sailing Business Report,* years **1988** – **2003**.

[6] *Boating Industry* **1996**, *4*

[7] *Boating Industry* **2002**, *4*

[8] *Boating Industry* **2003**, *2*

[9] *Boating Industry* **2002**, *6*

[10] T. G. Weld, *The Business Plan for Fiberspar,* Massachusetts Institute of Technology, *Master of Science Dissertation*, **1984**

[11] Reference U.S.A., http://www.referenceusa.com/ **2004**

[12] *Sail Magazine* **2000**, *4*

[13] Hall Spars and Rigging, www.hallspars.com, **2004**

[13] Abernathy, W. J. Clark, K.B. "Innovation: Mapping the Winds of Creative Destruction". *Research Policy. 14*, **1985**, pp 3-22

[14] Lindstrom, Assignee Selden Mast, U.S. Patent 6 575 108, **2003.**

[15] Lindstrom, Assignee Selden Mast, U.S. Patent 6 443 082, **2002.**

[16] Bernson, Assignee Selden Mast, U.S. Patent 5 560 311, **1996.**

[17] Kollberg, Assignee Selden Mast, U.S. Patent 5 493 988, **1996.**

[18] Montandon, Assignee Nirvana Espar System S.A., U.S. Patent 4 637 334, **1987.**

[19] Montandon, Assignee Nirvana Espar System S.A., U.S. Patent 4 712 500, **1987.**

[20] John McCabe, Hall Spars and Inc., Private conversation, **2004.**

[21] Hulse *et al.,* Isomat Inc., U.S. Patent 5 490 472, **1996.**

[22] Quigley, Assignee Fiberspar, U.S. 5 048 441 **1989.**

[23] Quigley, Assignee Fiberspar, Re. 85 081 **1995.**

[24] M.E. Porter, "Competitive Advantage: Creating and Sustaining Superior Performance" Boston, MA: Harvard Business School Press, **1985.**

[25] Hoover, http://premium.hoovers.com/, **2004**

[26] T. G. Weld, *The Business Plan for Fiberspar,* Massachusetts Institute of Technology, *Master of Science Dissertation*, **1984**

[27] Market Insight, http://mi.compustat.com/, **2004.**

Chapter 5

Conclusions

"If a man begins with certainties, he shall end in doubts;
but if he will be content to begin with doubts, he shall end in certainties."

Francis Bacon

Load-bearing tubular structures are widespread in engineering applications. Two types of design are used currently: thin-wall hollow shells and stiffened shells with rings and stringers. The former is common in small diameter applications (say less than 1 meter); the latter, which is more efficient against local buckling, is typical of large engineering tubular structure like aircraft fuselage or off-shore platform legs. Some load-bearing natural structures are characterized by a different design: they present an outer shell of dense material and an inner less dense compliant core. In this thesis, we discussed the possibility to improve the efficiency of small diameter engineering structures, by mimicking natural designs, focusing on the applications and commercial opportunities of these improved structures.

The fabrication of engineering structures, which resemble natural ones was shown to be feasible: metal foam and honeycomb materials are available in different shapes and densities and their cost is decreasing due to continuous improvements in their manufacturing processes. Sandwich shells with honeycomb cores can be manufactured easily adapting existing autoclave processing techniques. For foam-core shells, we considered two possibilities to create a shell sandwich structure: the first is a one-step process, co-forming metal powders; the second is a two-step process, fabricating first a hollow foam cylinder through the powder-metallurgical route and then bonding it to a metal sheet. For foam shells, we spot the greatest limit in the availability of viable technologies to join aluminium foam with solid metal. The opportunity to create foam sandwich structures in a two-step process, by nickel-plating the foam and brazing it, is currently under investigation.

In order to assess the viability, the technical performance of shells with a compliant core was compared to conventional engineering designs. This was done using the resistance to buckling as parameter and focusing only on structures in compression. The results of our analysis are encouraging: for small compression loads, biomimicked designs outperform traditional engineering ones. In this load range, aluminium sandwich shells with cellular metal core can be more efficient than CFRP tubes. We compared the cost of fabrication a honeycomb-core and foam-core sandwich shells with the cost of conventional hollow tubes: structures integrating cellular metals were found to have a manufacturing cost of 20-40 $/kg, which places them among extruded aluminium and autoclave-moulded CFRP tubes. Performance and cost feature makes aluminium sandwich shells with cellular metal core competitive in aerospace and/or sport applications. As aerospace applications were regarded too complex to introduce the product into the market, we focused on sport ones.

We pointed out that sailboat masts, which are columns subjected mainly to axial compression designed as light as possible, are an ideal field for the take-off of this technology. In particular, we considered the application of cellular metals in masts of sailboats of large dimension, which are currently designed against local buckling (see Figure 5.1)

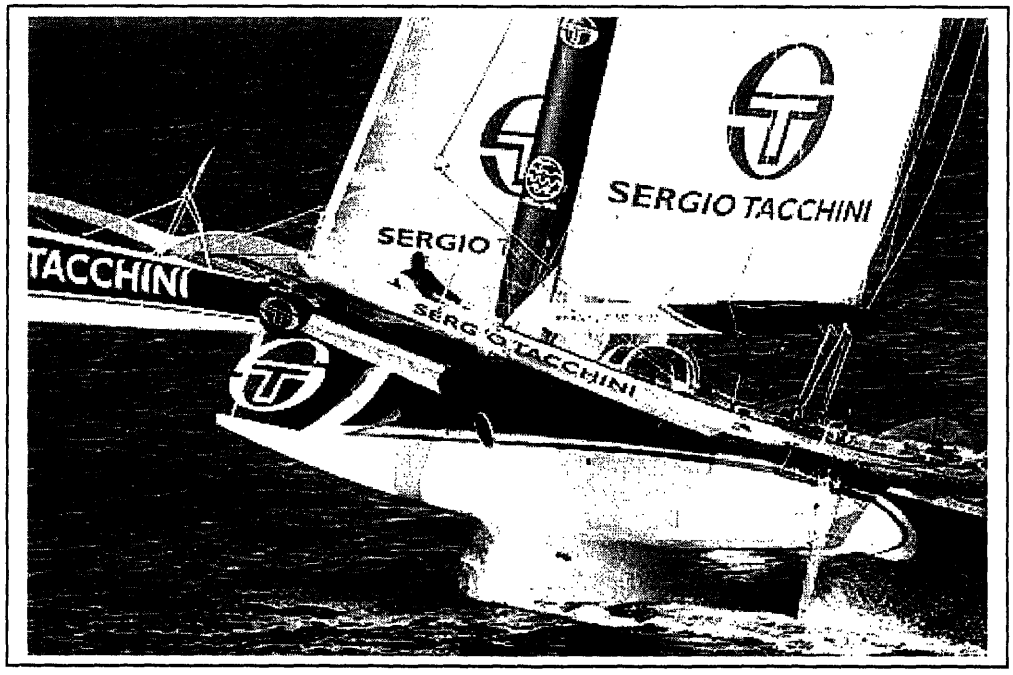

Figure 5.1: The carbon fiber mast of the trimaran Sergio Tacchini, produced by Espace Composite (Lunel, France) [1].

In order to evaluate the effectiveness of this application, we redesigned the mast of a typical 12-meter yacht using conventional engineering and compliant core designs. The results of the analysis were that foam-core shell designs, whose core thickness is limited by manufacturing constraints, do not perform well compared to hollow thin-wall mast. On the other hand, a sandwich construction employing thin layers of honeycomb as core metal allows a reduction of almost 30% in weight with small increments in the external mast dimension. Further decreases in weight, up to 60%, are possible employing a single-reinforced honeycomb-core design at larger mast diameters.

Different investments options were evaluated: the opportunity to start a Company specializing in the production of cellular metal mast does not seem feasible, mainly because the size mast of the market does not justify the risks of a start-up. The possibility to patent the invention and licensee to a CFRP mast manufacturers seems the best option.

References

[1] Giovanni Soldini, Giovanni Soldini website, http://www.soldini.it/eng/trimarano.html